(37)

PCT WORLD INTELLECTUAL PROPERTY ORGANIZATION
International Bureau

INTERNATIONAL APPLICATION PUBLISHED UNDER THE PATENT COOPERATION TREATY (PCT)

(51) International Patent Classification 6 : A61B 19/00 — A1

(11) International Publication Number: **WO 99/39650**

(43) International Publication Date: 12 August 1999 (12.08.99)

(21) International Application Number: PCT/US99/02045

(22) International Filing Date: 28 January 1999 (28.01.99)

(30) Priority Data:
09/018,435 4 February 1998 (04.02.98) US

(71) Applicant: AMERICAN CARDIAC ABLATION CO. INC. [US/US]; 125 John Hancock Road, Taunton, MA 02780 (US).

(72) Inventors: NARDELLA, Paul, C.; 12 Cromesett Point, Wareham, MA 02571 (US). WRUBLEWSKI, Thomas; 5 Tall Tree Road, Sharon, MA 02067 (US).

(74) Agents: GEARY, William, C., III et al.; Nutter, McClennen & Fish, LLP, One International Place, Boston, MA 02110–2699 (US).

(81) Designated States: CA, JP, European patent (AT, BE, CH, CY, DE, DK, ES, FI, FR, GB, GR, IE, IT, LU, MC, NL, PT, SE).

Published
With international search report.

(54) Title: CATHETER POSITIONING SYSTEM

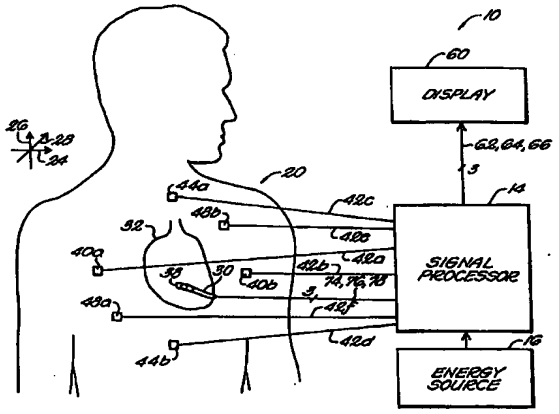

(57) Abstract

A system (10) for detecting the position of a catheter (30) in a patient includes three sets of excitation electrodes (40a, 40b; 44a, 44b; 48a, 48b), with one set disposed in each of the three intersecting axes. A signal processor (14) measures a voltage indicative of impedance between a detection electrode (38) disposed on the catheter (30), and each of the three sets of excitation signals in order to determine the X coordinate, Y coordinate and Z coordinate of the catheter (30). The detected position of the catheter (30) is recorded, and the detection of subsequent catheter positions is performed relative to the recorded catheter position. The difference between subsequent catheter positions, and the recorded position relative to the X, Y and Z axes is displayed in order to facilitate repositioning of the catheter (30) at the recorded position. Excitation electrode (38) embodiments utilizing as few as four excitation electrodes are disclosed. The excitation electrodes (38) may be surface, subcutaneous or intra-cardiac electrodes.

FOR THE PURPOSES OF INFORMATION ONLY

Codes used to identify States party to the PCT on the front pages of pamphlets publishing international applications under the PCT.

AL	Albania	**ES**	Spain	**LS**	Lesotho	**SI**	Slovenia
AM	Armenia	**FI**	Finland	**LT**	Lithuania	**SK**	Slovakia
AT	Austria	**FR**	France	**LU**	Luxembourg	**SN**	Senegal
AU	Australia	**GA**	Gabon	**LV**	Latvia	**SZ**	Swaziland
AZ	Azerbaijan	**GB**	United Kingdom	**MC**	Monaco	**TD**	Chad
BA	Bosnia and Herzegovina	**GE**	Georgia	**MD**	Republic of Moldova	**TG**	Togo
BB	Barbados	**GH**	Ghana	**MG**	Madagascar	**TJ**	Tajikistan
BE	Belgium	**GN**	Guinea	**MK**	The former Yugoslav Republic of Macedonia	**TM**	Turkmenistan
BF	Burkina Faso	**GR**	Greece			**TR**	Turkey
BG	Bulgaria	**HU**	Hungary	**ML**	Mali	**TT**	Trinidad and Tobago
BJ	Benin	**IE**	Ireland	**MN**	Mongolia	**UA**	Ukraine
BR	Brazil	**IL**	Israel	**MR**	Mauritania	**UG**	Uganda
BY	Belarus	**IS**	Iceland	**MW**	Malawi	**US**	United States of America
CA	Canada	**IT**	Italy	**MX**	Mexico	**UZ**	Uzbekistan
CF	Central African Republic	**JP**	Japan	**NE**	Niger	**VN**	Viet Nam
CG	Congo	**KE**	Kenya	**NL**	Netherlands	**YU**	Yugoslavia
CH	Switzerland	**KG**	Kyrgyzstan	**NO**	Norway	**ZW**	Zimbabwe
CI	Côte d'Ivoire	**KP**	Democratic People's Republic of Korea	**NZ**	New Zealand		
CM	Cameroon			**PL**	Poland		
CN	China	**KR**	Republic of Korea	**PT**	Portugal		
CU	Cuba	**KZ**	Kazakstan	**RO**	Romania		
CZ	Czech Republic	**LC**	Saint Lucia	**RU**	Russian Federation		
DE	Germany	**LI**	Liechtenstein	**SD**	Sudan		
DK	Denmark	**LK**	Sri Lanka	**SE**	Sweden		
EE	Estonia	**LR**	Liberia	**SG**	Singapore		

CATHETER POSITIONING SYSTEM

BACKGROUND OF THE INVENTION

Catheters of the type which are inserted into a vessel of a patient for carrying electrical signals to and from the patient are used in various applications. For example, cardiac catheters are inserted within a blood vessel into a patient's heart to detect cardiac electrical signals, to apply electrical stimulation for diagnostic testing and to apply treatment signals, such as tissue ablation signals which are used to eliminate the source of an arrhythmia. Other applications for ablation catheters include the treatment of tumors, such as breast or liver tumors, and the identification of tumor biopsy sampling sites. In addition to one or more electrodes, the catheter may include other structures, such as a lumen through which light, thermal energy or chemical agents are delivered and/or a sampling system for sampling a tissue or fluid specimen.

One multi-electrode catheter arrangement, described in U.S. Patent No. 5,341,807 (Nardella), includes signal processing circuitry for detecting contact of the catheter with tissue, such as a vessel wall. The Nardella catheter includes a tip electrode and a plurality of ring electrodes spaced along the catheter. The differential voltage indicative of impedance between the electrodes is measured to provide an indication of the catheter electrodes being disposed in different mediums (for example, when one electrode is in blood and another is in contact with tissue). The resulting indication of catheter contact is useful in many applications. For example, in cardiac ablation, the catheter must be in contact with, or at least in close proximity to, the treatment site in order to ensure that an effective level of RF energy reaches the tissue.

It is generally necessary to utilize a visualization technique of some sort in order to guide the catheter to a desired site of diagnosis and/or treatment and to ensure that the catheter remains at the desired location. Additionally, it is often desirable or necessary to re-position the catheter at a particular location. For example, in applications in which a cardiac ablation catheter is used for diagnosis and subsequent treatment of an arrhythmia, the catheter is moved around the heart while cardiac electrical signals are monitored, following which one or more sites identified as being the source of an arrhythmia are ablated. Thus, during such a procedure, it is necessary to determine the location of the catheter as the electrical signals are monitored in order to facilitate re-positioning the catheter at the site of an arrhythmia for ablation. Further, during any catheter

procedure, the catheter may slip and require re-positioning in order to successfully complete the procedure.

Catheter positioning and re-positioning has conventionally been achieved with the use of fluoroscopic techniques. However, since fluoroscopy typically provides only two-dimensional information, its accuracy in catheter positioning is limited. Furthermore, due to the potential risks associated with exposure to electromagnetic radiation, it is advantageous to limit the use of fluoroscopy.

SUMMARY OF THE INVENTION

The invention relates to a catheter positioning system for detecting the position of a catheter relative to intersecting X, Y and Z axes and for permitting the catheter to be accurately re-positioned with an accuracy on the order of about one millimeter. Once the catheter is placed at a desired location, its position is recorded. Subsequent positions of the catheter are processed relative to the recorded position and are displayed. The catheter is re-positioned at the recorded position by moving the catheter until the displayed difference between the subsequent and recorded catheter positions decreases to zero. With this arrangement, once a desired location is detected and recorded, the fluoroscopic equipment can be turned off, thereby advantageously limiting the patient's exposure to potentially harmful radiation. Further, the accuracy with which the catheter is re-positioned is enhanced, as compared to the use of fluoroscopic techniques for this purpose.

The position detection system includes a first set of excitation, or reference electrodes disposed along the X axis, a second set of excitation electrodes disposed along the Y axis, and a third set of excitation electrodes disposed along the Z axis. A signal processor measures the differential voltage indicative of impedance between a detection electrode on the catheter and each electrode of the first, second and third sets of excitation electrodes to determine the X coordinate, Y coordinate and Z coordinate of the catheter position, respectively. To this end, a first current provided by an energy source flows between the first set of excitation electrodes, a second current flows between the second set of excitation electrodes and a third current flows between the third set of excitation electrodes. Preferably, the first, second and third currents have different frequencies which minimize any cross-axis interference.

The signal processor includes an X axis processor unit coupled to the first set of excitation electrodes, a Y axis processor unit coupled to the second set of excitation electrodes and a Z axis processor unit coupled to the third set of excitation electrodes. Each of the processor units includes a demodulator coupled to the output of a differential amplifier for providing a DC signal proportional to the position of the catheter relative to the respective axis (i.e., the coordinate).

In one embodiment, the differential voltage indicative of impedance is measured by detecting the difference between the voltage at the detection electrode and a reference potential generated from each of the three sets of excitation electrodes. Specifically, an X axis reference node is provided by a resistor divider coupled between the X axis excitation electrodes and used to detect catheter position along the X axis by measuring the voltage between the detection electrode and the X axis reference potential. Similarly, a Y axis reference potential is provided by a resistor divider coupled between the Y axis excitation electrodes and used to detect catheter position along the Y axis by measuring the voltage between the detection electrode and the Y axis reference potential and a Z axis reference potential is provided by a resistor divider coupled between the Z axis excitation electrodes and used to detect catheter position along the Z axis by measuring the voltage between the detection electrode and the Z axis reference potential.

In another embodiment, catheter position detection measurements along each of the three axes are strict differential measurements made without the use of a reference potential or a separate reference electrode. For each of the three axes, a first amplifier measures the voltage between the detection electrode and one electrode of a excitation electrode pair for the given axis and a second amplifier measures the voltage between the detection electrode and the other one of the pair of excitation electrodes. A differential amplifier coupled to the outputs of the first and second amplifiers provides an output signal indicative of the position of the detection electrode relative to the excitation electrodes.

An optional EKG sensor detects an EKG signal of the patient for use in synchronizing detection of the catheter position. Further, an optional respiratory sensor detects a respiratory signal of the patient for use in synchronizing detection of the catheter position. In this way, artifacts due to cardiac motion and/or respiratory motion of the patient are reduced, thereby enhancing the accuracy of the catheter position detection.

The excitation, or reference electrodes may be subcutaneous electrodes, such as needle electrodes inserted into the patient's body in the region of catheter treatment or, alternatively, may be pad electrodes attached externally to the patient's body. In the later case, an additional set of electrodes, referred to as compensation electrodes, may be positioned along each of the X, Y and Z axes in order to compensate for any impedance effects due to external attachment of the pad electrodes.

As a further alternative, the excitation electrodes may be intracardiac electrodes. One suitable type of intracardiac electrode has a plurality of electrode supporting members at a distal end which, in use, are bowed outward to form a basket structure. The intracardiac electrode may support various numbers of excitation electrodes for applying three excitation signals along three intersecting axes.

In one embodiment, an intracardiac catheter supports eight or more electrodes which are grouped to define at least two X, Y, Z coordinate systems. This arrangement permits the signal processor to switch between excitation coordinate systems as the detection electrode approaches a region of large electric field non-linearity near one of the active excitation electrodes.

Also described is a catheter positioning system utilizing as few as four electrodes, either of the surface, subcutaneous, or intracardiac type or some combination thereof, for applying three excitation signals along three intersecting axes. One of the excitation electrodes provides an X axis electrode, one of the excitation electrodes provides a Y axis electrode and one of the electrodes provides a Z axis electrode. The fourth electrode is a "common" electrode shared by each of the three axis electrodes.

In one embodiment, the detection electrode is positioned at the tip of the catheter and the catheter further includes a proximal electrode and a reference electrode positioned between the tip and the proximal electrode. Contact of the catheter with tissue, such as a vessel wall, is detected by measuring the differential voltage indicative of impedance between the tip electrode and the proximal electrode relative to the reference electrode.

BRIEF DESCRIPTION OF THE DRAWINGS

Figure 1 illustrates a catheter positioning system in accordance with the invention.

Figure 1A is a perspective view of a multi-electrode catheter for use with the catheter positioning system of Figure 1.

Figure 2 is block diagram of the catheter positioning system of Figure 1.

Figure 3 is a schematic of the front end circuit of the catheter positioning system of Figure 2.

Figure 4 is a schematic of the demodulator circuit of the catheter positioning system of Figure 2.

Figure 4A is an alternative differential voltage circuit for the front end circuit for the catheter positioning system of Figure 2.

Figure 5 is a schematic of the demodulator switch of the catheter positioning system of Figure 2.

Figure 6 is a schematic of the sampling circuit of the catheter positioning system Figure 2.

Figure 7 is a schematic of a first portion of the EKG circuit of the catheter positioning system of Figure 2.

Figure 7A is a schematic of a second portion of the EKG circuit of the catheter positioning system of Figure 2.

Figure 8 is a schematic illustrating processing of signals from the detection, proximal and reference electrodes of the catheter of Figure 1A in order to detect contact of the catheter with tissue.

Figure 9 is a schematic of an alternate front end circuit of the catheter positioning system of Figure 2 including compensation electrodes for use in conjunction with externally attached reference electrodes.

Figure 10 illustrates an alternate catheter positioning system utilizing four surface excitation electrodes.

Figure 11 illustrates an intracardiac catheter supporting four excitation electrodes in accordance with a further embodiment of the invention.

Figure 12 illustrates an alternate intracardiac catheter supporting six intracardiac excitation electrodes in accordance with a still further embodiment of the invention.

Figure 13 illustrates an further alternate intracardiac catheter supporting twelve intracardiac excitation electrodes in accordance with another embodiment of the invention.

Figure 14 is a schematic of a signal processor and multiplexer circuit suitable for use with the intracardiac catheter of Figure 13.

DETAILED DESCRIPTION OF THE INVENTION

Referring to Figure 1, a catheter positioning system 10 for detecting the position of a catheter 30 having a detection electrode 38 is shown. The system 10 includes a signal processor 14 and three pairs of excitation, or reference electrodes 20, with one pair positioned along each of three intersecting axes, including the X axis 24, the Y axis 26 and the Z axis 28. Preferably, the three intersecting axes are mutually orthogonal, although they need not be, as discussed below. More particularly, a first set of excitation electrodes 40a, 40b is positioned along the X axis 24, a second set of excitation electrodes 44a, 44b is positioned along the Y axis 26, and a third set of excitation electrodes 48a, 48b is positioned along the Z axis 28. An energy source 16 supplies electrical energy to the excitation electrodes 20. A display 60, coupled to the signal processor 14, displays the detected catheter position in a manner that facilitates catheter re-positioning, as will be described. In applications in which the detection electrode 38 delivers ablation energy, the electrode may be referred to as an active electrode.

The illustrated catheter 30 is a cardiac ablation catheter adapted for insertion through a vessel into a patient's heart 32 for arrhythmia diagnosis and ablation. It will be appreciated by those of ordinary skill in the art, however, that the catheter positioning system 10 and related techniques described herein are suitable for use with any catheter application in which it is advantageous to re-position the catheter at a particular location.

The reference electrodes 20 may be subcutaneous electrodes, such as needle electrodes adapted for insertion into the patient's body. Alternatively, the reference electrodes 20 may be electrode pads, or patches adapted for external attachment to the patient's skin. Where the electrodes are externally attached, three additional sets of electrodes, referred to as compensation electrodes, may be provided to compensate for any impedance effects associated with attachment of the pads to the patient's skin, as will be described further in conjunction with Figure 9. As a further alternative, the reference electrodes 20 may be intracardiac electrodes, as described in conjunction with Figures 11-14.

Each of the excitation electrodes 20 is electrically coupled to the signal processor 14 via a respective signal line 42a - 42f, as shown. In the illustrative embodiment, the catheter 30 is coupled to the signal processor 14 via three signal lines 74, 76 and 78, with one signal line coupled to each electrode on the catheter, as described below in conjunction with Figure 1A.

The energy source 16 delivers AC energy, referred to herein as an excitation signal, in the form of voltage or current to the electrodes via the signal processor 14 in order to permit voltage measurements to be made by the signal processor. The measured voltage is indicative of impedance since voltage is proportional to impedance. In the illustrative embodiment, the energy source 16 provides a first excitation current to the first set of excitation electrodes 40a, 40b, a second excitation current to the second set of excitation electrodes 44a, 44b and a third excitation current to the third set of excitation electrodes 48a, 48b.

Preferably, each of these currents has a different frequency chosen to minimize any cross-axis interference. In one example, the first current is a 48 KHz AC current, the second current is a 50 KHz AC current and the third current is a 54 KHz AC current. In alternative embodiments, other distinguishing characteristics of the currents may be varied among the three axes to sense and differentiate the respective current signals. Distinguishing characteristics may include, for example, phase or timing variations between the current signals for each axis.

Signal processor 14 measures the differential voltage indicative of impedance between the detection electrode 38 of the catheter 30 and each of the six excitation electrodes 20 in order to determine the three-dimensional position of the catheter 30 and, specifically, to determine the X coordinate, Y coordinate and Z coordinate of the catheter 30. To this end, the signal processor 14 includes an X axis processor unit 50, a Y axis processor unit 52 and a Z axis processor unit 54 (Figure 2), with each processor unit measuring the differential voltage indicative of impedance between the detection electrode 38 and each one of the electrodes of the respective set of electrodes. For example, the X axis processor unit 50 measures the voltage indicative of impedance between the detection electrode 38 and excitation electrode 40a and also between detection electrode 38 and excitation electrode 40b in order to determine the X coordinate of the catheter 30 (i.e., the position of the catheter relative to the X axis).

The signal processor 14 provides an X axis output signal 62, a Y axis output signal 64 and a Z output axis signal 66 coupled to the display 60, which may be referred to alternatively as the catheter location map. The display 60 provides an indication of the position of the catheter

relative to the X, Y and Z axes and/or relative to a previously recorded position. More particularly, the catheter positioning system 10 is capable of operating in a "direct" mode of operation, during which the catheter position is continuously tracked and an indication thereof is displayed, or in a "relative" mode of operation, in which a position of the catheter is recorded, subsequent position measurements are made relative to the recorded position and the difference between the recorded and subsequent positions is displayed, as will be described further below.

The display 60 may take various forms, including analog or digital. In one embodiment, two axes are displayed on one graph and the third axis is displayed on a separate device, such as a digital meter. Alternatively, a three axis graphical representation, a wire frame representation, or a surface rendering technique, all of which are conventional Computer-Aided Design (CAD) system presentations, may be used to provide the display 60.

Referring also to Figure 1A, an enlarged view of the illustrative cardiac ablation catheter 30 is shown. The detection electrode 38 which may deliver ablation energy is positioned at the distal tip of the catheter and thus, may be referred to as the tip electrode 38. The catheter 30 further includes a proximal electrode 72 and a reference electrode 68 disposed between the proximal electrode and the tip electrode, with the proximal and reference electrodes being in the form of ring electrodes, as shown. The catheter 30 has an elongated insulating body 36 mounted at the end of a flexible tube 34 which is used for inserting and manipulating the catheter along a vessel. Signal lines 74, 76, and 78 extend from the tube 34 to electrically connect catheter electrodes 38, 68 and 72 to the signal processor 14, respectively. In accordance with a feature of the invention, a fourth current provided by the energy source 16 flows between the tip electrode 38 and proximal electrode 72 in order to facilitate measurements used to determine catheter contact, as described below in conjunction with Figure 8.

Referring also to Figure 2, a block diagram of the catheter positioning system 10 is shown to include the signal processor 14, energy source 16 and display 60. The energy source 16 includes three oscillators 100, 106 and 108 for providing the first current to the X axis excitation electrodes 40a, 40b, the second current to the Y axis excitation electrodes 44a, 44b and the third current to the Z axis excitation electrodes 48a, 48b, respectively.

The signal processor 14 includes the X axis processor unit 50 which is coupled to the X axis excitation electrodes 40a, 40b, the Y axis processor unit 52 which is coupled to the Y axis excitation electrodes 44a, 44b, and the Z axis processor unit 54 which is coupled to the Z axis

excitation electrodes 48a, 48b, all of which are substantially identical in construction. The processor units will be described with reference to exemplary X axis processor unit 50 for simplicity of discussion. Also provided in the signal processor 14 is an optional EKG circuit 105 (Figures 7 and 7A) which monitors the EKG signal of the patient and an optional respiratory detector 101 which monitors the respiratory signal of the patient. The output signals from the EKG circuit 105 and the respiratory detector 101 are processed by a trigger logic circuit 103 to provide a SYNC signal 107 which is used to synchronize catheter position detection, as will be described.

The processor unit 50 includes a front end circuit 120 (Figure 3) coupled to the excitation electrodes 40a, 40b via respective terminals 140a, 140b of a connector 140, a demodulator circuit 128 (Figure 4) coupled to the outputs of the front end circuit 120 and a sampling circuit 134 (Figure 6). The demodulator circuit 128 is responsive to a demodulator switch 132 (Figure 5). The sampling circuit 134 provides the X axis output signal 62 to the display 60, as shown. It will be appreciated by those of ordinary skill in the art that the particular circuitry arrangement and component values described herein are illustrative only and may be varied without departing from the spirit from the invention.

Referring also to Figure 3, the front end circuit 120 includes a gain and/or phase stage 104, an electrode interface 126 and buffers 150, 152. The output signal 102 from the X axis oscillator 100 is coupled to the gain and/or phase stage 104 which permits the magnitude of the AC energy signal 102 and/or the phase of demodulation of the signal from the X axis excitation electrodes 40a, 40b to be adjusted. More particularly, the oscillator output signal 102 is coupled to a first potentiometer 124 which can be adjusted to vary the magnitude of the oscillator output signal 102. The oscillator output signal 102 is further coupled to a second potentiometer 130 which is adjustable to vary the phase of demodulation of the signal from the excitation electrodes 40a, 40b. More particularly, the output of the potentiometer 130 provides a phase signal (DEMODX) which is coupled to the demodulator switch 132 (Figure 5). The phase signal is used to vary the demodulation phase in order to compensate for phase shifts resulting from signal processing.

The magnitude setting potentiometer 124 is coupled to an operational amplifier 110 which provides a voltage output signal at a circuit node 112. The output of voltage amplifier 110 is further coupled to an operational amplifier 113 which provides a current output signal at a

circuit node 116. A jumper 118 is provided for selectively connecting either the voltage output of amplifier 110 or the current output of amplifier 113 to a circuit node 114. With this arrangement, the jumper 118 can be positioned in order to provide an AC current or an AC voltage to the excitation electrodes 40a, 40b. In the preferred embodiment, an AC current is supplied to the excitation electrodes 40a, 40b, since this stimulus type provides a larger signal-to-noise ratio.

A transformer 122 coupled to the circuit node 114 isolates the oscillator 100 on the primary side 122a of the transformer from the reference electrodes 40a, 40b coupled to the secondary side 122b of the transformer. The X axis reference electrodes 40a, 40b are coupled to the signal processor 14 via respective terminals 140a, 140b of connector 140, as shown. More particularly, the terminals 140a, 140b are coupled to a buffer 150 via a resistor divider 125. The detection electrode 38 of the catheter 30 is coupled to the signal processor 14 via terminal 140c of connector 140. A buffer 152 buffers the electrical signal from the detection electrode 38.

The front end circuit 120 also includes a differential amplifier 200 having a first input coupled to output 154 of buffer 150 and a second input coupled to the output 156 of buffer 152. The output signal 158 of the differential amplifier 200 is coupled to demodulator circuit 128 (Figure 4).

Referring to Figure 4, the demodulator circuit 128 includes a gain stage 204 having an input coupled to output 158 of differential amplifier 200, as shown. Demodulation is provided by an amplifier 210 having an inverting input coupled to the output of the gain stage 204 and a non-inverting input coupled to the output of the gain stage 204 and further to a signal line 212 from the demodulator switch 132, as will be described below in conjunction with Figure 5.

In operation, the differential voltage indicative of impedance between the excitation electrodes 40a, 40b and the detection electrode 38 is measured by differential amplifier 200 such that the output of amplifier 200 is an AC signal having a phase and magnitude indicative of the position of the detection electrode 38 relative to the excitation electrodes 40a, 40b. That is, an output signal in phase with the excitation stimulus indicates that the detection electrode 38 is closer to one of the electrodes 40a, 40b and an output signal out of phase with the excitation stimulus indicates that the detection electrode 38 is closer to the other one of the electrodes 40a, 40b. Thus, when the output signal of the amplifier 200 is null, the detection electrode 38 is equidistantly positioned between the X axis excitation electrodes 40a, 40b. The magnitude of

the output signal of the amplifier 200 indicates the relative proximity of the detection electrode 38 to each of the excitation electrodes 40a, 40b.

The gain of the output signal of amplifier 200 is boosted by the gain stage 204 in order to enhance the detection sensitivity. For example, in the illustrative embodiment, the gain is boosted by a factor of twenty. The output of the gain stage 204 is demodulated by demodulator 210 in accordance with signals Xa and Xb provided by the demodulator switch 132 (Figure 5) in response to the respective phase signal DEMODX, as will be described.

Consideration of Figures 3 and 4 reveals that catheter position detection along the X axis (i.e., the measurement of the differential voltage indicative of impedance between the detection electrode and each of the X axis excitation electrodes 40a, 40b) is achieved by measuring the voltage between the detection electrode 38 and an electronically generated reference potential at the center of the resistor divider 125. That is, the voltage at the center of the resistor divider 125 is equal to one-half of the voltage between the X axis excitation electrodes 40a and 40b. The same signal measurement technique is used to detect catheter position relative to the Y and Z axes. Thus, for each of the three axes, a "virtual" or electronic reference potential is generated for measuring the signal at the detection electrode.

The voltage at the center of resistor divider 125 need not be equal to one half of the voltage between the X axis excitation electrodes 40a and 40b. While the one half value may be preferred for certain electrode configurations, this voltage may be varied to any level between the X axis excitation electrodes 40a and 40b. In fact, measurement of the differential voltage indicative of impedance between the detection electrode and the X axis may be achieved by measuring the voltage between the detection electrode and either of the X axis excitation electrodes 40a or 40b directly without the use of resistor divider 125. Accordingly, the reference potential may be varied in any amount from the voltage of one axis excitation electrode to the voltage of the other excitation electrode for that axis.

This technique advantageously permits elimination of a separate additional reference electrode to be placed on the surface of the patient which could move and render the catheter position detection inaccurate. Further, such an additional reference electrode has noise associated with its use.

This arrangement is also advantageous as compared to the use of a separate reference electrode provided in the form of an intracardiac electrode since such an intracardiac electrode

is susceptible to movement within the body due to the forces applied to the electrode by a beating heart. In addition, an intracardiac reference electrode is a low impedance electrode that will create an equipotential field based upon its size, shape and location within the heart. As a result, position detection of the detection electrode suffers from reduced sensitivity when the detection electrode nears the equipotential field. This reduced sensitivity is most significant when the intracardiac reference electrode and the detection electrode are located within the same chamber of a heart.

Referring to Figure 4A, an alternative technique for measuring the differential voltage indicative of impedance between the detection electrode 38 and each of the X axis excitation electrodes 40a, 40b is shown. This technique does not require the use of a separate reference electrode for attachment to, or insertion into the patient or "virtual" reference nodes as described above. The voltage difference between the detection electrode 38 and a first one of the X axis excitation electrodes 40a is measured with an amplifier 600 and the voltage difference between the detection electrode 38 and the other X axis excitation electrode 40b is measured with an amplifier 604. The outputs of amplifiers 600 and 604 are coupled to inputs of a differential amplifier 608 which detects the differential voltage between the detection electrode and the X axis electrodes, thereby indicating the location of the detection electrode relative to such excitation electrodes 40a, 40b. Thus, the output 658 of amplifier 608 is null when the detection electrode is located equidistantly between the X axis excitation electrodes. The output 658 of amplifier 608 may then be coupled to demodulation circuit 128 in place of signal 158 (Figure 4).

Referring also to Figure 5, the demodulator switch 132 provides demodulation input signals Xa/Xb, Ya/Yb and Za/Zb to the processor units 50, 52, and 54, respectively, as shown in Figure 2. The demodulator switch 132 is responsive to phase signals DEMODX, DEMODY and DEMODZ (Figure 2) from the phase portion of circuitry 104 of the front-end circuit 120 of each the X, Y and Z processor units 50, 52 and 54. More particularly, each of the DEMOD signals is coupled to a respective comparator 250, 252 and 254, as shown and the output of each of the comparators 250, 252, and 254 is coupled to an analog switch 260.

Switch 260 includes three inverters, each having an input coupled to an output of a respective one of the comparators 250, 252, 254. For example, the output of the X axis comparator 250 is coupled to the input of inverter 264. Each inverter has a switch associated therewith that is adapted for being in a first, open position when the inverter output signal is in

one logic state and in a second, closed position when the inverter output signal is in the second logic state. In the illustrative example, when the output signal of the inverter 264 is at a logic low level, the switch 262 is open, so that terminals 262a and 262b are disconnected, as shown. When the inverter output signal is at a logic high level, the corresponding switch 262 is closed, with terminals 262a and 262b electrically connected.

Referring again to Figure 4, switch 262 is coupled between signal lines 212 and 214 such that, when the switch 262 is closed, signal line 212 is connected to ground via signal line 214. Whereas, when the switch 262 is open, signal line 212 is floating. With this arrangement, the signal provided at the output of amplifier 204 is demodulated with respect to the phase signal (DEMODX). The output signal 220 of the demodulator 210 is thus a DC signal with varying amplitude having a mean value proportional to the position of the catheter 30 relative to the X axis (i.e., proportional to the X coordinate). An amplifier 230 forms a low-pass filter for establishing the mean value, in order to enhance the detection accuracy of the system. The filter output signal 234, referred to alternatively as the demodulated catheter position signal 234, is coupled to the sampling circuit 134 (Figure 6). The information from channels Y 52 and Z 54 present on channel X are also demodulated. However, since they are not synchronous with the demodulation signal, an AC signal is generated and this information is averaged to zero by the filter.

Referring to Figure 6, the sampling circuit 134 controls the sampling of the demodulated catheter position signal 234 (Figure 4) in order to generate the X axis output signal 62. More particularly, as noted above, the catheter positioning system 10 is adapted for operating in a "direct" mode of operation, during which the catheter position is continuously tracked, or in a "relative" mode of operation, in which the catheter position is recorded and subsequent catheter positions are detected relative to the recorded position.

To this end, a four-pole, double throw direct/relative switch 310 is provided for user control in order to select between the direct and relative modes of operation. Switch pole 310a is associated with the X axis processor unit 50 (Figure 6), pole 310b is associated with the Y axis processor unit 52 (Figure 2) and pole 310c is associated with the Z axis processor unit 54 (Figure 2). The fourth pole 310d of the switch 310 is common to all three of the processor units and is provided for controlling the sample and hold circuit 304, as will be described.

The demodulated catheter position signal 234 is coupled to a differential amplifier 300, the input of sample and hold circuit 304 and switch 310a, as shown. The output of the sample and hold circuit 304 is coupled to an input of the differential amplifier 300, the output of which is coupled to the switch 310a. Switch 310a selectively couples the non-inverting input of a gain stage 320 either to the catheter position signal 234 or to the output of operational amplifier 300. When the switch 310 is in the direct position, as shown, the non-inverting input of the gain stage 320 is coupled to the demodulated catheter position signal 234. Alternatively, when the switch 310 is in the relative position, the non-inverting input of gain stage 320 is coupled to the output of the amplifier 300. The output signal of amplifier 300 represents the catheter's position relative to the catheter's position when the switch 310 was in the direct position.

Switch 310d causes the S/H input of the sample and hold circuit 304 to be selectively coupled to +5V or to ground, as shown. When the switch 310 is in the direct position and the S/H input to the sample and hold circuit 304 is at +5V, the sample and hold circuit 304 tracks the signal 234 to provide output signal 316. When the switch 310 is in the relative position and the S/H input to the sample and hold circuit 304 is at ground, the output signal 316 of the sample and hold circuit 304 is held constant.

The gain of the operational amplifier 320 is adjustable in order to adjust the position detection sensitivity. To this end, a switch 330 is provided in feedback relationship with the gain stage 320 to selectively connect or disconnect the output of gain stage 320 to its inverting input. In this way, the gain of amplifier 320 can be set to one or to a gain set by resistors 322 and 323.

The output signal 328 of the gain stage 320 is coupled to the input of a sample and hold circuit 324 which is operative to track and sample the signal 328 in accordance with the SYNC signal 107. This sampling stage serves to reduce artifacts associated with the patient's EKG and/or respiratory signals, as will be described. The output of the sample and hold circuit 324 is a DC signal 62 (Figure 2) indicative of the X coordinate of the catheter position during the direct mode of operation or indicative of the difference between the X coordinate of the catheter position and a recorded catheter position during the relative mode of operation. Thus, the display 60 can display the catheter position relative to a previous position or the direct catheter position measurements relative to an arbitrary origin. For example, multiple catheter positions relative to the X, Y and Z axes may be captured and displayed.

In operation, when the switch 310 is in the direct position, the demodulated catheter position signal 234 is tracked by the sample and hold circuit 304 and is coupled to the gain stage 320 for processing and coupling to the input of the sample and hold circuit 324. The signal 328 is thus indicative of the present X coordinate of the catheter and is sampled by the circuit 324 every time the SYNC signal 107 transitions to a logic high level.

When the switch 310 is toggled to the relative position, the sample and hold circuit 304 causes the previously tracked catheter position signal 234 to be held to provide the output signal 316. Further, the output of the differential amplifier 300 is coupled to the gain stage 320 for processing and coupling to the sample and hold circuit 324. In this mode of operation, the signal 328 is indicative of the difference between the present X coordinate of the catheter (i.e., as represented by the catheter position signal 234) and its position at the time that the switch 310 was toggled (i.e., as represented by the value held at the output 316 of the sample and hold circuit 304). Stated differently, the differential amplifier 300 detects the difference between the signal 316 which is indicative of the catheter X coordinate when the switch 310 was toggled (i.e., the recorded position) and the X coordinate of the present catheter position (i.e., the subsequent position) and it is this difference signal that is coupled to the gain stage 320 and to the sample and hold circuit 324 to provide the X axis output signal 62 to the display 60.

Referring to Figures 7 and 7A, the EKG circuit 105 (Figure 2) is shown to include three leads 400, 404 and 408 adapted for attachment to the patient. Two of the leads 400 and 404 are pickup leads and the third lead 408 is a guard, or reference lead. The leads 400 and 404 are coupled to respective filter circuits 410 and 412 and to optional protection devices 414 and 418, as shown. The filtered signals are further coupled to a differential amplifier 420.

The output of the differential amplifier 420 is coupled to an amplifier 424 for signal amplification and further to a low-pass filter 428. The output of filter 428 is coupled to an adjustable gain stage 430 to provide an output signal EKGOUT, as shown. In the illustrative embodiment, the gain can be adjusted from between one and fifty-one.

The EKGOUT signal is coupled to a first input of a threshold detection comparator 434 (Figure 7A), the second input to which receives an adjustable threshold voltage. More particularly, the threshold voltage is adjustable with a potentiometer 436. The output signal 437 of the comparator 434 is a logic signal for triggering a one shot 438. Preferably, the threshold level coincides with the r-wave of the detected EKG signal. It will be appreciated by those of

ordinary skill in the art that the EKG detection circuitry shown and described herein is illustrative only and that other conventional EKG triggering circuitry and techniques could alternatively be used.

The one-shot circuit 438 generates a sampling pulse at a duration set by an adjustable resistor 440. The output of the one-shot 438 provides an EKG trigger signal which transitions to a logic high level when the detected EKG signal exceeds the predetermined threshold level (i.e., when an r-wave is detected). The EKG trigger signal is coupled to a trigger logic circuit 103 (Figure 2) or, in applications in which the SYNC signal 107 is based only on the EKG signal, the output of the EKG trigger signal is coupled directly to a switch 444 (Figure 2).

The optional respiratory detector 101 (Figure 2) includes similar circuitry and uses similar techniques to those described above in conjunction with EKG signal detection in order to detect the patient's respiratory signal. The output signal from the respiratory detector 101 is coupled to the trigger logic circuit 103 which combines the EKG trigger signal and the respiratory trigger signal to provide the SYNC signal 107 which indicates a predetermined point in the patient's respiratory and EKG cycles. The SYNC output signal of the trigger logic circuit 103 is coupled to a switch 444 which can be toggled between a SYNC position as shown and a "free-run" position in which the catheter position detection is not synchronized and the SYNC signal 107 is maintained at a logic high level, so that the X axis output signal 62 continuously tracks the input signal 328.

Referring to Figure 8, preferably, the signal processor 14 includes a catheter contact detection processor 70 for detecting contact of the catheter 30 with a vessel wall, or other tissue. Contact detection is achieved by providing a fourth current between the tip electrode 38 and the proximal electrode 72 and measuring the differential voltage representing impedance between the catheter electrodes, as described in U.S. Patent No. 5,341,807 (Nardella) which is incorporated herein by reference.

More particularly, the energy source 16 is coupled between the tip electrode 38 and the proximal electrode 72 of the catheter to provide a current between the two electrodes. A first differential amplifier 80 has a first input coupled to the proximal electrode 72 and a second input coupled to the reference electrode 68. A second differential amplifier 84 has a first input coupled to the tip electrode 38 and a second input coupled to the reference electrode 68, as shown. With this arrangement, each of the differential amplifiers provides an output signal indicative of the

impedance between the reference electrode 68 and a respective one of the proximal electrode 72 and tip electrode 38. The output of each of the differential amplifiers 80 and 84 is coupled to an input of a third differential amplifier 88 which detects a difference in the voltage representing a difference in the impedance between the tip electrode 38 and the reference electrode 68 and between the proximal electrode 72 and the reference electrode 68. When the impedance between electrodes 38 and 68 is substantially equal to the impedance between electrodes 68 and 72, the output of differential amplifier 88 is substantially null. Whereas, when the impedances differ (for example, as will occur when the tip electrode 38 contacts a vessel wall and the proximal electrode is disposed in blood), the output of the differential amplifier 88 increases. In this way, contact of the catheter 30 is indicated at the output of the differential amplifier 88 which may be coupled to a display (not shown).

Referring to Figure 9, a schematic of an alternate front end circuit 500 of the catheter positioning system of Figure 2 includes compensation electrodes for use in conjunction with externally attached reference electrodes 40a, 40b (Figure 1). The front end circuit 500 is similar to the front end circuit 120 (Figure 3), with like components being labeled with like reference numbers. Thus, the front end circuit 500 includes the gain and/or phase stage 104, the electrode interface 126, buffers 150 and 152, and differential amplifier 200.

The front end circuit 500 differs from the front end circuit 120 of Figure 3 in that the circuit 500 includes two additional electrodes, referred to as compensation electrodes PU1 and PU2, which are pad electrodes attached externally to the patient and electrically coupled to the signal processor via terminals 140d, 140e of connector 140. The compensation electrodes PU1 and PU2 are coupled to amplifiers 504 and 508, respectively, each of which has a high input impedance. Amplifier 504 has a non-inverting input capacitively coupled to the input terminal 140d and an inverting input coupled to its output. The output of amplifier 504 is further coupled to the resistor divider 125 (Figure 3). Similarly, amplifier 508 has a non-inverting input capacitively coupled to the input terminal 140e and an inverting input coupled to its output. The output of amplifier 508 is further coupled to the resistor divider 125. Use of the compensation electrodes PU1 and PU2 serves to minimize any impedance variations associated with external attachment of the reference electrodes 40a, 40b to the patient.

Referring to Figure 10, in which like reference numbers refer to like elements, an alternate catheter mapping system 10' utilizes only four excitation, or reference electrodes 40a,

44a, 48a, and 46 (collectively 20') positioned on the surface of the patient for detecting the position of the detection electrode 38 supported by the catheter 30. This is achieved by using one of the four electrodes 20' as common to each of the three axes of excitation. Specifically, one of the electrodes 40a is an X axis electrode and the return path for the current applied along the X axis is provided by a common electrode 46. Another electrode 44a is a Y axis electrode and the return path for the current applied along the Y axis is provided by the common electrode 46 and the last electrode 48a is a Z axis electrode and the return path for the current applied along the Z axis is provided by the common electrode. Thus, a first current having a first frequency passes between X axis electrodes 40a and 46, a second current having a second frequency passes between Y axis electrodes 44a and 46 and a third current having a third frequency passes between Z axis electrodes 48a and 46.

The same signal processing circuitry 14 (Figure 2) used to process the signals 42a - 42f from the six excitation electrodes 20 in Figure 1 can be used to process the signals 56a - 56d from the four excitation electrodes 40a, 44a, 48a, and 46. More particularly, the excitation electrodes 20' are coupled to the signal processor 14 by coupling the X axis excitation electrode 40a to one input of the X axis processor unit 50 (e.g., connector terminal 140a in Figure 2) and the common electrode 46 to the other input of the X axis processor unit 50 (e.g., connector terminal 140b in Figure 2). Similarly, the Y axis excitation electrode 44a is coupled to one input of the Y axis processor unit 52 and the common electrode 46 is coupled to the other input of the Y axis processor unit 52. Further, the Z axis excitation electrode 48a is coupled to one input of the Z axis processor unit 54 and the common electrode 46 is coupled to the other input of the Z axis processor unit 54. With this arrangement, two additional electrodes and their associated inaccuracies (e.g., due to inadvertent electrode movement and/or the impedance associated with surface electrodes) are eliminated.

Referring to Figure 11, an intracardiac catheter 632 supporting a plurality of electrodes 610, 614, 618, 622 (collectively 630) for use as excitation electrodes is shown. The catheter 632 is adapted for insertion through a vessel into a patient's heart. The catheter 632 has a plurality of flexible electrode supporting members 644, which may be provided in the form of wires, disposed at the end of a flexible tube 634. The electrode supporting members 644 are coupled together at a distal end 646 of the catheter which is attached to a pull wire 636. The pull wire 636 extends through the flexible tube 634 to the proximal end 650 of the catheter. Wire

conductors coupled to the electrodes 630 extend through the tube 634 to terminate at a connector 640 through which the electrodes are connected to an energy source which generates the excitation signals.

As the catheter 632 is inserted into a chamber of the patient's heart through a vessel, the flexible electrode supporting members 644 are pulled together (not shown). Once the catheter 632 is positioned at a desired location, the wire 636 is pulled from the proximal end 650 of the catheter (not shown), outside of the patient. Actuation of the wire 636 causes the flexible electrode supporting members 644 to bow outward, as shown, to form a basket, or cage structure 650. In use, some or all of the electrodes 630 may contact the chamber wall, although such contact is not necessary for catheter position detection. It may however be desirable to have the at least a portion of the basket structure 650 contact a chamber wall in order to stabilize the catheter and synchronize the excitation electrodes relative to cardiac movements.

The four excitation electrodes 630 are paired in the same way as the four surface excitation electrodes of Figure 10 to provide three intersecting excitation axes. Specifically, electrode 610 provides a first X axis electrode and the common electrode 622 provides the second X axis electrode, electrode 618 provides a first Y axis electrode and the common electrode 622 provides the second Y axis electrode, and electrode 614 provides a first Z axis electrode and the common electrode 622 provides the second Z axis electrode. Thus, the wire conductors extending from each of the electrodes to the connector 640 can be coupled to a signal processor of the type shown in Figure 2 in the manner discussed above in conjunction with Figure 10.

In use, the detection electrode 38 (Figure 1) is positioned in a location of the heart to be detected. Significantly, the detection electrode 38 need not be positioned within the region defined by the basket 650, although it can be. More particularly, because the electric field generated by passing an AC signal between a pair of excitation electrodes extends well beyond the straight line path between the electrodes in a conductive medium, the detection electrode 38 may in fact be located external to the basket 650. The detection electrode 38 need only be at a location in which it is subjected to the three electric fields generated by the three sets of excitation electrodes. In fact, the basket 650 may be located in one chamber of the heart, for example, the easier accessible right ventricle, and the detection electrode 38 located in the left ventricle where position detection for treatment, such as ablation, is desired.

Referring to Figure 12, an alternate intracardiac catheter 660 includes a plurality of electrode supporting members 664 coupled together at a distal end 666 of the catheter for supporting a plurality of excitation electrodes 668. The catheter 660 further includes a flexible tube 670 through which wire conductors coupled to the electrodes 668 extend. The wire conductors terminate at a connector 672 at the proximal end 674 of the catheter for permitting electrical connections to be made to the electrodes 668.

The catheter 660 differs from the catheter 632 of Figure 11 in that the former supports six excitation electrodes 668 and the latter supports four excitation electrodes as described above. More particularly, the catheter 660 has a pair of X axis excitation electrodes 680, 682, a pair of Y axis excitation electrodes 684, 686, and a pair of Z axis excitation electrodes 688, 690. The excitation electrodes 668 supported by the catheter 660 may be coupled to a signal processor of the type and in the manner described above in conjunction with Figure 2.

As will be appreciated by those of ordinary skill in the art, current density is greatest at the excitation electrodes and decreases as you move away from the electrodes, to a point of lowest current density half-way between two excitation electrodes in a given axis. This phenomena results in the greatest voltage gradient, and output sensitivity occurring when the detection electrode 38 is in close proximity to one of the excitation electrodes and also results in a non-linearity in the gain of the system relative to the excitation electrodes. Further, such non-linearity is exacerbated when the excitation electrodes are located close to one another, as occurs with intracardiac excitation electrodes as compared to surface excitation electrodes.

In catheter repositioning applications, this non-linearity is generally not of concern. This is because catheter repositioning is not dependent on the consistency of system gain, but rather on determining the difference between two or more detected positions in order to enable the operator to reposition the catheter at a point of interest.

However, in other applications, it may be desirable to determine the absolute distance between detected catheter positions. This can be achieved with the use of an additional electrode on the catheter 30 (Figure 1) located at a fixed, known distance from the detection electrode 38 or with a separate "calibration" electrode provided for reconciling the distance/voltage associated with movement of the catheter 30. Such absolute distance calibration requires three measurements to be made, with the detection electrode 38 located at three different positions relative to the excitation electrodes.

More particularly, assuming that the body between the excitation electrodes behaves linearly, the location of a detection electrode along any measured axis will be a constant multiplied by the voltage differential measured in the direction of that axis. With two electrodes placed a known distance apart on the catheter 30, the voltages measured in each axis for the two electrodes can be related to the known distance between the electrodes. The measurement of three data points then permits the three constants associated with voltage measurements in each of the three excitation axes to be determined and used to calibrate catheter position detection. Thus, with this arrangement, the absolute distance between two or more detected catheter positions can be determined.

In applications in which improved linearity or determination of the absolute distance between catheter positions is desired, various techniques can be used to compensate for non-linearity in the detected signals resulting from non-linearities in the electric fields. As one example, the technique noted above, of locating the excitation catheter in one heart ventricle and detecting position with an intracardiac electrode in another heart ventricle may reduce non-linearity since, the further away the detection electrode is moved from the excitation electrodes, the lower the voltage gradient and the more linear the electric fields.

As another alternative, the system gain may be set to a relatively high level which ensures that the detection sensitivity is at a minimum desired level, such as on the order of one millimeter, when the detection electrode 38 is positioned at a point of least sensitivity (i.e., midway between a pair of excitation electrodes for a given axis). A suitable system gain can be determined empirically based on the size and shape of the excitation electrodes and characteristics of the patient's heart chambers. With this arrangement, while catheter position can be determined to within a predetermined minimum value, such as one millimeter, when the detection electrode is located at the least sensitive location, midway between a pair of excitation electrodes for a given axis, catheter position is determined with even greater accuracy at locations closer to one of the excitation electrodes.

As a still further alternative technique for compensating for the non-linearity in the gain of the detected signals resulting from electric field non-linearities, the gain of the detection circuitry may be boosted as the catheter approaches positions of least sensitivity (i.e., at or near the midpoint between a pair of excitation electrodes, when the signal processor output approaches null). For example, the output of the signal processor 14 may be monitored for the signal gain

to fall below a predetermined threshold or to a minimum and/or for the signal to approach null. Once one or both of these conditions occurs, the system gain may be boosted. More particularly, the system gain may be boosted by a predetermined amount or, alternatively, may be boosted incrementally or continuously, as the output signal gain falls below the predetermined level and/or approaches null.

System gain in such a system may be boosted in various ways. For example, the gain of one or more amplifiers within the signal processor 14, such as the differential amplifier 200 (Figure 4), may be boosted. Alternatively, the current level of the excitation signals may be boosted.

A further technique for compensating for electric field non-linearities includes the use of an intracardiac catheter 700 supporting twelve electrodes 702 - 724 (collectively 730), as shown in Figure 13. The intracardiac catheter 700 includes a plurality of electrode supporting members 732 coupled together at a distal end 734 of the catheter for supporting the excitation electrodes 730. The catheter 700 further includes a flexible tube 740 covering wire conductors coupled to and extending from the electrodes. The wire conductors terminate at a connector 742 at the proximal end 744 of the catheter for permitting electrical connections to be made to the electrodes 730.

The twelve excitation electrodes 730 establish two X, Y, Z coordinate systems. A first X, Y, Z coordinate system is defined by a pair of X axis electrodes 708, 718, a pair of Y axis electrodes 702, 724, and a pair of Z axis electrodes 712, 714. A second X, Y, Z coordinate system is defined by a pair of X axis electrodes 706, 720, a pair of Y axis electrodes 704, 722 and a pair of Z axis electrodes 710, 716. Each of the pairs of excitation electrodes is coupled to a respective signal processor unit (like signal processor units 50, 52, 54 of Figure 2), as shown in Figure 14.

In use, at any given time, catheter position detection is achieved by applying an excitation signal along each of the three intersecting axes defined by excitation electrodes of a selected one of the coordinate systems and sensing the differential voltage indicative between the detection electrode 38 and each pair of excitation electrodes of the selected, active coordinate system, as described further below. However, when the detection electrode 38 approaches one of the excitation electrodes of the selected coordinate system, the excitation coordinate system may be

switched to the other coordinate system. Such switching may be achieved with a multiplexer arrangement as shown in Figure 14.

Referring to Figure 14, multiplexers 750, 752 and 754 couple the excitation electrodes of the selected one of the X, Y, Z coordinate systems to the X axis processor unit 50 (Figure 2), the Y axis processor unit 52 (Figure 2), and the Z axis processor unit 54 (Figure 2) of the signal processor 14. The multiplexers 750, 752, 754 are synchronized so that when multiplexer 750 couples the X axis electrodes 708, 718 of the first coordinate system to the X axis processor unit 50, multiplexer 752 couples Y axis electrodes 702, 724 of the first coordinate system to the Y axis processor unit 52 and multiplexer 754 couples Z axis electrodes 712, 714 of the first coordinate system to the Z axis processor unit 54. Conversely, when multiplexer 750 couples the X axis electrodes 706, 720 of the second coordinate system to the X axis processor unit 50, multiplexer 752 couples Y axis electrodes 704, 722 of the second coordinate system to the Y axis processor unit 52 and multiplexer 754 couples Z axis electrodes 710, 716 of the second coordinate system to the Z axis processor unit 54.

The multiplexers 750, 752, 754 are responsive to a control circuit 770, such as may be provided by a microprocessor, for coupling excitation electrodes from a selected one of the coordinate systems to the signal processor 14. More particularly, the control circuit 770 provides control signals 760, 762, 764 to the multiplexers 750, 752, 754, respectively, to cause the multiplexers to switch between one excitation coordinate system and the other when the detection electrode approaches one of the excitation electrodes of the active coordinate system (i.e., when the system output signal is furthest from null).

In one embodiment, control circuit 770 signals multiplexers 750, 752, 754 to switch to an alternate coordinate system when the detection electrode is within one quarter of the axial distance from one of a pair of active excitation electrodes defining a given axis. This may be accomplished by providing a threshold reference signal corresponding to one quarter of the distance along a given axis from each excitation electrode defining that axis. When the voltage difference measured at the detection electrode crosses the threshold reference value in a direction toward an excitation electrode, the alternate coordinate system is used.

Threshold reference signals may be provided by applying resistor dividers such as, and in the same location as, resistor divider 125 (Figure 3). By applying resistor dividers having one quarter values (such as one divider having 50K and 150K ohm resistors and a second divider

having 150K and 50K resistors) between the same signals as resistor divider 125 , threshold reference signals having the desired values may be provided and coupled to control circuit 770. While the values provided in this exemplary embodiment will serve to keep the catheter positioning systems described herein in a generally linear operating region, a person of ordinary skill in the art will recognize that other threshold signals may be used consistent with the invention.

It will be appreciated by those of ordinary skill in the art that the benefits achieved with the twelve excitation electrode embodiment of Figure 13 may likewise be achieved with as few as eight electrodes, when using the "common" electrode technique discussed in conjunction with Figures 10 and 11. It will be further appreciated that more than the two coordinate systems provided by twelve electrodes may be used. For example, an additional six electrodes would provide a third X, Y, Z coordinate system for use in the manner described above.

The above-described techniques which compensate for electric field non-linearities and which render the intracardiac excitation electrode embodiments well suited for absolute catheter distance determination, are useful in transmyocardial revascularization /percutaneous myocardial revascularization (TMR/PMR) applications. In TMR/PMR applications, it is beneficial to precisely detect the distance between a border of a lesion and a location to form a channel to permit blood flow to a recoverable region surrounding the lesion. The lesion border is generally located using fluoroscopic techniques. With the improved linearity resulting from the techniques described herein, the catheter positioning system may be able to mimic the shape of the lesion border provided by fluoroscopic techniques. Multiple points on the border may then be recorded and channel formation locations spaced by a predetermined distance from the lesion border can be located using the catheter positioning techniques described herein.

Embodiments utilizing eight or more excitation electrodes (i.e., two or more X, Y, Z coordinate systems) provide an additional advantage of permitting a cardiac chamber to be outlined quickly. Such an outline may be obtained by designating the electrodes of one of the coordinate systems to be the excitation electrodes and the electrodes of the other coordinate system to be the detection, or mapping electrodes. The designations of the electrodes as "excitation" or "detection" can then be swapped, resulting in twelve data points which may be used to generate a graphical image of the cardiac chamber.

The use of intracardiac excitation electrodes provides several advantages as compared to surface excitation electrodes. First, a higher signal to noise ratio is generally achieved since greater signal magnitudes (assuming the same signal source) flow through the region of interest due to the position of the excitation electrodes within the region of interest. Further, inaccuracies due to the impedance between the surface electrodes and the skin, as well as inaccuracies due to inadvertent movement of the surface electrodes, are eliminated. Additionally, the catheter supporting the excitation electrodes may serve additional purposes. For example, the excitation electrodes themselves may perform cardiac sensing functions, such as ECG sensing. Further, the excitation electrodes and/or other electrodes (not shown) supported by the same catheter may perform cardiac pacing and/or ablation functions.

It will be appreciated by those of ordinary skill in the art that the apparatus and techniques described herein may be used to detect the position of multiple detection electrodes which may be supported by a single catheter or, alternatively, may be supported by separate catheters. The signal processor of a multiple detection electrode system may comprise additional processor units (like processor units 50, 52, and 54 shown in Figure 2) for each additional detection electrode. Alternatively, the signal processor units 50, 52 and 54 may be multiplexed to detect the position of the multiple detection electrodes. In addition to detection of the position of the multiple detection electrodes, this arrangement advantageously permits the direction of the electrodes to be determined. One application for such a system is atrial fibrillation, in which an elongated continuous lesion is created.

In general, the catheter positioning techniques of the present invention require, at a minimum, three excitation signals to be applied in three intersecting (i.e., non-parallel) planes. While some of the above-disclosed embodiments utilize excitation signals in mutually orthogonal planes (i.e., along three mutually orthogonal axes), the excitation signals may be applied in three orthogonal or non-orthogonal planes, such as planes separated by between 30-90 degrees. In catheter repositioning applications, perhaps the most robust applications of the system of the invention, axis orthogonality is of less concern than in absolute positioning applications. The ability to use non-orthogonal excitation signals reduces the need to precisely place surface excitation electrodes or to rely on precise geometries of an intracardiac excitation catheter.

The use of non-orthogonal excitation signals reduces signal gain somewhat. In some applications, it may be desirable to compensate for such gain reduction. One way to compensate for the gain reduction associated with non-orthogonal excitation signals is to mathematically correct for the non-orthogonality of the AC signals. However, this technique is possible only if the angles between the three excitation axes are known. In applications using eight or more intracardiac excitation electrodes which define at least two X, Y, Z coordinate systems, gain reduction can be compensated, at least in part, by selecting the excitation coordinate system which comes closest to providing orthogonal excitation signals. In practice, exact determinations of the angles between the three excitation axes are difficult, but measurement of angles may be aided by the application of fluoroscopic techniques or by using alternate X, Y, Z coordinate systems to locate the excitation electrodes of the other coordinate system.

It will be appreciated by those of ordinary skill in the art that the techniques described herein may be practiced with the use of various excitation electrode types and configurations. For example, it will be apparent to those of ordinary skill in the art, that multiple intracardiac catheters, each supporting less than all of excitation electrodes for the particular application, or a combination of intracardiac and surface excitation electrodes, may be used to establish three excitation signals in three intersecting planes.

The foregoing description of the illustrative embodiments of the invention is presented to indicate the range of constructions to which the invention applies. Variations in the invention will be apparent to those having ordinary skill in the art based upon the disclosure herein, and such variations are considered to be within the scope of the invention in which patent rights are asserted, as set forth in the claims appended hereto. All publications and references cited herein are expressly incorporated herein by reference in their entirety.

What is claimed is:

CLAIMS

1. An apparatus for detecting a position of a catheter in contact with a patient, said position characterized by an X coordinate relative to an X axis, a Y coordinate relative to a Y axis, and a Z coordinate relative to a Z axis, comprising:

a detection electrode disposed on the catheter;

an X axis excitation electrode;

a Y axis excitation electrode;

a Z axis excitation electrode;

a common excitation electrode;

a signal generator adapted for applying a first excitation signal between the X axis excitation electrode and the common electrode, a second excitation between the Y axis excitation electrode and the common electrode, and a third excitation signal between the Z axis excitation electrode and the common electrode; and

a signal processor for measuring the differential voltage indicative of impedance between the detection electrode and X axis excitation electrode and the common electrode in order to determine the X coordinate, the differential voltage indicative of impedance between the detection electrode and the Y axis excitation electrode and the common electrode in order to determine the Y coordinate, and the differential voltage indicative of impedance between the detection electrode and the Z axis excitation electrode and the common electrode in order to determine the Z coordinate.

2. The apparatus of claim 1 wherein the X axis excitation electrode, the Y axis excitation electrode, the Z axis excitation electrode, and the common electrode are surface electrodes for external attachment to the patient.

3. The apparatus of claim 1 wherein the X axis excitation electrode, the Y axis excitation electrode, the Z axis excitation electrode, and the common electrode are subcutaneous electrodes for insertion into the patient.

4. The apparatus of claim 1 wherein the X axis excitation electrode, the Y axis excitation electrode, the Z axis excitation electrode, and the common electrode are intracardiac electrodes for insertion into the cardiac regions of the patient.

5. The apparatus of claim 1 wherein the first excitation signal has a first frequency, the second excitation signal has a second frequency, and the third excitation signal has a third frequency.

6. A method for detecting a position of a catheter in contact with a patient, said position characterized by an X coordinate relative to an X axis, a Y coordinate relative to a Y axis, and a Z coordinate relative to a Z axis, comprising the steps of:

applying a first excitation signal generating a first electric field between an X axis excitation electrode and a common electrode disposed along the X axis;

applying a second excitation signal generating a second electric field between a Y axis excitation electrode and the common electrode disposed along the Y axis;

applying a third excitation signal generating a third electric field between a Z axis excitation electrode and the common electrode disposed along the Z axis;

locating a detection electrode within the first, second, and third electric fields; and

measuring the differential voltage between the detection electrode and the X axis excitation electrode and the common electrode to determine the X coordinate, measuring the differential voltage between the detection electrode and the Y axis excitation electrode and the common electrode to determine the Y coordinate, and measuring the differential voltage between the detection electrode and the Z axis excitation electrode and the common electrode to determine the Z coordinate.

7. The method of claim 6 further comprising the step of providing the X axis excitation electrode, the Y axis excitation electrode, the Z axis excitation electrode, and the common electrode as surface electrodes for external attachment to the patient.

8. The method of claim 6 further comprising the step of providing the X axis excitation electrode, the Y axis excitation electrode, the Z axis excitation electrode, and the common electrode as subcutaneous electrodes for insertion into the patient.

9. The method of claim 6 further comprising the step of providing the X axis excitation electrode, the Y axis excitation electrode, the Z axis excitation electrode, and the common electrode as intracardiac electrodes for insertion into the cardiac regions of the patient.

10. The method of claim 6 wherein the first excitation signal applying step comprises providing the first excitation signal with a first frequency, the second excitation signal providing step comprises providing the second excitation signal with a second frequency, and the third excitation signal providing step comprises providing the third excitation signal with a third frequency.

11. An apparatus for detecting a position of a catheter in contact with a patient, said position characterized by an X coordinate relative to an X axis, a Y coordinate relative to a Y axis, and a Z coordinate relative to a Z axis, comprising:

a detection electrode disposed on the catheter;

a pair of X axis intracardiac excitation electrodes disposed along the X axis;

a pair of Y axis intracardiac excitation electrodes disposed along the Y axis;

a pair of Z axis intracardiac excitation electrodes disposed along the Z axis; and

a signal processor for measuring the differential voltage indicative of impedance between the detection electrode and each electrode of the pair of X axis intracardiac excitation electrodes in order to determine the X coordinate, the differential voltage indicative of impedance between the detection electrode and each electrode of the pair of Y axis intracardiac excitation electrodes in order to determine the Y coordinate, and the differential voltage indicative of impedance between the detection electrode and each electrode of the pair of Z axis intracardiac excitation electrodes in order to determine the Z coordinate.

12. The apparatus of claim 11 wherein each of the first, second and third pairs of intracardiac excitation electrodes shares a common electrode.

13. The apparatus of claim 11 further comprising:

a second pair of X axis intracardiac excitation electrodes disposed along a second X axis;

a second pair of Y axis intracardiac excitation electrodes disposed along a second Y axis; and

a second pair of Z axis intracardiac excitation electrodes disposed along a second Z axis.

14. The apparatus of claim 13 wherein the signal processor is adapted for being selectively coupled to either the first pair of X axis electrodes, the first pair of Y axis electrodes, and the first pair of Z axis electrodes or to the second pair of X axis electrodes, the second pair of Y axis electrodes, and the second pair of Z axis electrodes.

15. A method for detecting a position of a catheter in contact with a patient, said position characterized by an X coordinate relative to an X axis, a Y coordinate relative to a Y axis and a Z coordinate relative to a Z axis, comprising the steps of:

positioning a detection electrode on the catheter;

positioning a pair of X axis intracardiac excitation electrodes along the X axis;

applying a first excitation signal between the X axis intracardiac excitation electrodes;

positioning a pair of Y axis intracardiac excitation electrodes along the Y axis;

applying a second excitation signal between the Y axis intracardiac excitation electrodes;

positioning a pair of Z axis intracardiac excitation electrodes along the Z axis;

applying a third excitation signal between the Z axis intracardiac excitation electrodes;

measuring the differential voltage indicative of impedance between the detection electrode and each electrode of the X axis intracardiac excitation electrodes in order to determine the X coordinate;

measuring the differential voltage indicative of impedance between the detection electrode and each electrode of the Y axis intracardiac excitation electrodes in order to determine the Y coordinate; and

measuring the differential voltage indicative of impedance between the detection electrode and each electrode of the Z axis intracardiac excitation electrodes in order to determine the Z coordinate.

16. The method of claim 15 further comprising the step of providing one of each of the X axis intracardiac excitation electrodes, the Y axis intracardiac excitation electrodes, and the Z axis intracardiac excitation electrodes as a common electrode.

17. The method of claim 15 further comprising the steps of:

positioning a second pair of X axis intracardiac excitation electrodes along a second X axis;

positioning a second pair of Y axis intracardiac excitation electrodes along a second Y axis; and

positioning a second pair of Z axis intracardiac excitation electrodes along a second Z axis.

18. The method of claim 17 further comprising the steps of:

measuring the differential voltage indicative of impedance between the detection electrode and each electrode of the second pair of X axis intracardiac excitation electrodes in order to determine the X coordinate;

measuring the differential voltage indicative of impedance between the detection electrode and each electrode of the second pair of Y axis intracardiac excitation electrodes in order to determine the Y coordinate; and

measuring the differential voltage indicative of impedance between the detection electrode and each electrode of the second pair of Z axis intracardiac excitation electrodes in order to determine the Z coordinate.

19. A method for detecting a position of a catheter in contact with a patient, said position characterized by an X coordinate relative to an X axis, a Y coordinate relative to a Y axis and a Z coordinate relative to a Z axis, comprising the steps of:

positioning a detection electrode on the catheter;

positioning a pair of X axis excitation electrodes along the X axis;

applying a first excitation signal between the X axis excitation electrodes;

positioning a pair of Y axis excitation electrodes along the Y axis;

applying a second excitation signal between the Y axis excitation electrodes;

positioning a pair of Z axis excitation electrodes along the Z axis;

applying a third excitation signal between the Z axis excitation electrodes;

determining the X coordinate by measuring a first voltage between the detection electrode and a first electrode of the pair of X axis excitation electrodes, measuring a second voltage between the detection electrode and a second electrode of the pair of X axis excitation electrodes and determining the difference between the first and second measured voltages;

determining the Y coordinate by measuring a third voltage between the detection electrode and a first electrode of the pair of Y axis excitation electrodes, measuring a fourth voltage between the detection electrode and a second electrode of the pair of Y axis excitation electrodes and determining the difference between the third and fourth measured voltages; and

determining the Z coordinate by measuring a fifth voltage between the detection electrode and a first electrode of the pair of Z axis excitation electrodes, measuring a sixth voltage between the detection electrode and a second electrode of the pair of Z axis excitation electrodes and determining the difference between the fifth and sixth measured voltages.

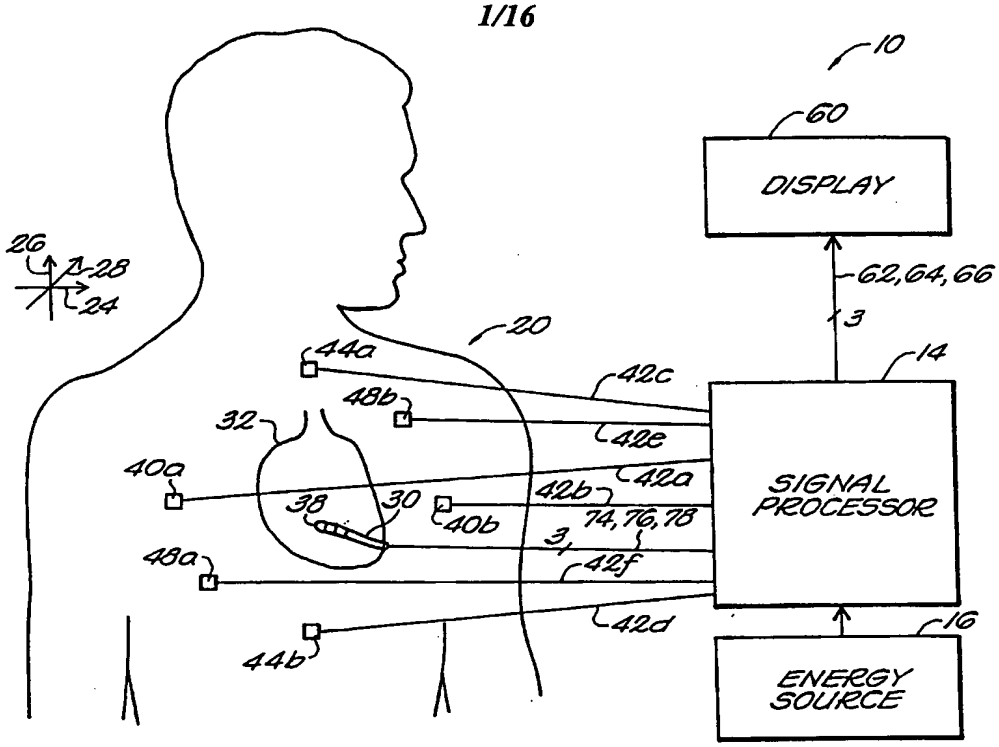
10
60
DISPLAY
62,64,66
3
14
SIGNAL PROCESSOR
16
ENERGY SOURCE
26
28
24
20
44a
42c
48b
42e
32
40a
42a
42b
38
30
40b
74,76,78
3'
48a
42f
42d
44b

FIG. 1

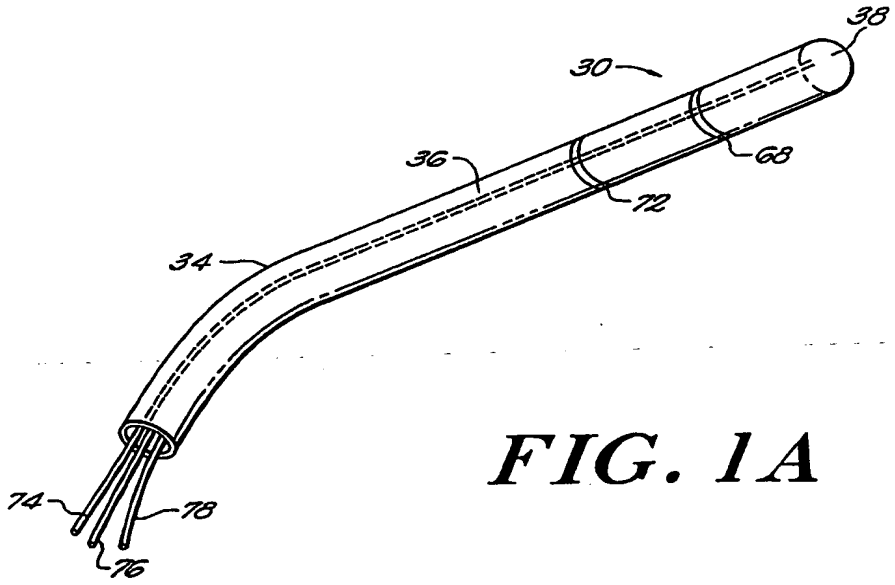
38
30
36
68
72
34
74
78
76

FIG. 1A

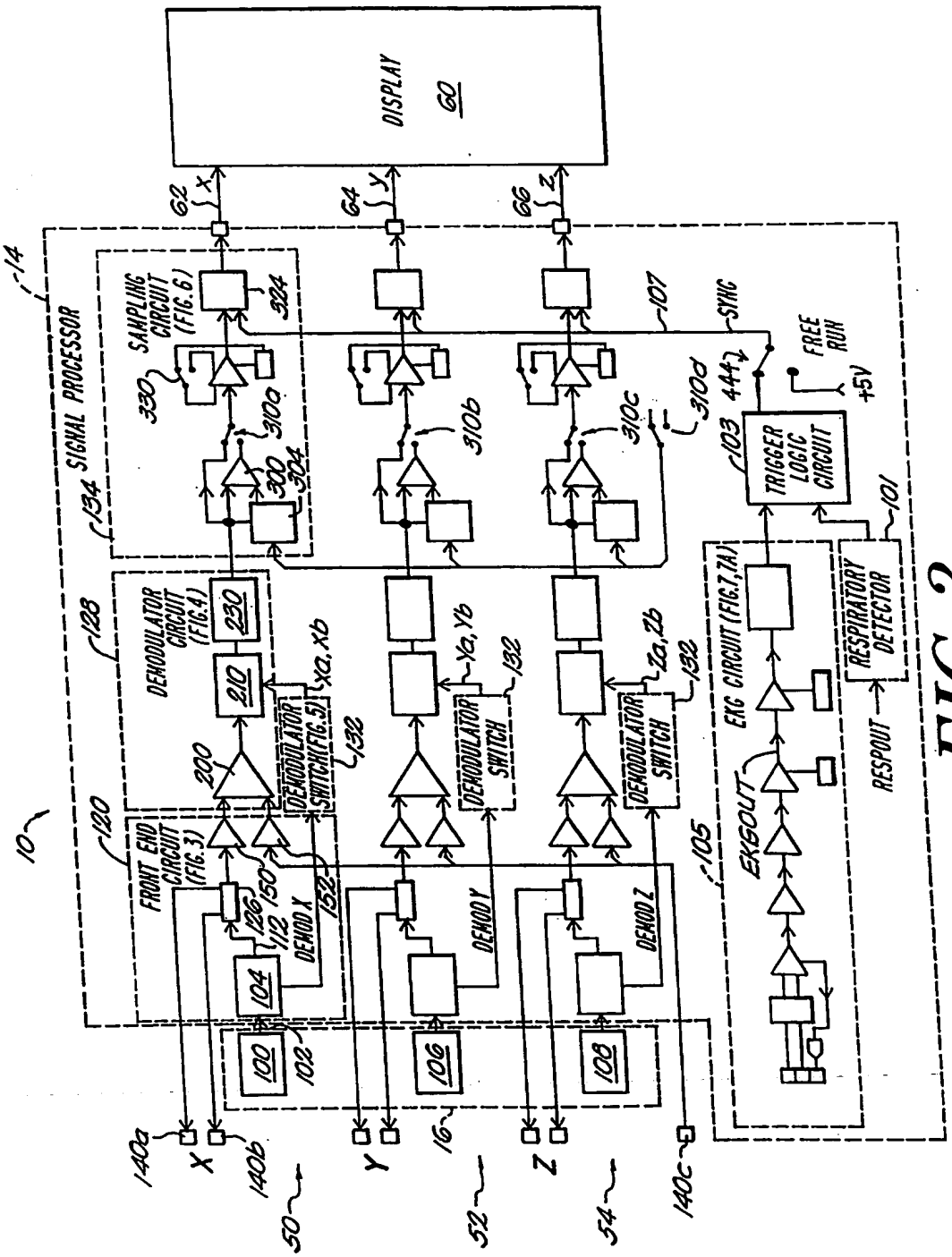
DISPLAY
60
62 X
64 Y
66 Z
14
SIGNAL PROCESSOR
SAMPLING CIRCUIT (FIG. 6)
324
330
300
304
310a
310b
310c
310d
444
107
SYNC
FREE RUN
+5V
103
TRIGGER LOGIC CIRCUIT
101
RESPIRATORY DETECTOR
RESPOUT
DEMODULATOR CIRCUIT (FIG. 4)
230
210
200
DEMODULATOR SWITCH (FIG. 5)
138
Xa, Xb
Ya, Yb
Za, Zb
132
DEMODULATOR SWITCH
DEMODULATOR SWITCH
128
FRONT END CIRCUIT (FIG. 3)
120
EKG CIRCUIT (FIG. 7, 7A)
105
EKGOUT
10
126
112
150
152
DEMOD X
DEMOD Y
DEMOD Z
104
106
108
100
102
140a
X
140b
50
Y
16
52
Z
54
140c

FIG. 2

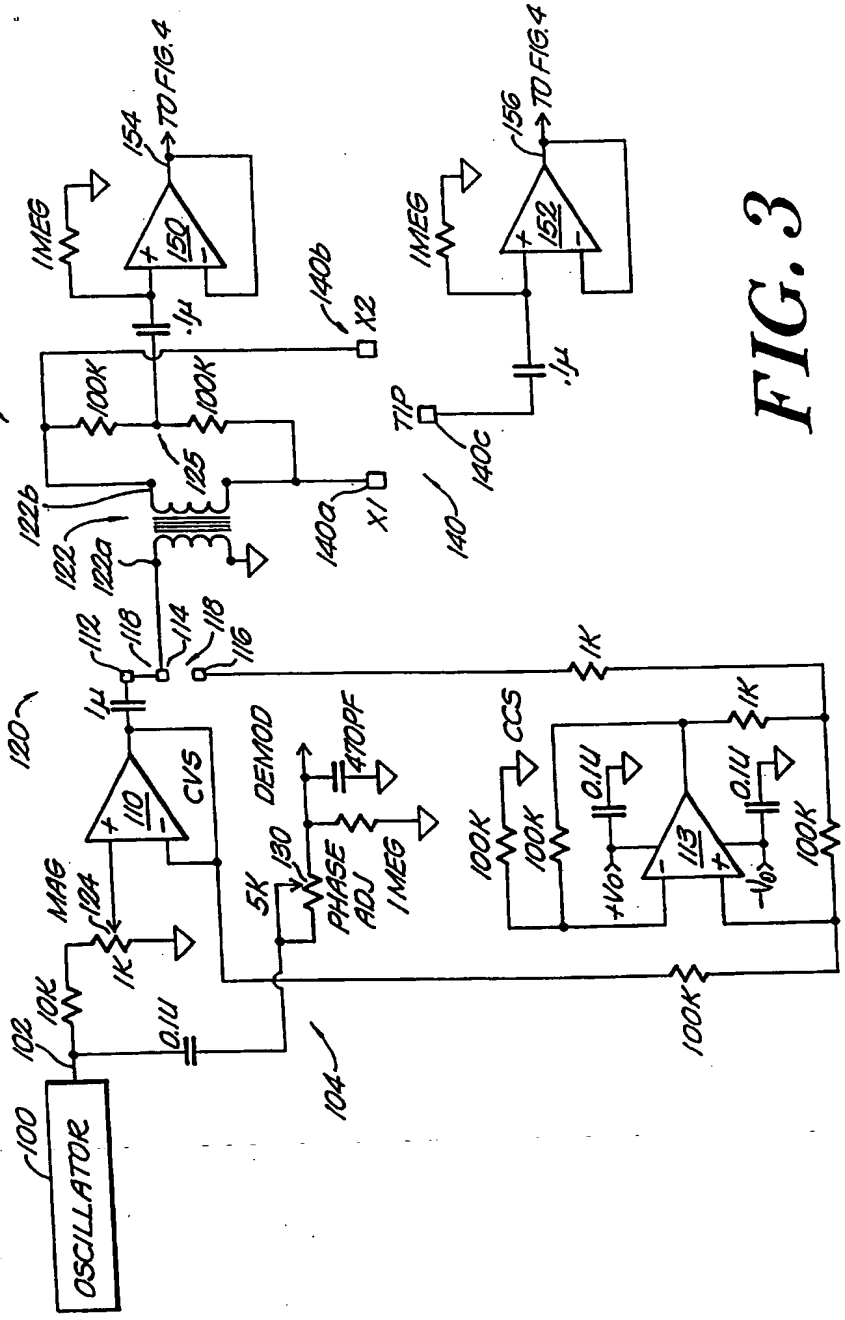
OSCILLATOR
100
102
10K
0.1U
104
MAG
124
1K
5K
130
PHASE ADJ
1MEG
DEMOD
470PF
CVS
110
120
1U
112
118
114
118
116
122
122a
122b
125
126
100K
100K
1MEG
150
154
TO FIG. 4
.1U
140b
X2
140a
X1
TIP
140c
140
1MEG
152
156
TO FIG. 4
.1U
1K
CCS
100K
100K
0.1U
+Vo1
113
0.1U
-Vo1
1K
100K
100K

FIG. 3

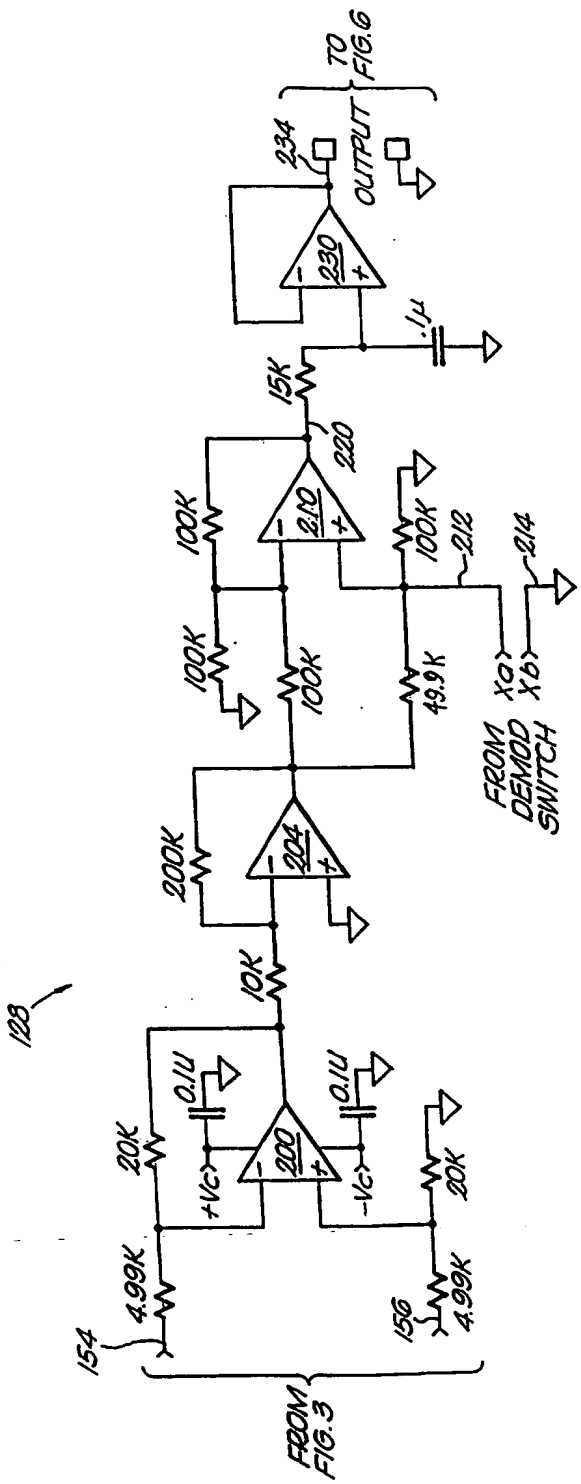
TO FIG.6
234
OUTPUT
230
.1μ
15K
220
100K
210
100K
212
214
100K
100K
49.9K
X0
X6
FROM DEMOD SWITCH
200K
204
10K
128
0.1μ
0.1μ
20K
200
20K
+Vc
-Vc
4.99K
4.99K
154
156
FROM FIG.3

FIG. 4

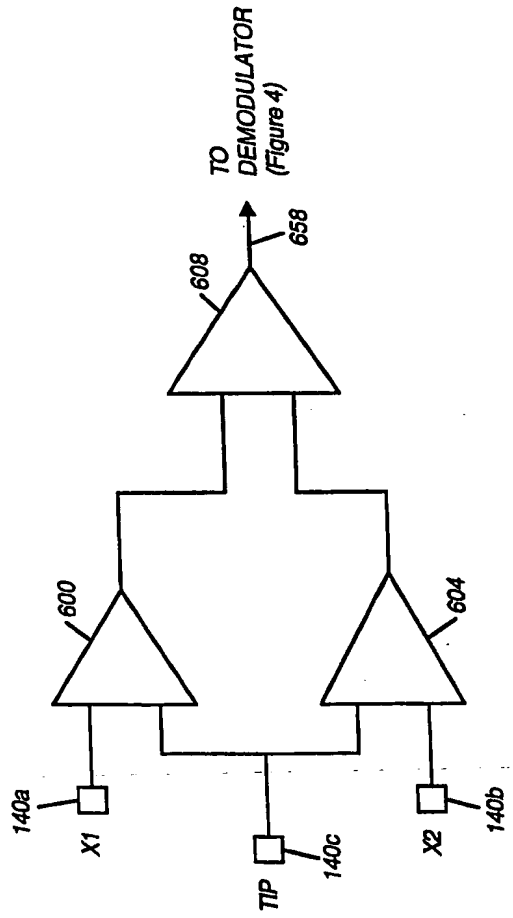
TO DEMODULATOR (Figure 4)
658
608
600
604
140a
X1
TIP
140c
X2
140b

FIG. 4A

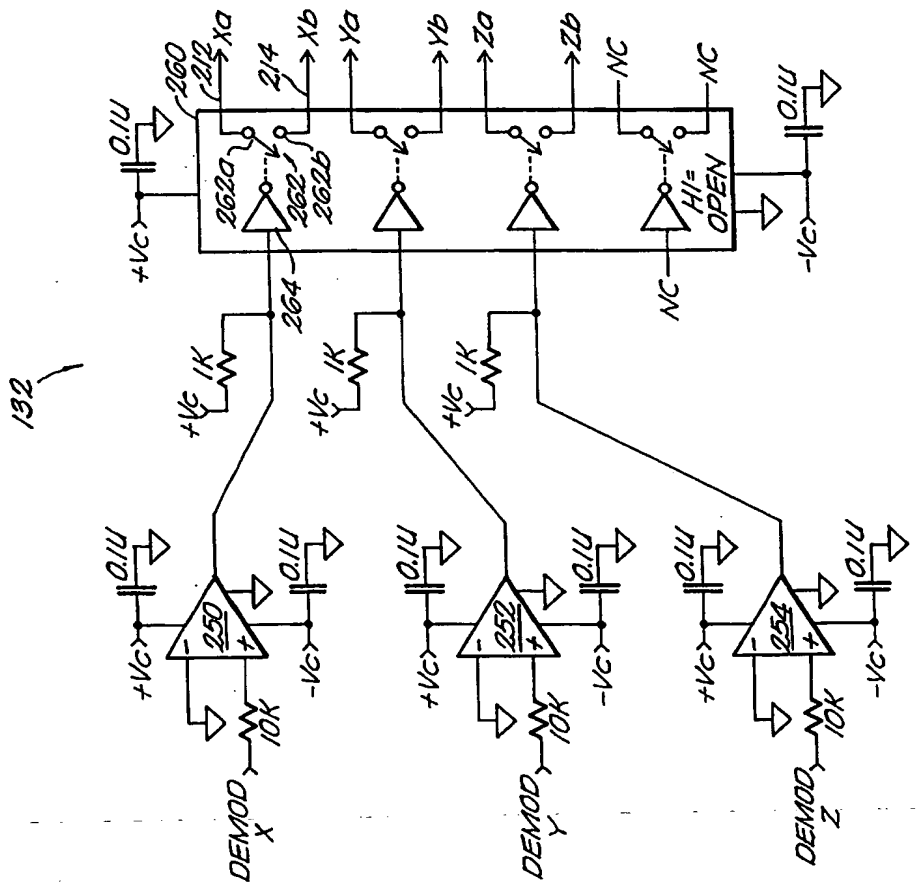
132
260
212
Xa
214
Xb
Ya
Yb
Za
Zb
NC
NC
0.1U
+Vc
262a
262
262b
HI=
OPEN
-Vc
264
NC
1K
+Vc
250
252
254
10K
DEMOD
X
Y
Z

FIG. 5

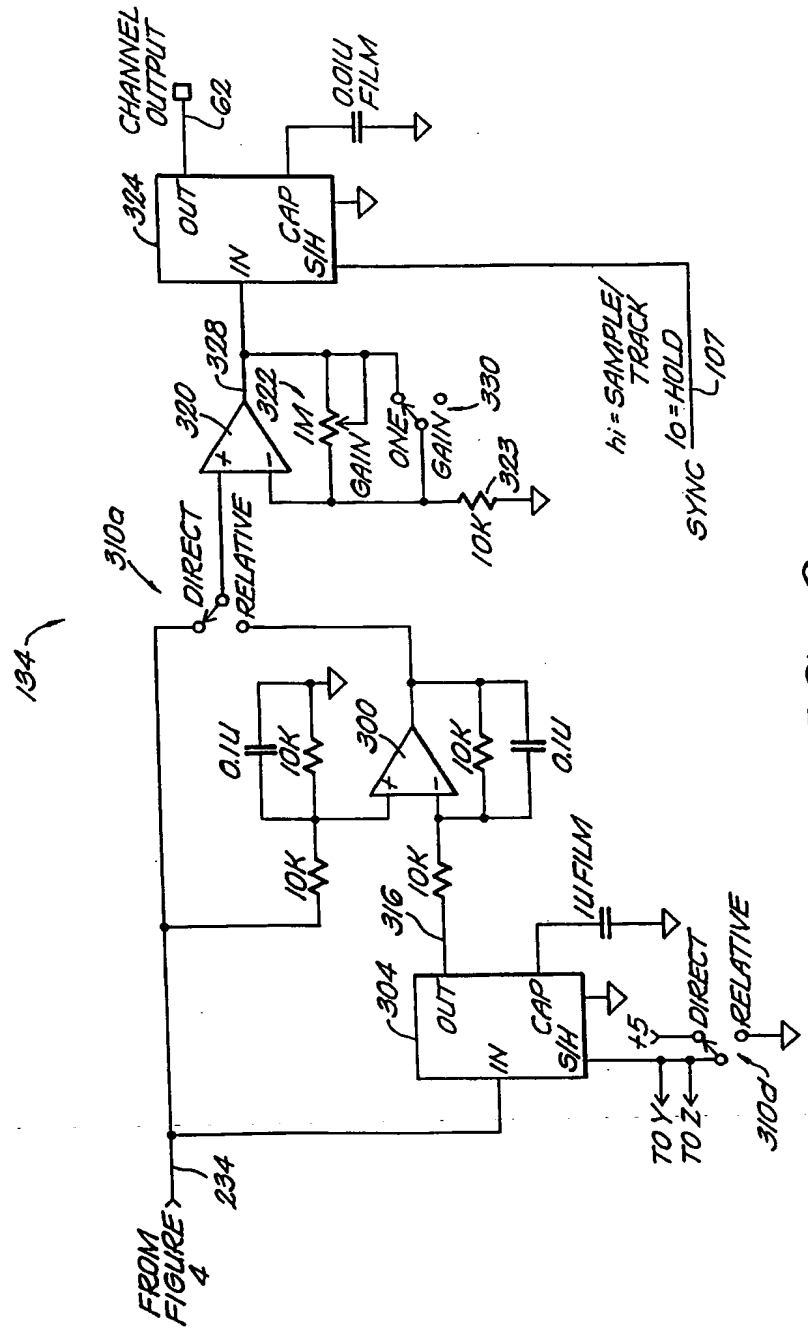
CHANNEL OUTPUT
62
0.01U FILM
324
OUT
IN
CAP S/H
328
322
330
1M
GAIN
ONE
GAIN
323
10K
hi = SAMPLE/TRACK
lo = HOLD
SYNC
107
310a
DIRECT
RELATIVE
134
0.1U
10K
300
10K
0.1U
10K
316
10K
1U FILM
304
OUT
IN
CAP S/H
+5
DIRECT
RELATIVE
TO Y
TO Z
310d
FROM FIGURE 4
234

FIG. 6

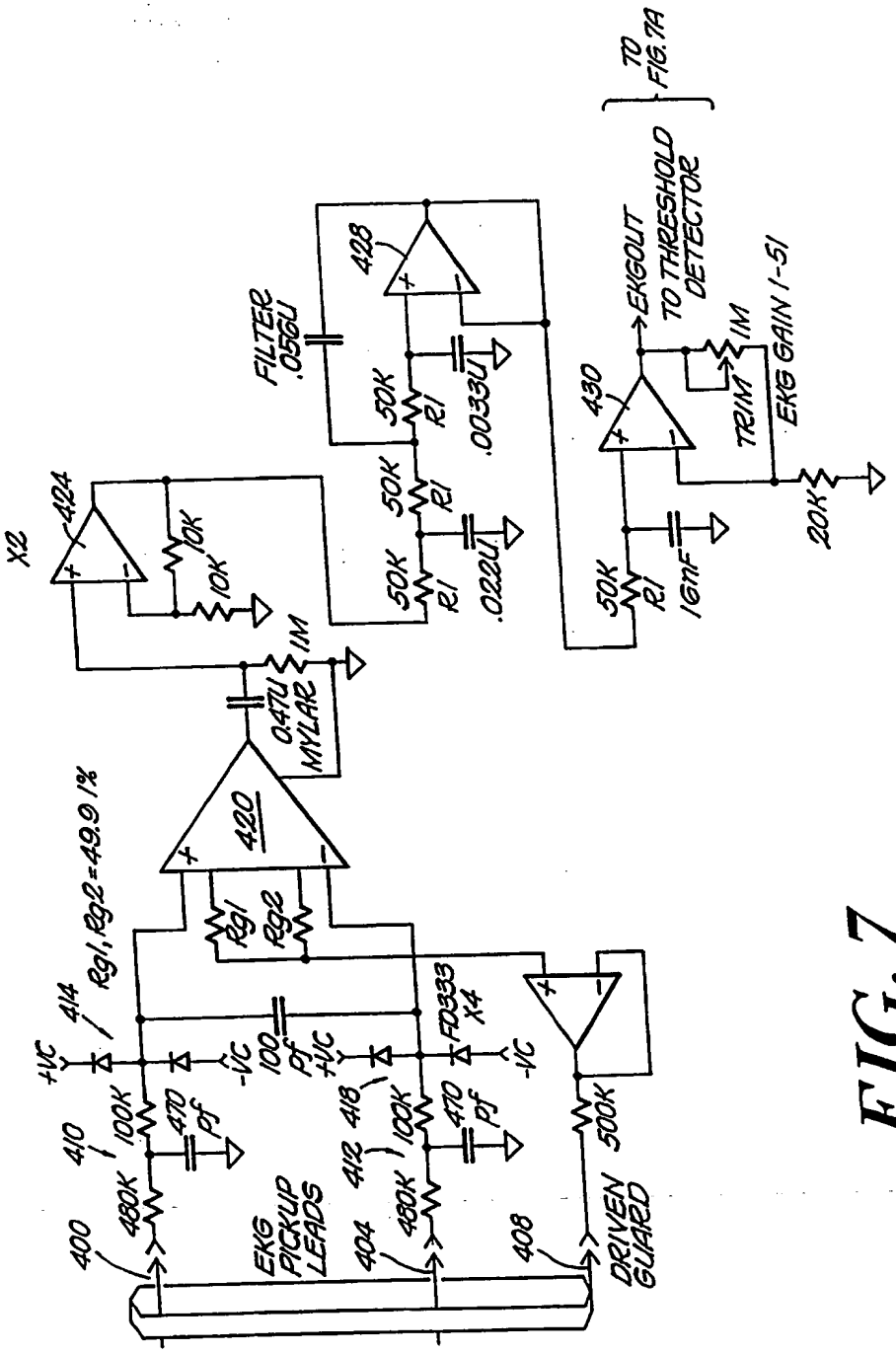
400
EKG PICKUP LEADS
404
408
DRIVEN GUARD
410
412
414
480K
100K
470 pf
+VC
-VC
100 pf
FD333 X4
500K
Rg1, Rg2=49.9 1%
420
Rg1
Rg2
.047U MYLAR
1M
X2
424
10K
10K
FILTER .056U
428
50K
21
.0033U
50K
21
.022U
50K
21
430
16nF
EKGOUT
TO THRESHOLD DETECTOR
TRIM 1M
EKG GAIN 1-51
20K
TO FIG. 7A

FIG. 7

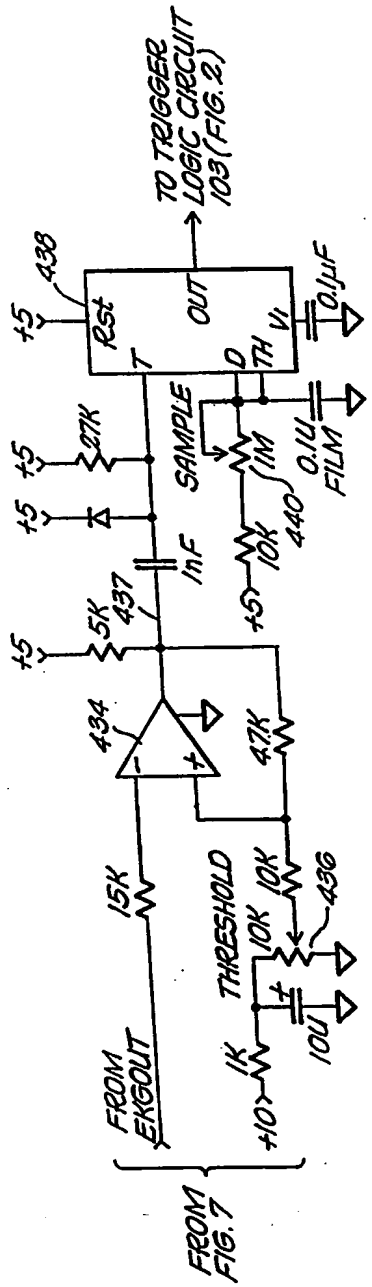
TO TRIGGER LOGIC CIRCUIT 103 (FIG. 2)
438
+5
Rst
OUT
0.1μF
T
D
TH
Vi
SAMPLE
27K
1M
0.1U FILM
440
10K
1nF
5K
437
47K
434
15K
THRESHOLD
10K
436
1K
10U
FROM EKGOUT
FROM FIG. 7

FIG. 7A

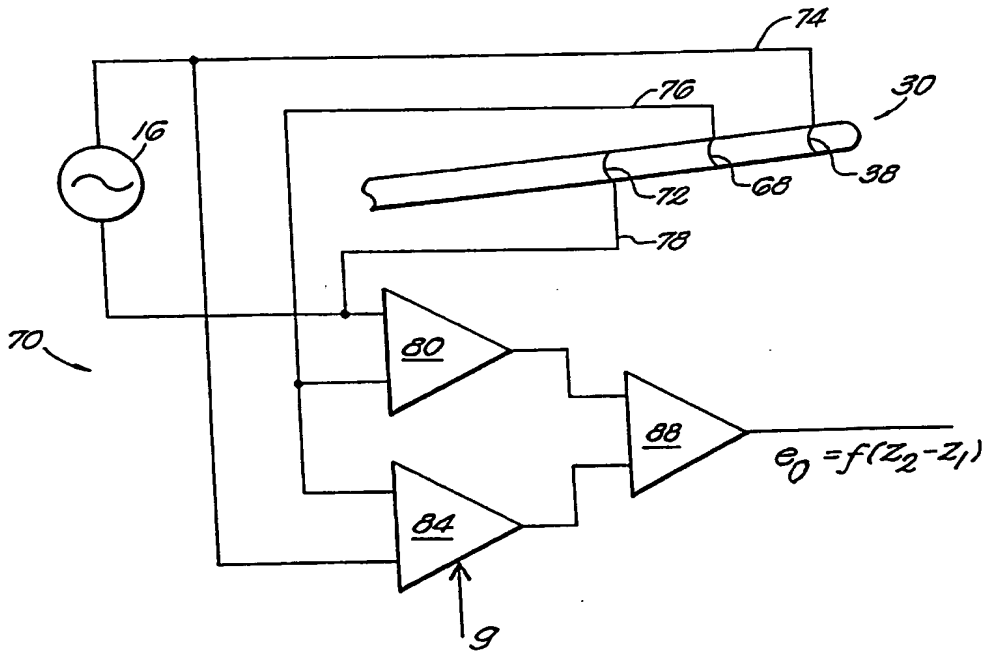

FIG. 8

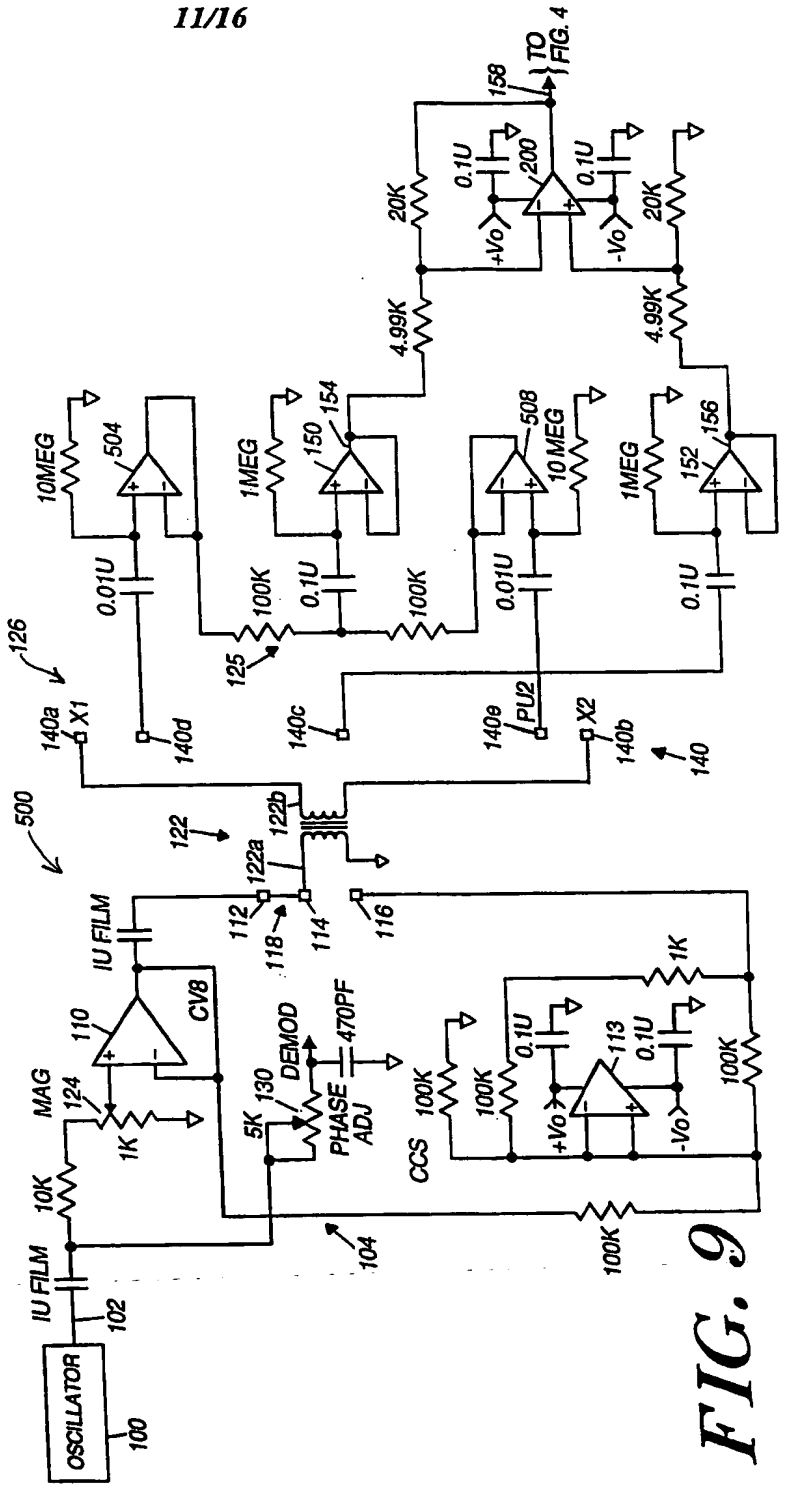
TO FIG. 4
158
20K
0.1U
200
+Vo
-Vo
4.99K
10MEG
504
1MEG
150
154
508
10 MEG
152
156
0.01U
100K
0.1U
125
126
140a
X1
140d
140c
140e
PU2
X2
140b
140
500
122
122b
122a
112
118
114
116
IU FILM
CV8
110
MAG
124
1K
10K
5K
130
DEMOD
PHASE ADJ
470PF
CCS
113
OSCILLATOR
100
102
104

FIG. 9

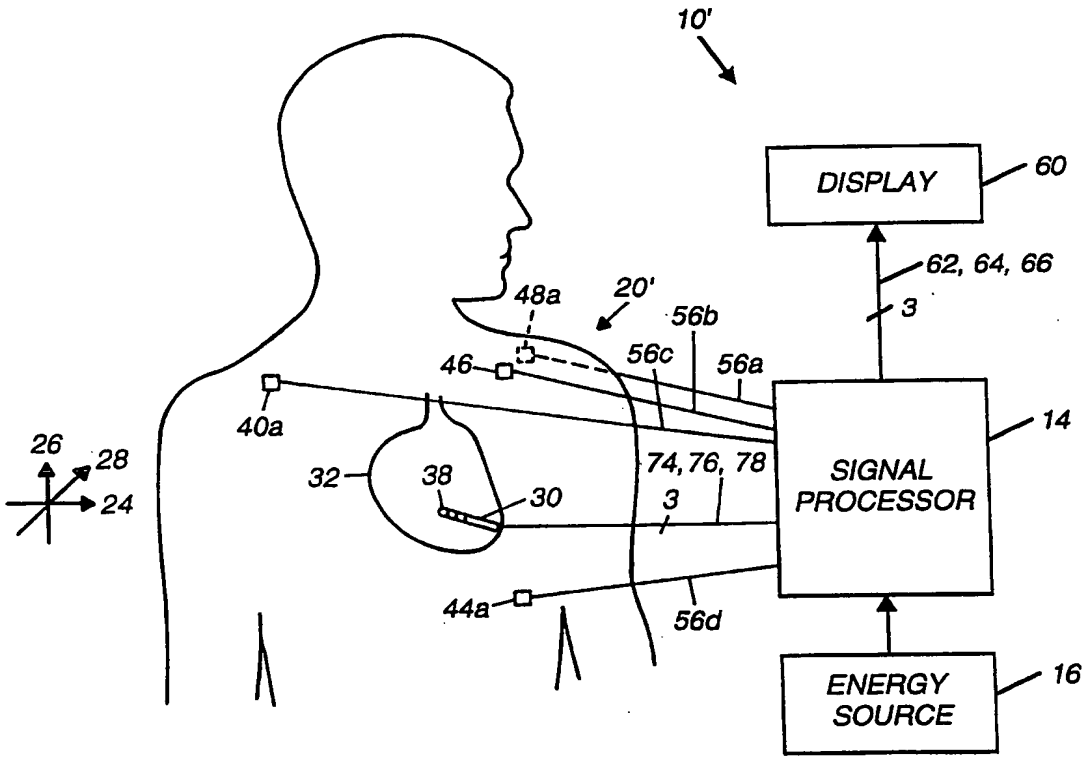
10'
DISPLAY
60
62, 64, 66
3
48a
20'
56b
56c
56a
46
40a
14
SIGNAL PROCESSOR
74, 76, 78
3
26
28
24
32
38
30
44a
56d
ENERGY SOURCE
16

FIG. 10

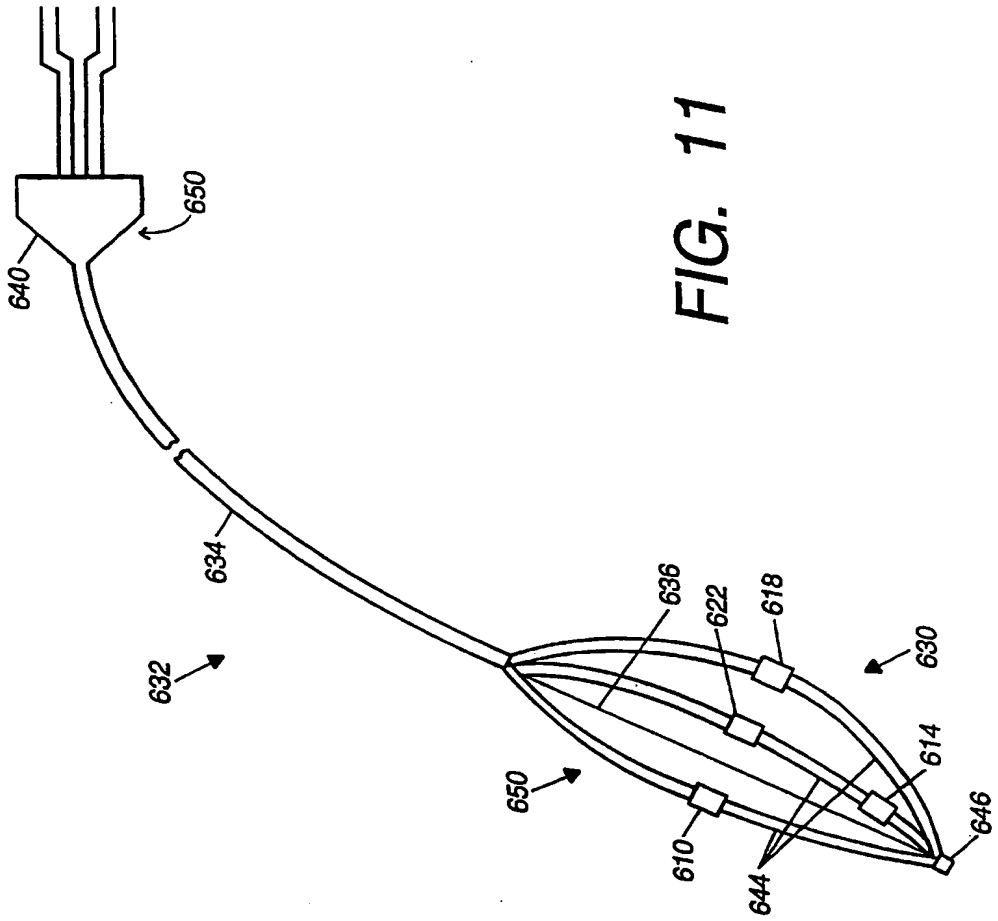

FIG. 11

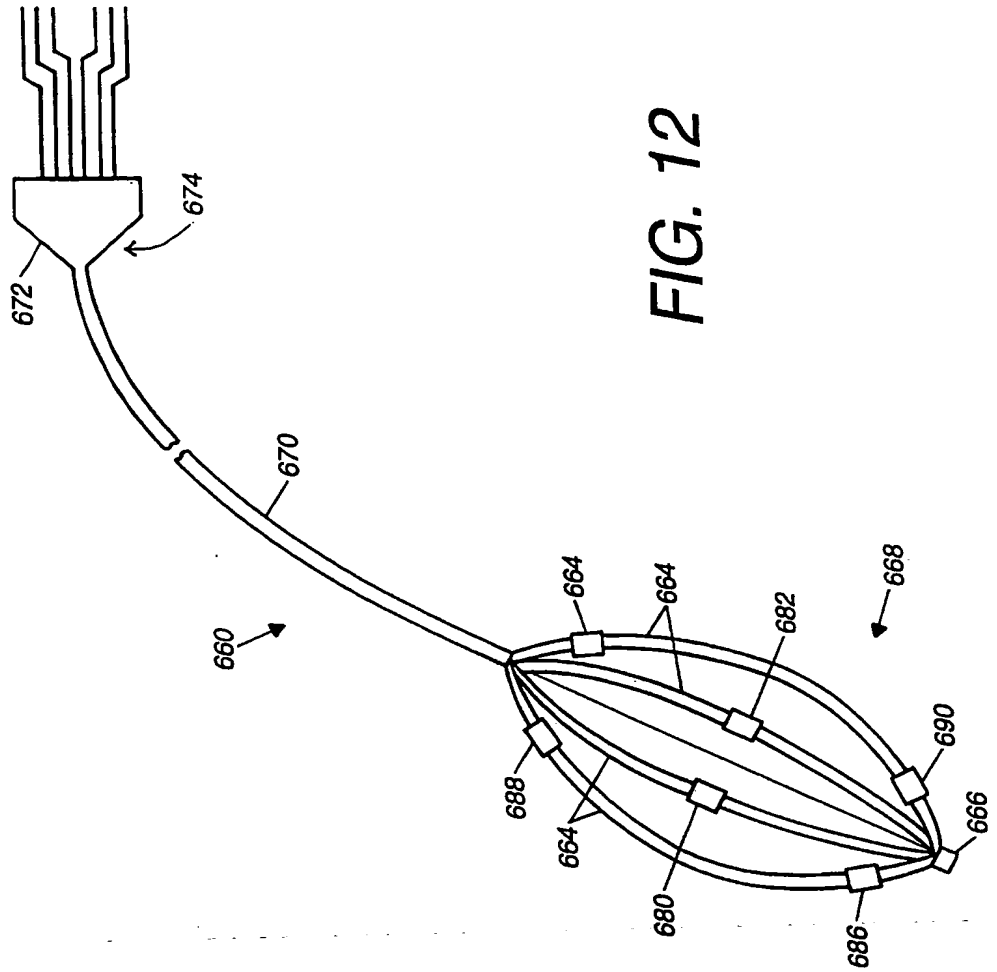

FIG. 12

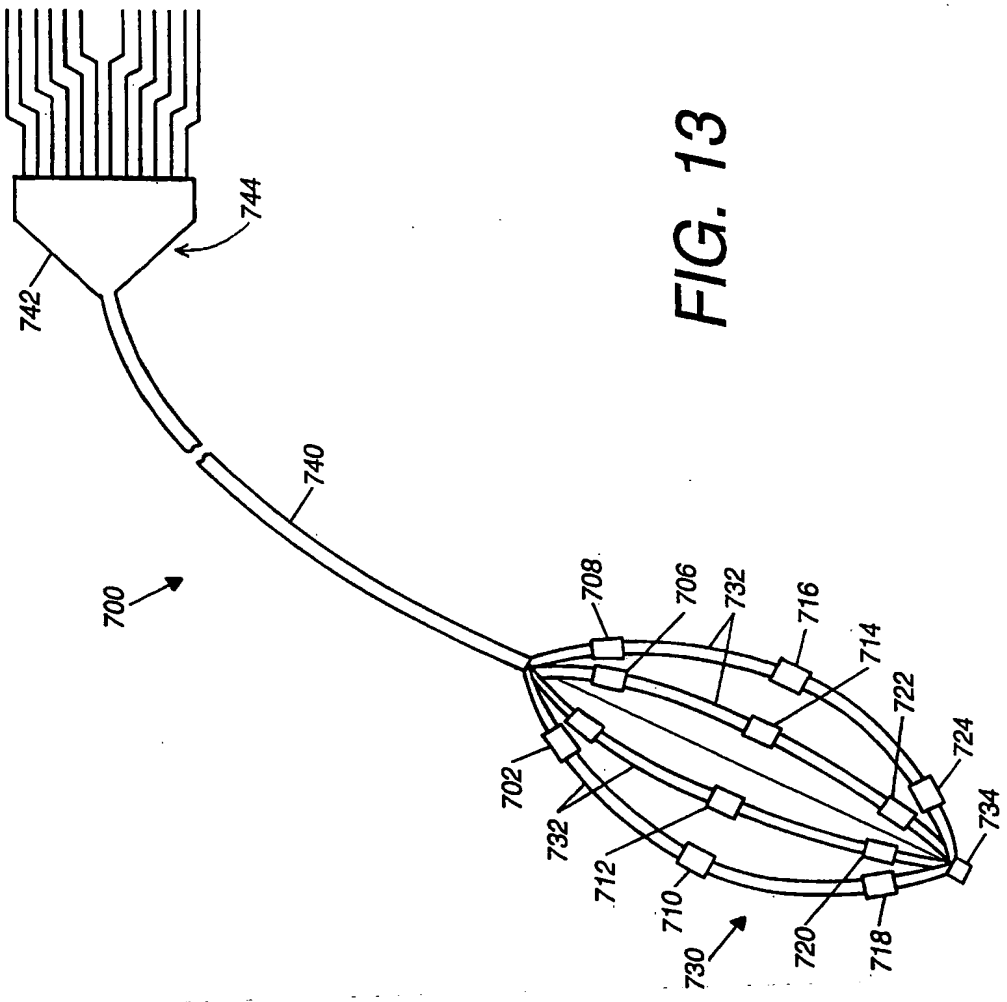
744
742
740
700
708
706
732
716
714
722
724
734
702
732
712
710
730
720
718

FIG. 13

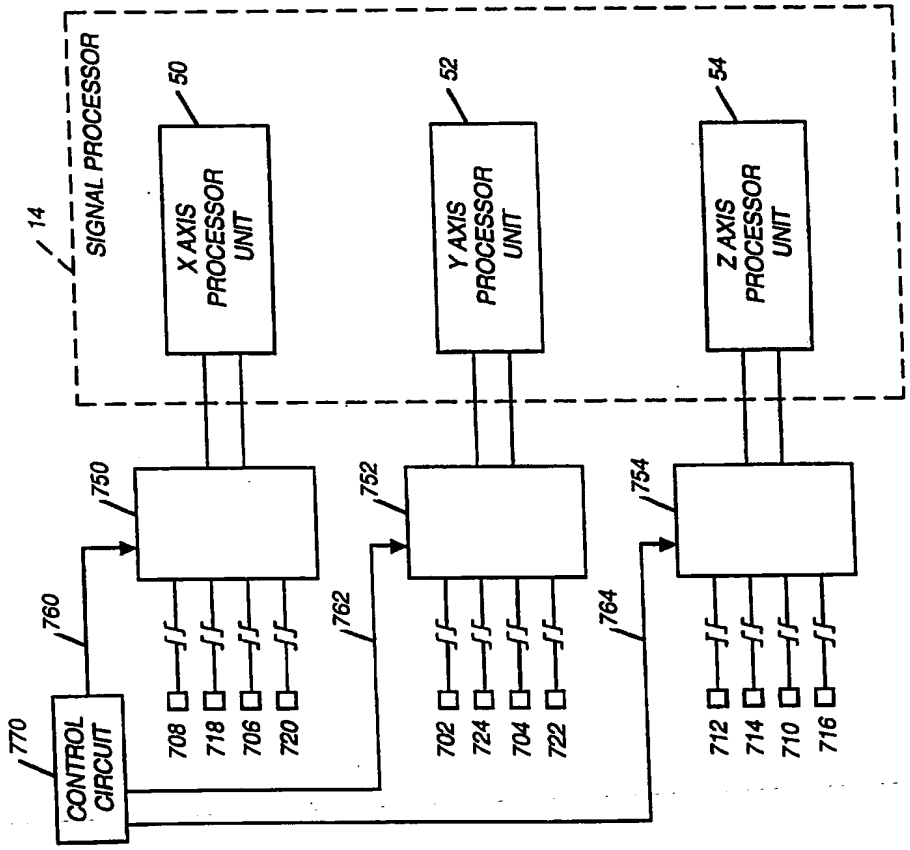
SIGNAL PROCESSOR
14
X AXIS PROCESSOR UNIT
50
Y AXIS PROCESSOR UNIT
52
Z AXIS PROCESSOR UNIT
54
750
752
754
760
762
764
770
CONTROL CIRCUIT
708
718
706
720
702
724
704
722
712
714
710
716

FIG. 14

INTERNATIONAL SEARCH REPORT

International application No.
PCT/US99/02045

A. CLASSIFICATION OF SUBJECT MATTER
IPC(6) :A61B 19/00
US CL :128/899
According to International Patent Classification (IPC) or to both national classification and IPC

B. FIELDS SEARCHED

Minimum documentation searched (classification system followed by classification symbols)

U.S. : 128/899; 600/373, 382, 547

Documentation searched other than minimum documentation to the extent that such documents are included in the fields searched

Electronic data base consulted during the international search (name of data base and, where practicable, search terms used)

C. DOCUMENTS CONSIDERED TO BE RELEVANT

Category*	Citation of document, with indication, where appropriate, of the relevant passages	Relevant to claim No.
A	US 5,697,377 A (WITTKAMPF) 16 December 1997, entire document.	1-19

☐ Further documents are listed in the continuation of Box C. ☐ See patent family annex.

*	Special categories of cited documents:	"T"	later document published after the international filing date or priority date and not in conflict with the application but cited to understand the principle or theory underlying the invention
"A"	document defining the general state of the art which is not considered to be of particular relevance	"X"	document of particular relevance; the claimed invention cannot be considered novel or cannot be considered to involve an inventive step when the document is taken alone
"E"	earlier document published on or after the international filing date	"Y"	document of particular relevance; the claimed invention cannot be considered to involve an inventive step when the document is combined with one or more other such documents, such combination being obvious to a person skilled in the art
"L"	document which may throw doubts on priority claim(s) or which is cited to establish the publication date of another citation or other special reason (as specified)	"&"	document member of the same patent family
"O"	document referring to an oral disclosure, use, exhibition or other means		
"P"	document published prior to the international filing date but later than the priority date claimed		

Date of the actual completion of the international search 11 MARCH 1999	Date of mailing of the international search report 30 MAR 1999
Name and mailing address of the ISA/US Commissioner of Patents and Trademarks Box PCT Washington, D.C. 20231 Facsimile No. (703) 305-3230	Authorized officer JOHN LACYK Telephone No. (703) 308-2995

Form PCT/ISA/210 (second sheet)(July 1992)*

(38)

Absolute Quantitation of Regional Myocardial Blood Flow of Rats Using Dynamic Pinhole SPECT

Toshiyuki Aoi[1,2,3], Hiroshi Watabe[2], *Member, IEEE* ,Hossain M. Deloar[2], Mikako Ogawa[2], Noboru Teramoto[2], Nobuyuki Kudomi[2], Toshihiro Oota[4], Kyeong Min Kim[2], *Member, IEEE,* Tetsuya Matsuda[1], Hidehiro Iida[2] *Member, IEEE*

Abstract— **PET and SPECT have been widely used to investigate the physiological function of animals in vivo. However, little efforts have been done to estimate absolute physiological parameters i.e. blood flow of small animals. The present study was aimed at the absolute quantitation of myocardial blood flow of rats by means of the dynamic SPECT fitted with a pinhole collimator with a careful determination of the arterial input function (IF). The center-of-rotation was carefully aligned to the center of the field-of-view of a fixed gamma camera with the accuracy < 0.05 mm. A rat was placed on a rotating device that fixes the rat in a stand position. The arterial blood samples were frequently collected and their radioactivity concentration was measured using a well counter cross-calibrated to the SPECT images. Dynamic SPECT (the step-and-shoot mode) was initiated at 5 min after the injection of 201TlCl into the tail vein. Acquisition period was 10 sec at each rotation angle, and 120 view projection data were obtained. The 360-degree complete data sets were obtained at approximately 20 min interval for 5 time frames. Images were reconstructed by filtered-back projection technique with Feldkamp algorithm. The cross-calibration factor was determined using a cylindrical phantom of 5 cm diameter filled with the 201TlCl solution. Regions-of-Interest were placed on the left ventricular wall to generate the tissue time activity curve (TTAC). TTAC and IF were fitted to the previously validated single-tissue compartment model to estimate the regional myocardial blood flow (rMBF) and volume of distribution (Vd) of thallium. The present system provided clear images of myocardial uptake of 201TlCl, and the time-dependent change of the tissue radioactivity concentration in regional basis, which was statistically sufficient for applying the compartment model analysis. The kinetic analysis yielded the rMBF of approximately 0.77 ml/min/g, which appeared to be an acceptable value with a consideration of contribution of partial volume effect and other error sources. Vd of approximately 91.9 ml/ml was also consistent with the know value of potassium potential across the cell membrane. These results strongly suggested the potential of the dynamic pinhole SPECT as a tool for absolute quantitation of physiological parameters in small animals.**

I. INTRODUCTION

Among a large number of studies aimed at developing small animal imaging devices using PET and SPECT technologies, little efforts have been made for in vivo quantitation of physiological parameters [1,2,3] such as regional myocardial blood flow or cerebral perfusion. This study was aimed at developing a system for the absolute quantitation of physiological functions in small animals using a dynamic pinhole SPECT. To achieve the spatial resolution of approximately 1.84mm, a pinhole collimator of 1mm diameter was employed [4,5] for the field-of-view of 6.75 cm diameter. A special rotating device was designed to carefully align the center-of-rotation to the center of the field-of-view of the imaging device [6,7]. Feasibility of applying the kinetic analysis for quantitation of regional myocardial blood flow and potassium potential of the myocardial cells in a rat was tested using the data obtained following the intravenous injection ^{201}TlCl and the dynamic pinhole SPECT.

II. MATEERIALS AND IMETHODS

A: Rotation unit and data acquisition

A rotating device consists of the small animal rotation section and a control section . The device gives signal of rotation as TTL into the commercial SPECT camera (GCA7100A, Toshiba Tokyo, Japan). The rotation was syncronized to the data acquisition. (Fig.1. a, b). A rat was placed on a rotating device that fixes the rat in a stand position (Fig.2. a, b).

Toshiyuki Aoi
Email: toshiaoi@ri.ncvc.go.jp;t-aoi@nifty.com
Hiroshi Watabe
Email: watabe@ri.ncvc.go.jp
Hossain M. Deloar
E.mail: hossain@ri.ncvc.go.jp
Hidehiro Iida
Email: iida@ri.ncvc.go.
1. The Dept. of System Science, Graduate school of informatics, Kyoto University, Yoshida-Honmachi, Sakyo-ku, Kyoto 606-8501 JAPAN.
2. The Dept. of Investigative Radiology, National Cardiovasucular Center Research Institute, Suita, Osaka, 565-8565 Japan.
3. The Dept. of Radiology, Osaka Rosai Hospital, Nagasone Sakai, Osaka, Japan
4 Eikoh company Co.Ld, Takahata Hiraoka-cho Kakogawa Hyogo 675-0103 Japan

0-7803-7636-6/03/$17.00 ©2003 IEEE.

Fig.1a Rotation maintenance unit and pinhole camera

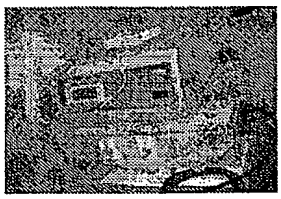

Fig1.b Control unit

Fig. 2a. A rat holder
Fig.2b. A rat was placed on a rotating device that fixes the rat in a stand position.

B: System sensitivity & Special Resolution

The system sensitivity was determined using an uniform phantom containing a homogeneous concentration of 148 MBq ^{201}TlCl solution(diameter=40mm, height =50mm).
The special resolution was determined from the profiles of planar and reconstructed SPECT images of three-line sources phantom (each 50mm length × 1mm diameter). The radioactivities of the line sources were 148 MBq/ml and the line sources were positioned in a cylinder with an interval of 5mm. The SPECT image was reconstructed by Feldkamp FBP algorithm. The radius of rotation (ROR) i.e. distance between the collimator aperture and object center was 67.5mm.

C: Dynamic SPECT of a rat

^{201}TlCl of 148 MBq was intravenously injected into the tail vein of a rat (230 g). Arterial blood was frequently collected using capillary tube from the femoral artery (Table.1). 5 minutes after injecting, dynamic SPECT acquisition (20 minutes x 5) was started. Each projection data had the matrix size of 128 ×128. Projections were obtained for 120 views with a step angle of 3 degree. The acquisition time per projection was 10 seconds. Tomographic images were reconstructed by filtered back-projection technique with the Feldkamp algorithm.

Table.1 Planning of arterial blood collection

I. TIME CORCE	II. INTERVAL
Injected 201-TlCl ~1min.	5 sec.
1~2min.	10 sec.
2~3min.	30 sec.
3~4min.	1 min.
4~10min.	2 min.
10~60min	10 min.

D: Cross Calibration

Prior to the SPECT study with a rat, a uniform phantom filled with ^{201}Tl solution was scanned to compute cross calibration factor (CCF) between the Well counter and the SPECT image.

E: Kinetic Analysis

^{201}TlCl is recognized as a potassium analog, and this kinetics have been extensively investigated. Kinetics of ^{201}TlCl is same as K^+, and ^{201}TlCl is rapidly accumulated into the myocardial tissue due to a high trans-capillary extraction fraction, and initial regional uptake of this tracer predominantly reflects regional blood flow. ^{201}TlCl from arterial blood was rapidly delivered to the myocardium. When an equilibrium between myocardium and ^{201}TlCl concentration of blood is reached, the myocardial concentration of ^{201}TlCl no longer reflects flow, but reflects the ability of myocardium to retain ^{201}Tl and is related to number of myocytes with maintained membrane potential in a given volume of myocardium. This equilibrium uptake is related to the volume of distribution (Vd) in kinetic modeling.

In this study, the tissue radioactivity curves were fitted to the two-compartment model [8,9] and estimated the regional myocardial blood flow and the Vd. In the two-compartment model, it is assumed that ^{201}TlCl extracted from the capillaries is diffused immediately into the extra vascular, myocardial tissue space, and is cleared slowly by venous drainage. Influx and out flux rate constants between capillaries and myocardial tissue are defined as K1 and K2. It is also assumed that ^{201}TlCl activity is retained in the tissue according to the regional affinity for ^{201}TlCl . Because of a high first-pass extraction of ^{201}TlCl by the myocardium, the influx rate of ^{201}TlCl reflects the rate of ^{201}TlCl supply to the capillary bed. In this modeling, the time course of regional radioactive concentration is expressed by

$$\frac{dc_t(t)}{dt} = f.C_a(t) - \frac{f}{Vd} C_t(t) \qquad (1)$$

and the time passed regional radioactivity concentration after injection is expressed as

$$Ct(t) = f.Ca(t) \otimes e^{\frac{f}{Vd}-t} \qquad (2)$$

where, Ct(t) is regional myocardial radioactive concentration by measurements with SPECT; Ca(t) is input function; Vd is the volume of distribution; f is regional myocardial blood flow (rMBF) ; k2 is f / Vd, and ⊗ is convolution integral.

Time integration of radioactive concentration can be obtained by the SPECT measurement after the time interval (Δ T).

Therefore, formula of Eq. (2) can be expressed by

$$\int_{MST-\Delta T/2}^{MST+\Delta T/2} ct(t)\,dt = f.\int_{MST-\Delta T/2}^{MST+\Delta T/2} ca(t) \otimes e^{-(\frac{f}{Vd})t}\,dt \qquad (3)$$

III. RESULTS

FWHM with the planar image of the line source phantom was 1.84 mm and in reconstructed image it was 2.86mm by using 1mm pinhole at the ROR of 67.5 mm (Fig.3).

Clear dynamic images were obtained with the scan duration employed in this study as typically shown in (Fig.4). Tissue time activity curve (TTAC) generated for given regions of interests (ROI's) were statistically sufficient enough for the kinetic analysis to be applied (Fig. 5). Input function (IF) can be accurately determined with the frequent collection of the arterial blood obtained from the femoral artery for the whole scan period (Fig.5). The cross-calibration factor was rather stable and did not change more than 5% when changing the size of the phantom from 2.5 to 5 cm diameter.

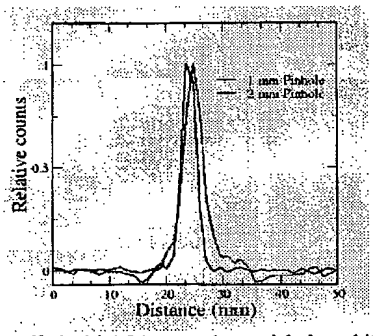

Fig.3 FWHM is1.84mm on 1mm pinhole and it was obtained from the planner profiles of the line source.

Special Resolution (FWHM, mm)

Planar image	**1.84**
Reconstructed image	**2.86**

Reconstructed by Feldkamp FBP algorithm

Fitting the observed TTAC and IF to the tissue compartment model resulted in K1, namely the rMBF of 0.76 ml/min/g and Vd of 75.1 ml/ml, if the whole blood radioactivity was used as IF. If the plasma radioactivity concentration curve is employed for IF, the analysis resulted in K1 of 0.77 ml/min/g and Vd of 91.9 ml/ml (Fig.5).

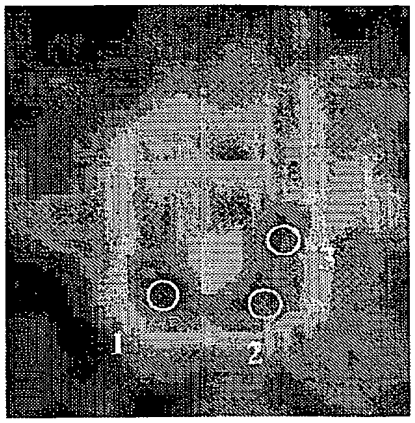

Fig.4 Set ROI to left ventricle, 1 to 3. Actually, use average counts of 1,2 and 3,

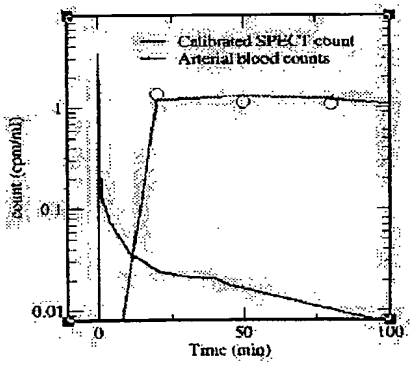

Fig.5 Typical fit by a two-compartment model to the regional radioactivity curve in the myocardium after ^{201}TlCl administration for rat. K_1=0.759 Volume of distribution (V_d) = 75.04 and after plasma correction was 0.77 ml/min/g and 91.9 ml/ml.

IV. DISCUSSION

The ^{201}TlCl exists only in plasma at the beginning, but should gradually be trapped into the red cells. The radioactivity in the red cells unlikely contributes to the extraction to the myocardial tissue, and thus the plasma radioactivity concentration should be used for the rMBF and Vd quantitation. Errors in K1 appeared to however be minimal, and only Vd was affected. Further investigation should be carried out regarding the ideal methodology for the IF determination.

The true rMBF of alive rats is unknown, and reference values have not been measured by the gold-standard technique of radiolabeled microspheres. However, K1 of 0.77ml/gm-min

is probably a reasonable value if considering the contribution of the partial volume effects, which was attributed to the small transmural thickness of the myocardial wall relative to the imaging device. The true rMBF value is probably greater than the double of the observed value. Vd of approximately 91.9 ml/ml was also consistent with the known value of potassium potential across the cell membrane. These considerations may support the feasibility of the quantitation of rMBF and Vd in small animals.

Imaging of mice is even more challenging, as it requires even higher spatial resolution. This could however be achieved by employing a small diameter pinhole collimator. Rotation radius needs to be further shortened in order to maximize the sensitivity, which may be achievable. Further careful manufacturing is required.

Due to the limited sensitivity of the pinhole SPECT system, the duration of the frame needs to be prolonged. A previously established Optimized-Sampling Schedule theory would be of use in order to minimize the loss of accuracy and precision in determination of the kinetic parameters when reducing the number of time frames in the dynamic SPECT acquisition [5]. This study did not consider the attenuation and scatter correction.

In the myocardium of small animal, we must set ROI attentively because of partial-volume effects. Partial-volume effect in SPECT usually refers to the loss of counts in small organs or regions because of the limited resolution of SPECT. The degree of underestimation depends on the myocardial wall thickness and wall motion. This effect is similar to a further degradation of special resolution or additional blurring of the SPECT images. Farther study should be carried out.

V. CONCLUSION

We measured the time course of regional myocardial radioactive concentration in rat after interveners injection of ^{201}TlCl using pinhole dynamic SPECT and estimated the parameters of K1 and Vd considering the assumption that two-compartment model was fitted the kinetics of ^{201}TlCl across the myocardium.

These results strongly suggested that the potential of the dynamic pinhole SPECT as a new tool for absolute quantitation of physiological parameters in small animals.

VI. ACKNOWLEDGEMENT

This study was financially supported by the Budget for Nuclear Research of the Ministry of Education, Culture, Sports, Science and Technology, based on the screening and counseling by the Atomic Energy Commission.

REFERENCES

[1] Z. Liu, G. A. Kastis, G. D. Stevenson, et al. " Quantitative Analysis of Acute Myocardial Infarct in Rat Hearts with Ischemia-Reperfusion Using a High-Resolution Stationary SPECT System," J Nucl Med, Vol.43, pp.933-939, 2002.

[2] M. Yukihiro, T. Inoue, T. Iwasaki, et al. " Myocardial infraction in rats: high-resolution single-photon emission tomographic imaging with a pinhole collimator," Europ. J Nucl Med, Vol.23, 1996.

[3] C. Scherfler, E. Donnemiller, M. Schocke, et al. " Evaluation of Striatal Dopamine Transporter Function in Rats by in Vivo beta-[^{123}I] CIT Pinhole SPECT," NeuroImage , Vol.17, pp.128-141,2002.

[4] K.Ogawa, T.Kawada, K,Nakamura, et al. " Ultra high resolution pinhole SPECT for small animal study," IEEE Trans Nucl Science, vol.45, pp.3122-3126, 1998.

[5] D.A. Weber, M. Ivanovic, D. Franceschi, et al. " Pinhole SPECT: An Approach to In Vivo High Resolution SPECT Imaging in Small Laboratory Animals," J Nucl Med, vol.35, pp.342-348 ,1994.

[6] L.J.Jaszczak, R.J.Greer KL, Coleman RE," A filtered backprojection algorithm for pinhole SPECT with a displaced center of rotation," Phys Med Biol, vol39, pp165-176, 1994.

[7] J.B.A.Habraken, K. Bruin, M. Shehata, et al. "Evaluation of High-Resolution Pinhole SPECT Using a small Rotating Animal," J Nucl Med, vol.42, pp.1863-1869,2001.

[8] H. Iida and S. Eberl," Quantitative assessment of regional myocardial blood flow thallium-201 and SPECT," J Nucl Cardio, vol.5 pp.313-331, 1998.

[9] C.H. Lau, S. Eberl, D. Feng, et al. " Optimized Acquisition Time and Image Sampling for Dynamic SPECT of Tl-201," IEEE Trans Med , vol.17, pp.334-34

PHYS. MED. BIOL., 1978, VOL. 23, NO. 2, 302–308.

A Radiotelemetry Pill for the Measurement of Ionising Radiation using a Mercuric Iodide Detector

M. A. HASSAN,† PH.D. and G. PEARCE, M.SC.

Department of Physics, Electronics and Electrical Engineering, UWIST, Cardiff CF1 3NU, U.K.

J. P. N. EDWARDS,‡ PH.D.

Department of Physics, Velindre Hospital, Cardiff CF4 7XL, U.K.

Received 13 *January* 1977, *in final form* 30 *September* 1977

ABSTRACT. A small radiation measuring pill is briefly described which utilises the principles of radiotelemetry and the properties of a room temperature semiconductor radiation detector such as mercuric iodide. By transmitting a radio signal to a remote receiver the pill could be an effective tool in localising bleeding sites along the gastrointestinal tract and also possibly in the diagnosis of gastrointestinal carcinoma. Other uses of the radiopill are suggested. The size of the pill is 27 mm × 10 mm diameter and consists of a mercuric iodide crystal, an amplifier, a frequency modulated transmitter and one battery. The radiotransmitter operates at about 106 MHz and has a range of about 10 m, and the sensitivity of the pill has been found for $^{99}Tc^{m}$, ^{131}I and ^{32}P.

1. Introduction

This paper describes the initial results obtained from a small inexpensive radiation pill designed in the first instance for investigating *in vivo* gastrointestinal bleeding, although the radiopill can also serve as a general purpose telemetric γ-ray detector.

Recent methods used to diagnose bleeding of the gastrointestinal tract include the use of X-rays, endoscopic instruments and medical probes. X-ray methods using contrast media are not very suitable because studies cannot be carried out continuously over a period of days while endoscopes involve a greater degree of clinical preparation and can cause considerable discomfort to the patient. The second technique is limited to the investigation of the oesophagus, stomach and rectum. Alternatively, a radiation pill might be employed which permits a continuous measurement along the gastrointestinal tract with little discomfort to the patient. The technique would involve injecting the patient with a suitable low Γ factor radioisotope such as $^{99}Tc^{m}$ before the radiation pill was swallowed. $^{99}Tc^{m}$ with its convenient half-life and easily detected γ-ray is envisaged as the isotope of choice. Gastrointestinal bleeding could in theory give rise to a local concentration of radioactivity which could be detected and the measurement transmitted to external

† Present address: University of Jordan, Amman, Jordan.
‡ Present address: Mt Vernon Hospital, Harrow, Middlesex.

apparatus. On a more speculative level, should one find increased uptake of particular isotopes at tumour sites, the radiation pill might then prove a suitable tool in the diagnosis of carcinoma of the gastrointestinal tract.

Two reports of radiation pills have been given previously. In the first (Mackay 1970), the radiation pill consisted of a GM tube, DC/DC converter to generate the high voltage for the tube, and two batteries, one for the DC/DC converter and the other for the radiotransmitter circuit. In the second report, Gugnin, Kalantarov, Pluzhnikov, Zemstov and Semenov (1972) described the use of a piezoelectric transformer to generate a high voltage for a GM tube and also to act as a modulator. The battery required had a lifetime of 20–30 h and the pill measured 29 mm long and 12 mm in diameter.

The use of GM tubes in radiation pills is limited because of such drawbacks as the high voltage supply required which usually limits the miniaturisation of the pill, and the poor sensitivity which restricts its use to medium or high energy β^- emitters for low activity in tracer and diagnostic use. Following the development of semiconductor radiation detectors as spectrometers, considerable effort has been made to utilise them in medical applications such as medical probes (Martini 1973, Walford and Parker 1973) and gamma cameras (McCready, Parker, Gunnersen, Ellis, Moss, Gore and Bell 1971).

Recent reports (Llacer, Watt, Schieber, Carlston and Schnepple 1974, Swierkowaski, Armantrout and Wichner 1974, Ponpon, Stuck, Siffert, Meyer, and Schwab 1975) relating to mercuric iodide detectors suggest the use of such material in the medical field.

Because of its high density (6·28 g ml^{-1}) and high average atomic number (Hg = 80, I = 53) mercuric iodide crystals can combine small size (millimetres or sub-millimetres) with efficient gamma ray detection at low voltages and at room temperatures (E_g = 2·13 eV).

With the low melting point of $\simeq$ 257 °C the crystal growth of the compound is easier and less expensive than other semiconductor radiation detectors such as CdTe, Si or Ge.

The basic mechanism of operation of semiconductor pulse radiation detectors can be summarised as follows. The detector consists of two conducting electrodes with a semiconductor region between them. A potential is applied across the electrodes which produces an electric field in the crystal. When a gamma ray interacts with the crystal, it loses energy by producing free charge carriers in the crystal, i.e. electrons and holes. If it is totally absorbed, the number of these carriers is proportional to the energy of the gamma ray and they move under the influence of the electric field until they are collected at the electrodes or trapped internally in the crystal. The resulting collected current pulses represent the basic signal information.

2. Description of the radiation pill

The radiation pill consists of a mercuric iodide crystal, amplifier, transmitter and a 1·35 V battery. Mercuric iodide crystals of good quality and up to 8 mm diameter and 20 mm long have been grown in our laboratory using a dynamic sublimation technique (Llacer *et al.* 1974, Ponpon *et al.* 1975) after

triple purification by sublimation *in vacuo* ($\simeq 10^{-5}$ torr). Crystals of about 2 mm × 2 mm × 0·4 mm were cut for use in the radiation pill or as spectrometer crystals. Aquadag paint served as the electrode contacts and the crystal was placed in a small PTFE mounting.

Some of the spectra which have been obtained from our crystals are shown in figs 1 and 2. The resolutions obtained are comparable to the most recent published results (Llacer *et al.* 1974, Martin, Bach and Guetin 1974, Swierkowski *et al.* 1974, Ponpon *et al.* 1975).

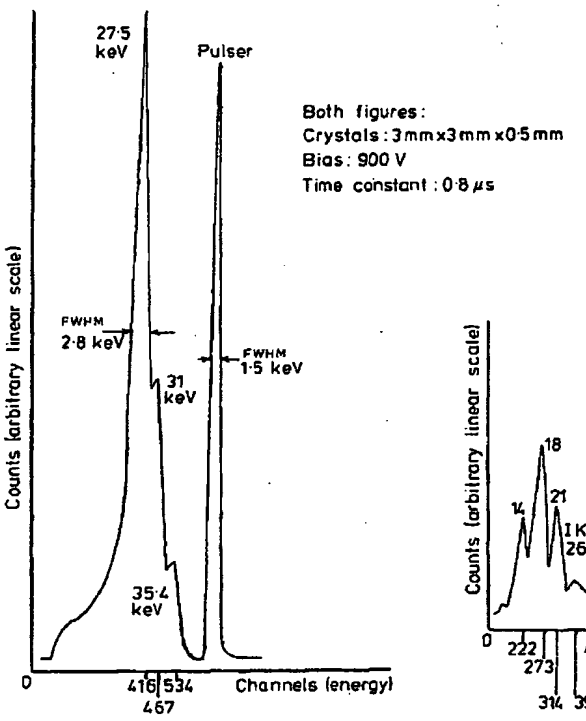

Fig. 1. Spectrum of ^{125}I source.

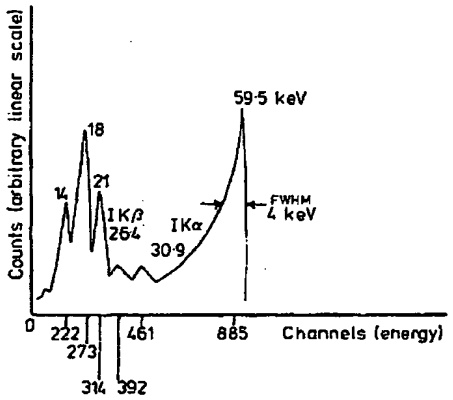

Fig. 2. Spectrum of ^{241}Am source.

Due to the small thickness of the crystal a small bias voltage (1·35 V) has been found sufficient to give adequate counting performance when subjecting the device to isotopes commonly used in hospitals. The output pulses from the crystal are very small (< 1 mV) and they need additional amplification before they can be transmitted. A small voltage amplifier was used (first half of fig. 3) for this purpose. A low pinch-off voltage FET was selected from a small batch so that it was operational with a gate-source voltage of −0·3 V. Similarly, a low noise diode was selected so that with the high resistivity of the crystal ($\simeq 10^{13}$ Ω cm) the first stage operated as a linear amplifier. To minimise thermal drift (which was considered to be important in view of the detectors'

in vivo applications) the three stages of the amplifier were AC coupled with 1 μF capacitors. The noise performance of this amplifier was measured using a multichannel analyser (MCA) and it was found to be about 12 keV FWHM The current drain on the battery was less than 500 μA. This amplifier was assembled on a small circular printed board of 9·5 mm diameter.

The output of the amplifier shown in fig. 3 is applied to the base of T_4 via a 1 μF capacitor C_5. T_4 is the active device in a grounded-base Colpitts oscillator circuit which performs two functions; those of an RF oscillator and of an FM transmitter. Frequency modulation is accomplished by varying the operating point of T_4 (due to the incoming pulses from the amplifier) which in turn varies its collector capacitance, thus changing the resonant frequency of the tank circuit. The coil L serves as both a tuning coil and a transmitting antenna.

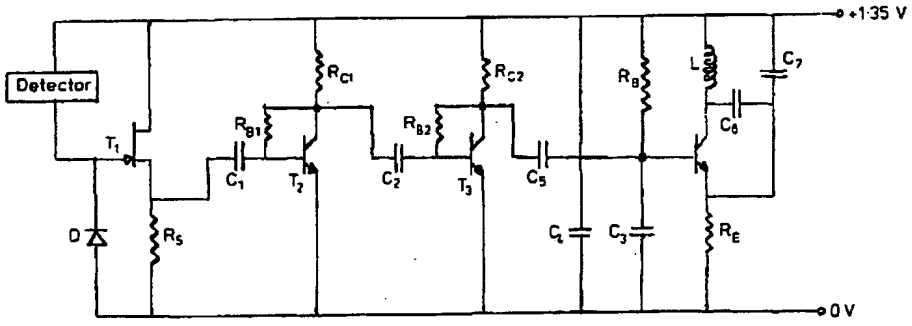

FIG. 3. Radiopill circuit diagram.

$R_S = 4{\cdot}7\ k\Omega$ $R_B = 68\ k\Omega$ $C_1 = C_2 = C_5 = 1\ \mu F$
$R_{B1} = R_{B2} = 100\ k\Omega$ $R_C = 560\ \Omega$ $C_3 = C_4 = 390\ pF$
$R_{C1} = R_{C2} = 2{\cdot}9\ k\Omega$ $C_6 = C_7 = 8{\cdot}2\ pF$
$T_1 = E201$ $L = 6$ turns 34 swg
$T_2 = T_3 = D26E\text{-}1$ (air core)
$T_4 = MMT\ 3904$ $D = IN\ 4531$

This transmitter operates at about 106 MHz with a range of about 10 m. The elementary characteristics of the transmitter are summarised in table 1.

Table 1. Transmitter characteristics

Current drain	< 450 μA
Frequency response	200 Hz–5 kHz (± 3dB)
Signal strength (at 30 cm from the receiver)	130 μV
Polar diagram	Isotropic to ± 10%
Noise (input signal 1 kHz)	Better than 8 μV

To power the radio transmitter and detector circuits, one small hearing aid battery (Mallory type RM-13H) was used. When continuously loaded, its useful lifetime of the battery was found to be about two days.

3. The radio receiver and the counting system

To receive and count the transmitted pulses, an FM receiver–amplifier was connected to a conventional discriminator and scaler units.

Any commercial FM receiver with minor modifications was found suitable to receive the signals from the radiation pill. The FM receivers commercial aerial proved adequate.

4. Performance

To make a preliminary evaluation of the radiopill, tests were carried out in air and water tanks in order to simulate the use of the pill *in vivo*. Measurements permitted the determination of the polar diagram, temperature dependence and sensitivity to several radioactive sources. Fig. 4 shows the polar diagram response of the radiopill using a 1 mm radius 'point source' of 1·7 mCi $^{99}Tc^{m}$. It is seen that the polar diagram is fairly isotropic except on the battery side which shields some of the incoming radiation. Similar results are shown for a

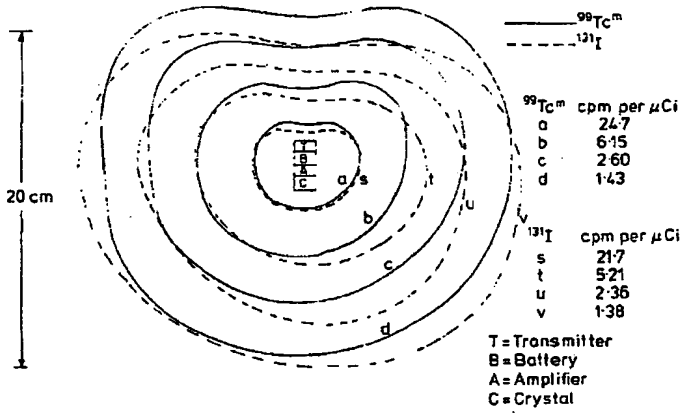

Fig. 4. Polar diagrams of pill in air using $^{99}Tc^{m}$(1·7 mCi) and ^{131}I(125 μCi) point sources.

point source of ^{131}I of strength 125 μCi. The β-rays from this source are not detected due to the moderate absorption characteristic of the pill's plastic encapsulation. It has been verified by simple calculation with $^{99}Tc^{m}$ and ^{131}I that the sensitivity of the radiation pill follows the inverse square law at distances $\gtrsim 4$ cm. To assess the variation of sensitivity with temperature the radiation pill was immersed in a beaker (3 cm diameter and 4 cm deep) of water containing ^{131}I such that the volume activity was about 1 μCi ml^{-1}. The overall count rate was measured in the temperature range 5–40 °C and the results are shown in fig. 5. The small increase of count rate with temperature is due mainly to the change in the operating points of the transistors and also the increasing leakage current of the mercuric iodide crystal. This current was measured on a sensitive electrometer and found with 1·35 V bias to be 0·26 pA at 25 °C increasing to about 0·6 pA at 37 °C.

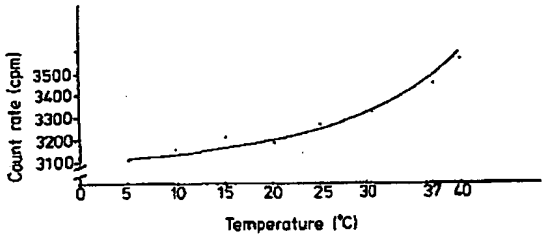

Fig. 5. The relation between the count rate and the temperature when the pill was immersed in a beaker (3 cm diameter and 4 cm deep) of water solution and of strength of about 1 μCi ml^{-1} of ^{131}I.

The radiopill was also tested as a beta detector using ^{32}P in aqueous solution. The average energy of the electrons is $\sim$0·6 MeV and has a range in water of $\simeq$2·4 mm, whilst the maximum range of the electrons (energy 1·71 MeV) is about 8·2 mm. For ^{131}I and considering only the 87% 0·61 MeV beta transition, the ranges in water of the average and maximum energy beta particle are 0·95 mm and 2·4 mm respectively. After the discriminator had been adjusted to give a background counting rate of $<$ 1 cpm, the sensitivity of the radiopill to ^{99}Tc^{m}, ^{131}I and ^{32}P was determined and is given in table 2.

Table 2. Radiopill sensitivity

Isotope	Strength	Beaker volume, diameter × height	Counts per minute
^{99}TC^{m}	1·0 μCi ml^{-1}	3 cm × 4 cm	4106
^{131}I	1·0 μCi ml^{-1}	3 cm × 4 cm	3200
^{32}P	1·0 μCi ml^{-1}	Large volume	2052

5. Conclusion

The material presented in this paper describes the preliminary work in using a mercuric iodide crystal as a radiation detector in conjunction with a small radio transmitter for use *in vivo*. The performance of the pill indicates it would be possible to use the pill *in vivo* for several radioactive isotopes but the problems of sensitivity to gut bleeding and localisation of bleeding site are still to be determined. The resolution obtained with mercuric iodide as a radiation detector indicates its application in imaging and spectrometer systems and as a possible alternative to detectors currently used in medical probes. It also appears suitable for some areas in radiation protection, e.g. in detecting X-ray leakage through inadequate shielding, and again in radiotherapy.

We are indebted to Professor J. R. Bristow (Head of Applied Physics and Electronics Department) for his encouragement, to the technical staff of the Applied Physics and Electronics Department for their assistance, to Dr. T. J. Deeley (Director of Velindre Hospital) and to Mrs. S. Kirkham (Head of the Isotopes Department at Velindre Hospital) for providing technical facilities.

One of us (M. A. H.) would like to acknowledge the considerable contribution made to this work by Dr. C. Schwab, University of Strasbourg.

This work was supported by a UWIST Research Studentship.

Résumé

Un comprimé à radiotélémétrie pour mesurer les rayonnements ionisant au moyen d'un détecteur à iodure mercurique

Brève description d'un petit comprimé pour mesurer les rayonnements; il utilise les principes de la radiotélémétrie et les propriétés d'un détecteur de rayonnement de semiconducteur à température ambiante, comme l'iodure mercurique. En transmettant un signal radio à un télérécepteur, le comprimé pourra être un instrument utile pour localiser les lésions hémorragiques au long des voies gastro-intestinales, et peut-être aussi pour le diagnostic des carcinomes gastro-intestinaux. D'autres usages de ce comprimé sont suggérés. Ses dimensions sont de 27 mm × 10 mm et il est composé d'un cristal d'iodure mercurique, d'un amplificateur, d'un émetteur à modulation de fréquence et d'une pile. Le radio-émetteur fonctionne à environ 106 MHz et à une gamme d'environ 10 m et la sensibilité du comprimé a été notée pour $^{99}Tc^{m}$, ^{131}I et ^{32}P.

Zusammenfassung

Eine radiotelemetrische Pille zur Messung der Ionisieurungsstrahlung unter Verwendung eines Quecksilberjodid-Detektors

Eine kleine Strahlungsmessungspille wird kurz beschrieben. Hierbei werden die Prinzipien der Radiotelemetrie und die Eigenschaften eines Halbleiter-Strahlungsmessers für Raumtemperatur, wie beispielsweise Quecksilberjodid, verwertet. Die Pille übermittelt ein Funksignal an einen ferngesteuerten Empfänger und könnte sich dadurch für die Lokalisieurung von Blutungen entlang des Magen-Darm-Kanals sowie auch möglicherweise für die Diagnose von Magen-Darm-Karzinomen als äusserst nützlich erweisen. Weitere Einsatzgebiete für die Funkpille werden vorgeschlagen. Die Pille hat einen Durchmesser von 27 mm × 10 mm und besteht aus einem Quecksilberjodid-Kristall, einem Verstärker, einem frequenzmoduilerten Sender und einer Batterie. Der Funksender arbeitet mit rund 105 MHz und hat eine Reichweite von rund 10 m, die Empfindlichkeit der Pille wurde für $^{99}Tc^{m}$, ^{131}I und ^{32}P festgestellt.

References

Gugnin, Yu. Ya., Kalantarov. K. D., Pluzhnikov, V. M., Zemskov, V. P., and Semenov, V. S., 1972, *Biomed. Engng*, **6**, 19.

Llacer, J., Watt, M. M. K., Schieber, M., Carlston, R., and Schnepple, W., 1974, *IEEE Trans. Nucl. Sci.*, **NS-21**, 305.

McCready, V. R., Parker, R. P., Gunnersen, E. M., Ellis, R., Moss, E., Gore, W. G., and Bell, J., 1971, *Br. J. Radiol.*, **44**, 58.

Mackay, R. S. 1970, *Bio-Medical Telemetry* (London: John Wiley).

Martin, G. M., Bach, P. and Guetin, P., 1974, *Appl. Phys. Lett.*, **25**, 286.

Martini, M., 1973, *IEEE Trans. Nucl. Sci.*, **NS-20**, 294.

Ponpon, J. P., Stuck, R., Siffert, P., Meyer, B., and Schwab, C., 1975, *IEEE Trans. Nucl. Sci.*, **NS-22**, 182.

Swierkowski, S. P., Armantrout, G. A., and Wichner, R., 1974, *IEEE Trans. Nucl. Sci.*, **NS-21**, 302.

Walford, G. V., and Parker, R. P., 1973, *IEEE Trans. Nucl. Sci.*, **NS-20**, 318.

(40)

Review article

Intraoperative probes and imaging probes

Edward J. Hoffman[1], Martin P. Tornai[2], Martin Janecek[1], Bradley E. Patt[3], Jan S. Iwanczyk[3]

[1] Division of Nuclear Medicine, Department of Pharmacology, UCLA School of Medicine, 10833 Le Conte Avenue, Los Angeles, CA 90095-6948, USA
[2] Department of Radiology, Duke University Medical Center, Durham, N.C., USA
[3] Photon Imaging Inc., Northridge, Calif., USA

Abstract. Intraoperative probes have been employed to assist in the detection and removal of tumors for more than 50 years. For a period of about 40 years, essentially every detector type that could be miniaturized had been tested or at least suggested for use as an intraoperative probe. These detectors included basic Geiger-Müller (GM) tubes, scintillation detectors, and even state-of-the-art solid state detectors. The radiopharmaceuticals have progressed from $^{32}PO_4^-$ injections for brain tumors to sophisticated monoclonal antibodies labeled with iodine-125 for colorectal cancers. The early work was mostly anecdotal, primarily interdisciplinary collaborations between surgeons and physical scientists. These collaborations produced a few publications, but never seemed to result in an ongoing clinical practice. In the mid 1980s, several companies offered basic gamma-detecting intraoperative probes as products. This led to the rapid development of radioimmunoguided surgery (RIGS) and sentinel node detection as regularly practiced procedures to assist in the diagnosis and treatment of cancer. In recent years intraoperative imaging probes have been developed. These devices add the ability to see the details of the detected activity, giving the potential of using the technique in a low-contrast environment. Intraoperative probes are now established as clinical devices, they have a commercial infrastructure to support their continued use, and there is ongoing research, both commercial and academic, that would seem to ensure continued progress and renewed interest in this slowly developing field.

Key words: Intraoperative probes – Sentinel node detection

Eur J Nucl Med (1999) 26:913–935

Correspondence to: Edward J. Hoffman, e-mail: ehoffman@mednet.ucla.edu, Tel.: +1-310-8258851, Fax: +1-310-8254517

Introduction

The concept of employing a hand-held radiation detector to assist a surgeon in locating and removing tumors was part of the "fallout" from the Manhattan project. In the years following World War II (1946–1949), several investigators [1–5] realized that if one could label a tumor by making an intravenous injection with a compound labeled with a radioactive isotope, it should be possible to locate the tumor by surveying the region under suspicion with a radiation detector. In this early work the isotope was phosphorus-32 (14.3-day half-life, 1.71 MeV β^-) and the detector was a simple Geiger-Müller (GM) tube. This combination worked because the GM tube had a very high detection efficiency for the β^- from ^{32}P, and the relatively high energy of the β^- allowed penetration of up to 8 mm of tissue to reach the GM tube. The success of this approach was limited in part because the absorbed dose per unit activity for ^{32}P is 300–600 times that of the currently most frequently used isotope, technetium-99m. From 1.2 to 2.4 MBq (30–60 μCi) is equivalent in dose to the 740 MBq (20 mCi) that is typical in diagnostic nuclear medicine. This meant that there would be very low count rates from the tumor or the physician would need to inject larger doses. In the early work with ^{32}P [3–5], 37 to 148 MBq (1–4 mCi) doses were injected for intraoperative probe-assisted surgery. It should be pointed out that this work was performed before guidelines had been established for medical applications of radiation. The usefulness of procedures utilizing an intraoperative probe must be considered in terms of a measurement system. This system consists of the radiation detector, the radioisotope, and the compound that is labeled. First, the compound needs to have the following properties: (a) it must be extracted from the blood into the tumor, (b) the amount in the tumor must be significantly higher than that in the surrounding tissue, and (c) it must be extracted into the tumor and remain in the tumor with a time course that is consistent with the requirements of the surgery and the half-life of the isotope. Secondly, the radioisotope must have both (a) the chemical properties that allow it to form a stable labeled compound and (b) an appropriate half-life; furthermore, the

emitted radiation must be compatible with the detector system and patient safety. Thirdly, the detector system must have some combination of the following properties: (a) efficient detection of the emitted radiation, (b) insensitivity to background radiation or ability to suppress or measure and subtract background events, (c) good energy resolution to discriminate against background radiation, (d) collimation to shield against background radiation, and/or (e) good spatial resolution to resolve tumor from adjacent background.

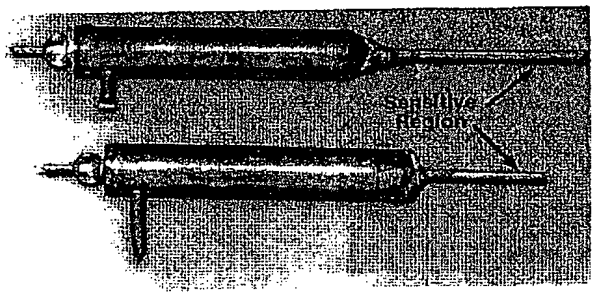

Fig. 1. Photograph of the earliest GM tubes used as intraoperative probes [8]. (Courtesy of Melvin Griem, M.D., Emeritus Prof., University of Chicago, assistant to C. Robinson in 1948)

Early intraoperative probes

Geiger-Müller counters

The earliest intraoperative probes were GM counters, which are among the most basic kind of gas-filled radiation detectors, and ^{32}P was the isotope of choice [1–7]. Fortuitously, the properties of the GM tube plus ^{32}P matched well the requirements of the good measurement system outlined above. First the compound, inorganic phosphate, was extracted into and remained in the tumor for a long period (many days). The tumor to background activity ratio was measured to be from 5.5 to 110 [3–5] for various types of brain tumors. The isotope, ^{32}P, was used as a label in PO_4^- ion, which is the most stable form of phosphorus. The emitted radiation is a beta particle. Beta radiation is not mono-energetic, as is the case with gamma rays, but is emitted in a continuous distribution of energies, in this case from 0 to 1.71 MeV. This maximum energy beta can penetrate up to 8 mm in tissue, but the average penetration is 2.8 mm. The properties of beta radiation reduce the technical requirements of the probe. The short range of the beta means that all detected radiation comes from a source that is almost touching the probe. Thus, there is no background from distal parts of the body, and the probe does not require collimation or other shielding. The simplest gas detectors (ionization chambers) simply collect the ions produced in the gas by the radiation. The GM tube is designed with a fine wire central electrode, which gives a very high electric field near the electrode. The high field can be produce by a simple 100-V external supply (e.g., 11 9-V batteries in series). The high field accelerates the electrons released by the absorbed radiation in the gas to a high enough velocity to cause secondary ionizations, releasing more electrons. The secondary electrons are also accelerated and cause more ionizations with the process continuing until enough charge builds up around the electrode to cause a reduction in the electric field, stopping the ionization. The process can be initiated by a single ionization. Thus, the GM tube only requires that a small fraction of the energy of the beta particle be absorbed, causing ionization of gas atoms in its sensitive volume. A few initial ionizations in the counter gas leads to the same cascade of ionizations in the gas as a large number of initial ionizations, and produces a signal just as strong. This means that essentially all betas striking the detector are counted, giving close to 100% efficiency or sensitivity.

The early probes were more invasive than the modern intraoperative probes, which tend to be used on exposed surfaces. Figure 1 is a photograph of two of the earliest probes. The GM tube is about 3 mm in diameter, about the same diameter as the needle that was used in ventriculography, and only about 1–1.5 cm at the tip is sensitive to radiation. After exposing the brain, the probe is introduced into a convolution of the brain as far from the expected tumor location as possible to get a control reading. Then the probe is introduced into convolutions of the brain near the expected location of the tumor. A large increase in the count rate indicates the location of the tumor.

The GM tube is limited in that its sensitive volume is a gas, which is essentially transparent to gamma rays; as a consequence, typically less than 1% of the gamma rays that pass through a GM counter are detected. A higher density detector consisting of higher atomic number materials is required for efficient detection of gamma rays.

A technical improvement in gas detector-based probes was made by Robinson [9], who created a probe based on the proportional counter. However, the use of the gas detector was only rarely reported in the literature [6, 7, 10–12]. Since one rarely reports on the failure of a technique, unless it has caused serious harm, the reasons for the phasing out of gas detectors is not well documented. It could be presumed that the use of doses that were on the order of 100 times that normally accepted in nuclear medicine may have been a factor, as well as the fact that these detectors could not be used with gamma-emitting isotopes.

Scintillation detectors

The only readily available solution for a gamma ray-sensitive probe in the 1950s was the scintillation detector

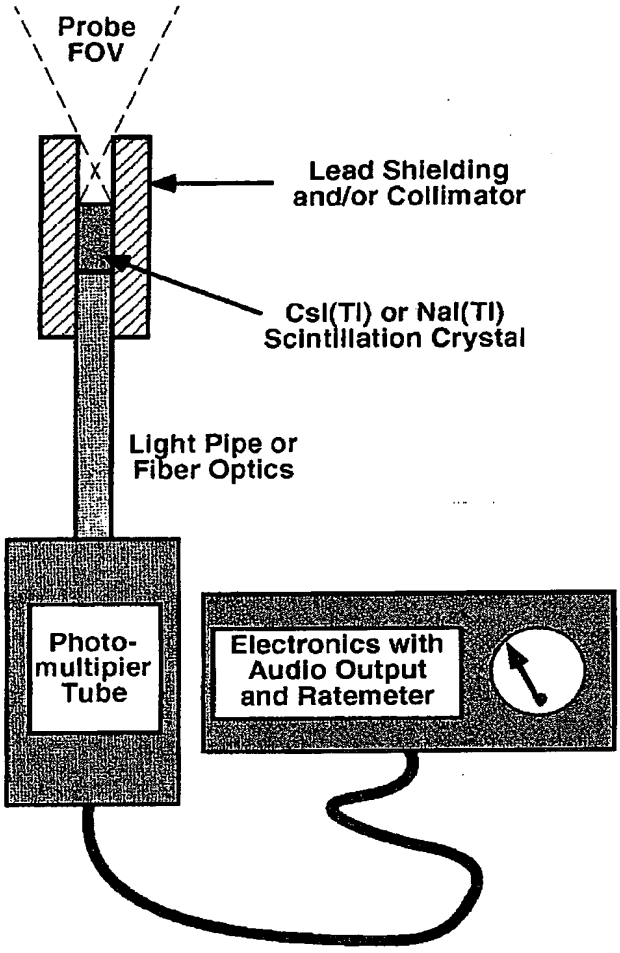

Fig. 2A–E. The basic configuration of scintillation detector-based intraoperative probe. The system consists of: **A** a simple shield/collimator; **B** a scintillation detector, initially CsI(Tl) and eventually NaI(Tl); **C** a light pipe or fiber optics; **D** a photomultiplier; **E** electronics with a ratemeter and audio output

[13]. The typical configuration is illustrated in Fig. 2 and is basically the configuration used by Harris et al. in 1956 [13]. In this type of detector, the scintillator absorbs the radiation and emits visible light in proportion to the energy absorbed. The visible light must be measured with a photon detector, usually a photomultiplier (PMT). In the early versions, CsI(Tl) was used as the scintillator because it was easy to handle and was only slightly hygroscopic. The reliable PMTs of the day were on the order of 2.5 cm (1 in.) in diameter or larger. Therefore, a light pipe [13, 14] or fiber optics [15–19] were used to optically couple the small scintillators of the probe to these relatively large PMTs. Eventually, reliable PMTs became available in sizes as small as 10 mm in diameter and modern probes have eliminated the light pipe [20, 21]. The elimination of the light pipe or fiber optic allowed a significant improvement in light collection from the scintillator. This in turn led to improved energy resolution and, since a scattered gamma ray loses energy, also enabled the rejection of scattered gamma-rays.

The high penetration power of gamma rays means that background events could come from any part of the patient. These events would be reduced to some extent by absorption in the patient and to a greater extent by the low solid angle for detection of distant radiation sources, which is governed by an inverse square law relation with distance. However, since it is rare to have more than a few percent of the isotope in the tumor, the total background from the rest of the body can be very significant. The early scintillation detectors were shielded by varying amounts of platinum [13, 14], or lead [16, 20, 21]. The collimators/shielding were little more than cylinders of absorber designed to shield the detector from most of the body and provide a modest amount of collimation for the detector. A typical collimator for a scintillation camera reduces the number of gamma rays that strike the detector by a factor of 10^3 to 10^4. This type of collimation would be too severe for the probe, which depends on its high sensitivity for its usefulness. The fact that a gamma probe has a large distal field of view (FOV) is a factor that must be remembered in its employment in surgery. The final elements in the system are the electronics and readout. Since the scintillation detector provides a signal proportional to the energy of the gamma ray, it is possible to do some crude spectroscopy to set the sensitive energy range of the probe to select the desired gamma ray energy and eliminate at least part of the scattered gamma rays. The count rate of the probe is then fed to a rate-meter, which in turn drives an audio output. The surgeon uses this output, either an increase in loudness or an increase in frequency, to locate the tumor. The ratemeter itself is used to check the level of increased uptake after the tumor has been located. These basic elements are still used in a modern system, as shown in Fig. 3.

More recently, plastic scintillators have been employed to directly detect the positrons, rather than detect the annihilation radiation from positron-emitting radiopharmaceuticals. One such device [22], essentially the same as the design in Fig. 2, was developed after the very high tumor to tissue ratio of fluorine-18 5-fluorodeoxyuridine [23] was seen in positron emission tomography (PET) scans. A second system employs a long fiber optic cable [24, 25], and has been used to detect ^{18}F-fluorodeoxyglucose (FDG) in abdominal tumors.

Solid state detectors

The reduction in the use of GM tubes was due in part to the introduction of solid state detectors. The advantages of solid state detectors are generally that: (1) they have

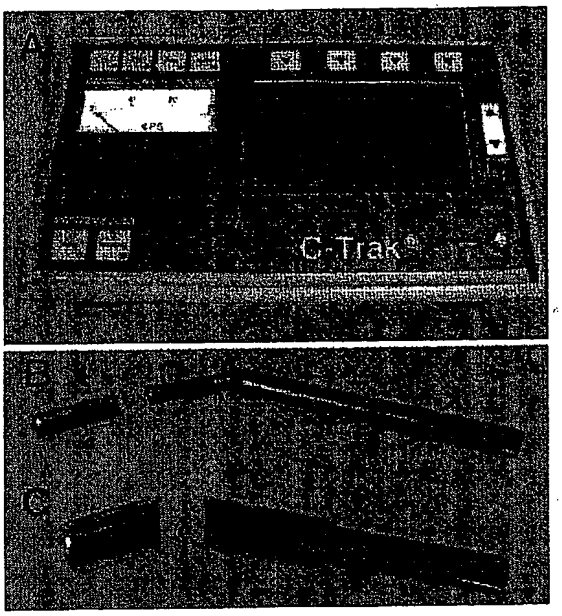

Fig. 3A–C. Scintillation detector-based intraoperative probe[21]. A Control unit with electronics, audio tone generator, ratemeter, and LCD (liquid crystal display) readout of counts; B ^{99m}Tc probe and collimator; C ^{111}In probe and collimator. (Courtesy of Carewise Medical Products Corp., Morgan Hill, CA)

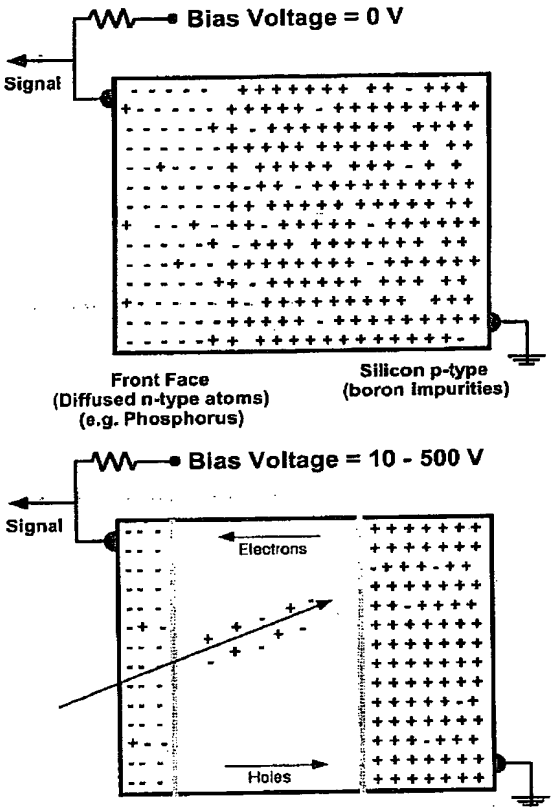

Fig. 4. Diagram of one method used to create a detector from a semiconductor. One surface of silicon with 1 ppm boron is diffused with phosphorus. A bias pulling the electrons to the phosphorus surface and holes to the other creates a carrier-free region. Radiation from gamma or beta rays will cause ionization in this region, and the electrons and holes are collected to provide the signal

better energy resolution, (2) they can be manufactured in very small sizes, and (3) they can have very thin entry windows to allow the counting of very low energy beta and gamma rays [26]. When radiation is absorbed by a solid state detector, ionization occurs by promoting electrons out of the bound state in the crystal to a free state called a conduction band, where the electrons can flow almost as freely as in a metal. The positive charge is carried in the opposite direction by the electric field by having the holes left by the excited electrons move to the opposite electrode. The motion of the holes in the crystal lattice is a key property of semiconductors (silicon, germanium, etc.). The free movement of the holes tends to occur only in very pure well-formed crystals, as impurities or disruptions in the crystal structure tend to trap or slow down the migration of the holes. As a result, solid state detectors tend to be very small and expensive. If the material is not pure, it is sometimes possible to manipulate the semiconductor with judicious addition of impurities. For instance silicon, which shares four valence electrons in the crystal, always has some level of impurities. If, as in Fig. 4, 1 part per million boron is added to the silicon, the boron with one less outer electron than silicon will fit into the matrix, creating excess "holes." The net effect is to reduce the number of electrons that are free to conduct current. If one face has a thin layer of phosphorus diffused into the surface, the pentavalent phosphorus will provide local suppression of the holes and an excess of electrons (upper part of Fig. 4). A bias across the device that draws the electrons to the left and holes to the right sweeps an area in the middle free of both kinds of charge carriers (lower part of Fig. 4). After the initial application of bias sweeps the central region free of charge carriers, the bias is trying to extract electrons from a sea of holes, and holes from a sea of elections. The net effect is very low current through the crystal. At this point if radiation is absorbed in the central region, the number of electron hole pairs produced is large compared with the leakage current, and the resulting pulse is collected and amplified for counting and/or energy measurement.

The earliest uses of solid state probes were as direct replacements for GM tubes to detect ^{32}P in eye tumors [27, 28]. The possibilities for miniaturization were demonstrated by Lauber [29] by placing a detector inside a

needle with an outside diameter of 1.1 mm and multiple detectors inside a 1.5-mm-diameter needle. These detectors were a variation of the silicon device in Fig. 4.

Avalanche detectors

The solid state detectors discussed above are analogous to gas ionization counters in that the electron hole pairs are created and simply collected by the electrodes. As in gas detectors, it is possible to design solid state detectors that have regions of very high electric field that accelerate the electrons to high velocities. At medium fields the amplification is controlled and the output is proportional to the input energy, and at high fields the output is large and independent of the input energy, much like a GM tube. This internal amplification is primarily amplification of the true signal, and the device has potentially better signal to noise ratios than the standard silicon detector. These devices are referred to as avalanche detectors.

The initial application of avalanche detectors was for plutonium contamination in the lungs of nuclear power plant workers [30]. The emissions were 13.5–20 keV L X-rays from the uranium daughter produced in plutonium decay. This application took advantage of the gain and good signal-to-noise ratio of the avalanche detector to detect these very low energy emissions. Production of avalanche detectors has been fraught with difficulties, and only recently has reemerged in some medical imaging applications.

Cadmium telluride detectors

Cadmium telluride (CdTe) detectors have a relatively high atomic number with respect to silicon: Cd and Te have atomic numbers of 48 and 52, respectively, while Si has a Z of 14. This translates into a factor of 100 improvement in the photoelectric stopping power for the 140-keV gamma ray from ^{99m}Tc. Thus, while the silicon-based probes were used in beta detection and low-energy gamma ray detection, the CdTe detectors could be used with the relatively high-energy gamma rays from ^{99m}Tc. One difficulty that has been seen with CdTe, the similar CdZnTe and CdHgTe, as well as HgI_2, is the trapping of holes in the material. This has had the practical effect of limiting the thickness of the detectors. As long as the radiation is absorbed near the surface, the holes have only a short distance to travel. This results in complete charge collection, and narrow, symmetric photopeaks. At higher energy, the interactions occur throughout the crystal, and a significant fraction of the charge is uncollected. This results in photopeaks with low energy tails, which essentially nullify the potential high resolution of this material. Even with this limitation, CdTe is the detector of choice for one of the most widely used intraoperative probe systems. The key to this success is the use of ^{125}I-labeled radiopharmaceuticals, with emissions ideally suited for CdTe's best energy range (27–37 keV). By limiting the system to ^{125}I, the detector can be relatively thin and low cost and the shielding/collimation requires only about 0.2 mm of lead for a factor of 1000 absorption of ^{125}I photons.

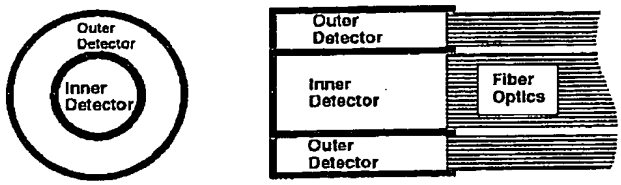

Fig. 5. Dual-detector configuration with cylindrical detector inside annular detector. Fiber optic bundles transport light to PMTs

Detector configurations

Until now the discussion has been about the basic detectors. There have been a number of ways in which multiple detectors have been configured to improve sensitivity or to measure or suppress background.

Dual-detector probes

The simplest configuration is the dual-detector probe, in which Hickernel [31] and Daghighian [22] used the second detector to provide a measure of the background. The basic configuration is shown in Fig. 5. In both cases there was an inner cylindrical detector and an outer annular detector with optical fiber bundles providing the optical coupling to the PMTs. Hickernel's system was for gamma ray detection and had lead shielding and collimation. The operating principle was that if the central detector had a higher count rate than the outer detector, the tumor was in the FOV.

Daghighian's system was designed to detect the positrons and the background was primarily the annihilation radiation produced in other parts of the body. Thus the outer detector was shielded from the positrons, and its count rate was assumed to be only the annihilation radiation. The system was calibrated with annihilation radiation before use to determine the ratio of the efficiencies of the inner and outer detectors for the 511-keV radiation. The count rate in the outer detector was multiplied by this ratio and subtracted from the inner detector online to give the net β^+ signal.

Coincident dual-detector probes

If the radioisotope of interest emits two gamma rays simultaneously, the probability that both gamma rays will

strike the same detector is the square of the probability that one will strike the detector. That is, if there is a 10% chance of one striking the detector, the second has essentially an equal 10% chance. Thus the probability of two gamma rays striking at the same time is 10% of 10% or 1%. For a 1-cm-diameter probe the sensitivity would be about 10% at 2 mm from the detector, 3% at 4 mm, 0.6% at 8 mm, and 0.05% at 16 mm. The drop in sensitivity for the detection of both gamma rays is a factor of 200 in 14 mm. This provides a system that is very sensitive to activity at or just below the surface and essentially immune to background events more than 2 cm away.

The simplest implementation of this technique is to use the sum peak on a single detector [32, 33]. For instance indium-111 emits a 171-keV and a 245-keV gamma ray almost simultaneously. If both strike the detector, the event will register as a 416-keV sum peak. By placing the energy window on the sum peak, the system is effectively selecting those events that are in coincidence. One problem with this method is that if the second gamma ray is from another decay and falls within about 1 μs of the first, the two unrelated events will sum to the same energy and will give a false event. One way to minimize these events is to use two detectors and accept only those events that are electronically measured to be within 10–100 ns of each other. This would reduce the error rate by a factor of 10–100. Saffer et al. [34] describe and model an array of detectors using the coincidence concept, extending the idea to include any pair of detectors in an array of detectors. Of course, a critical limitation to this approach is the requirement of an isotope with coincident gamma rays. This is the antithesis of the ideal isotope for most nuclear medicine procedures. The ideal choice has been considered to be a single gamma ray in the 100–200 keV range. Multiple gamma rays tend to lower image quality and increase patient dose.

Watabe et al. [35] used the dual coincidence probe concept in an unusual manner. The rate of accidental coincident events is proportional to the product of the rates on the two detectors. For a source that is moved to various distances from the detector pair, the accidental count rate will vary in the same manner as the coincidence count rate described above. Thus, if you have an isotope that only emits one gamma ray, there can be no true coincidences but rather only accidental coincidences. Monitoring the accidental rate would then have the same shallow depth of field described above. In addition, if one were to survey a region with tumors that were the same size, but with different amounts of isotope, the count rate over the hotter tumors would increase with the square of the activity. This would give an enhanced visibility to hotter tumors, or conversely, a diminished visibility to cooler tumors.

Stacked silicon detectors for beta detection

Raylman and Wahl [36, 37] have developed a solid state version of the dual detector of Daghighian et al. [22]. This device consists of two ion-implanted-silicon detectors with an 8-mm-diameter active area. The two detectors are stacked in such a manner that the second detector is shielded from all direct betas or positrons, ensuring that all events seen by the second detector are due only to the annihilation radiation. The two detectors are essentially identical in geometry and physical position relative to the flux of annihilation radiation from the body. Although there must be some calibration between the detectors, the count rate on the second detector is the background for the first detector. This means there is no variation due to a significantly different detector shape, which might distort the energy spectrum, as could be the case for the Daghighian device [22].

Summary of intraoperative probe instrumentation

In the first section of this review, the basic principles of intraoperative probe detectors were introduced. Each type of detector was described as a general category. There are many variations of the gas detector, solid state detector, and scintillation detector, and the reference list will provide a good starting point for those requiring a more detailed knowledge of a particular device. Most of the early work with probes is essentially anecdotal. Usually, a surgeon and an engineer or physicist find they have a mutual interest, and they work together to build a probe. We usually hear of this in a paper covering a few patients with some preliminary, and usually promising results.

Clinical applications

The key to continued use of a technology, such as an intraoperative probe, is a commercial interest in the product. Each surgeon cannot depend on developing a relationship with a nuclear engineer or physicist, to allow him access to detector technology. In recent years the industrial backing has been developing for the use of scintillator and cadmium telluride probes. A relatively widespread use of intraoperative probes has been developed based on these technologies.

A fairly extensive literature has been accumulating on the use of intraoperative probes in two specific applications: (1) A technique that is called radioimmunoguided surgery (RIGS) seems to be the most widely accepted application [38–76]. (2) A technique which allows the surgeon to identify the first lymph node downstream from a tumor, usually a melanoma or a breast tumor, has been rapidly gaining on RIGS as the most used procedure. The first node is the most likely place to find cancer cells, and if there are no cancer cells in this "senti-

nel" node, the probability that the cancer has spread is low, and vice versa [77–125].

Radioimmunoguided surgery (RIGS)

RIGS was developed as a measurement system by a commercial vendor (Neoprobe Corp., Columbus, Ohio). The radiolabeled compounds were monoclonal antibodies (MAbs) [126] of colorectal cancers. Many attempts to develop MAbs as nuclear medicine imaging agents were only partially successful. Among the difficulties was the time required for tumor uptake and blood clearance of the isotope. The times required varied from several days to more than 3 weeks [47]. Iodine was the labeling agent of choice, but the best imaging agent of the iodine isotopes is ^{123}I, which has only a 13.2-h half-life, much too short for these clearance times. The RIGS system allows for this long biological time course by using a relatively long-lived isotope, ^{125}I, which has a half life of 60 days. ^{125}I decays by electron capture to a 35.5-keV gamma-emitting state, most of which is internally converted. The emissions per decay are 6% 35.5-keV gamma rays, 115% 27-keV K_α x-rays, and 25% 31-keV K_β x-rays. The low energy of the emissions is useful for localizing activity because of the relatively short attenuation length. A 30 keV x-ray is attenuated by a factor of 2 in only 1.9 cm of water. The low energy provides two other benefits in terms of the instrumentation. First, the shielding/collimation only requires the equivalent of 0.2–0.3 mm of lead (1–1.5 mm stainless steel) to reduce background by a factor of 1700–70, 000. Second, RIGS uses CdZnTe (an improved version of CdTe), which, at these energies, is a very good detector with essentially no trapping to degrade resolution. Both of these factors reduce the weight requirements of the probe. The CdTe detector requires no PMT, just signal and bias lines and the thin shielding which means that the probe can weigh less than 0.3 kg [127].

The primary reason that the probe gives satisfactory results relative to imaging is the high sensitivity of the probe, which has open collimation similar to that shown in Fig. 2. Thus at close ranges the sensitivity per unit area is a factor of 1000 higher than with a gamma camera. RIGS has been used with some form of MAbs labeled with ^{125}I since the mid 1980s [46]. Essentially all the reports in the literature have been positive [38–43, 45–49, 51, 53, 54, 56–60, 62, 63, 65–67, 71–74, 76, 127]. One critical article about radioimmunotargeting (RIT) [70], which included RIGS as a special case, stated that RIGS with ^{125}I was the most successful of all the related RIT techniques. One key criticism was that it had not been shown that there was any improvement in patient survival. Since the bulk of the work has been performed in the 1990s, and this paper was written in 1995, it was probably too early to make a strong argument about patient survival. The other major criticism was that there have been no randomized clinical trials with patients treated by standard or RIGS-based procedures. Each group of patients has been chosen according to the criteria of the individual investigator to answer a different question. Most of the conclusions have been positive, but vague, with statements about RIGS being very useful and worthy of further investigation

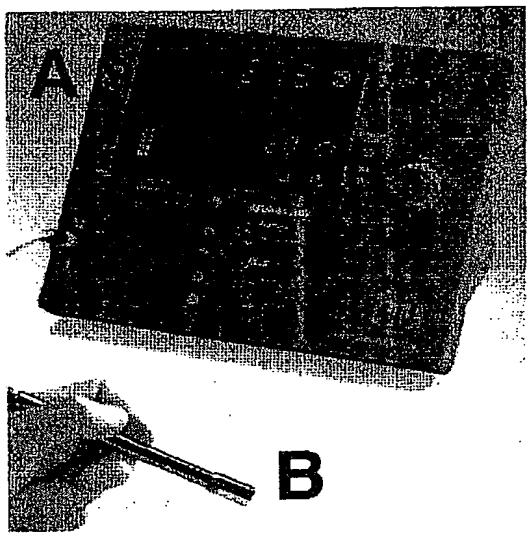

Fig. 6A, B. Picture of Neoprobe Model 2000 RIGS system. **A** Neoprobe neo2000 control unit with digital readout instead of ratemeter, and automated energy windowing. **B** One of the two probes currently available. Custom shielding and collimation are available for each isotope. (Courtesy of Neoprobe Corp., Dublin, Ohio)

The fact that the CdZnTe probe is available has led a number of investigators to look at other isotopes such as ^{99m}Tc, ^{111}In, ^{123}I, and ^{131}I [63, 69, 71]. The term RIGS is a registered trademark of Neoprobe, Corp.; however, the term seems to have been adopted by the field as a general term for any MAb gamma-guided intraoperative procedure (e.g., [68]). Neoprobe has adjusted to the use of other radionuclides by producing probes, electronics, and collimation appropriate for their use with the higher energy isotopes (Fig. 6, Table 1).

Location of sentinel nodes

The sentinel node concept [128] is that in the spread of melanoma or breast cancer, the metastasis will pass down the lymph system and deposit some cells in the first or "sentinel" lymph node. If the location of this node can be identified and it can be biopsied, the spread or the lack of spread of the cancer can be identified and many times the lymphatic drainage can be spared [125]. The sentinel node can be identified by injecting a ^{99m}Tc-labeled colloid in or around the tumor, and collecting a

Table 1. Manufacturers and properties of intraoperative probes

Manufacturer	Location	Model	Detector	Detector size
Capintec[a] in USA	6 Arrow Rd., Ramsey, N.J. USA	GAMMED II B	CdTe CsI(Tl) (Si photodiode)	5×5×3 mm 5 mm diam. by 10 mm
Eurorad[b] in Europe	23 rue de Loess, BP20, F-67037 Strasbourg Cedex 2, France	GAMMED II	CdTe CsI(Tl) (Si photodiode)	5×5×3 mm 5 mm diam. by 10 mm
Carewise[c]	P.O. Box 1655, Morgan Hill, CA 95038-1655, USA	C-Trak	Indium probe Technetium probe NaI(Tl) Mini-probe	25 mm[i] 19 mm[i] 15 mm[i]
DAMRI/ORIS[d]	Gif sur Yvette, France	Modelo 2	NaI(Tl)	5 mm diam. by 15 mm
Diagnostic Technologies[e]	150 Glover Ave., Norwalk, CT 06856, USA	Navigator GPS	CdTe	10 mm diam.
Intra Medical Imaging, LLC[f]	1444 Carmelina Ave., Suite 227, Los Angeles, CA 90025, USA	Node Seeker	LSO	8 mm diam. by 7 mm deep
Neoprobe[g] (RIGS)	425 Metro Place North, Suite 300, Dublin, OH 43017, USA	Neoprobe 1500 neo2000	CdZnTe CdZnTe	14 mm diam. 19 mm diam.
STRATEC Biomedical Systems AG[h]	Gewerbestr. 11, D-75217 Birkenfeld, Germany	Tec Probe 200	CsI(Na)	9.5 mm diam. by 15 mm

[a]Capintec Product Specification Catalog, volume 3, 1998, p.120. www.capintec.com
[b]www.eurio.net/eurio/eurorad.nsf/Probes [119, 130]
[c]www.carewise.com/
[d]Refs. [68, 130]
[e]www.ussurg.com
[f]www.intra-medical.com
[g]www.neoprobe.com/ and ref. [119]
[h]www.stratec-biomedical.de/Product_Line/TecProbe/tec-probe.html, refs. [51 130]
[i]Outer diameter of probe casing

series of images to follow the motion of the activity through the lymphatic system [79, 80, 129]. The dynamic part of the study allows the identification of the sentinel node in those cases where there are multiple visible nodes. The static image can be used to locate the node and the location is marked on the skin for the surgeon, who will then use a gamma probe to locate the node surgically. Figure 7 is the static image from a lympho-scintigraphy study.

One of the key features of the image is the high contrast of the sentinel node. The activity is almost solely confined to the lymph system and the tumor, with very little activity anywhere else in the body. The exceptions, of course, are those cases in which the anatomy of the patient places the sentinel node within or near to the injection site. With the nuclear medicine images as a guide, the surgeon can be confident in locating the node with a gamma probe. Again, the whole system must be considered in the procedure. In this case the contrast is so high that the requirements of the instrumentation are reduced. A simple scintillation probe is more than adequate for this type of procedure.

The earliest and greatest quantity of work has been in the diagnosis and treatment of melanoma [78, 82, 84, 88, 89, 92, 93, 98, 99, 101, 103, 105–107, 110, 111, 113, 114, 118, 120, 122–124]. The early work on sentinel nodes used a blue dye as the tracer, and the surgeon would use visual inspection of the lymph nodes to locate the sentinel node [128]. This technique was tricky to use [117]. [98]; not only was the use of the gamma probe more accurate, it was also easier to learn to use it effectively [95, 111]. There has been a strong interest in applying the sentinel node technique to breast cancer [85, 87, 90, 94–96, 104, 108, 109, 112, 115, 116, 121]. A large multicenter study on the use of the sentinel node technique in breast cancer was completed in 1998 [102]. It was positive, but still somewhat skeptical, basically saying that the method worked, but the accuracy depended on the physician. The technique has also been applied to squamous cell carcinoma [91, 100] and Merkel cell carcinoma [83].

Table 1 lists the manufacturers and some of the properties of intraoperative probes [119, 130]. Although Neoprobe had originally designed its system for ^{125}I, many

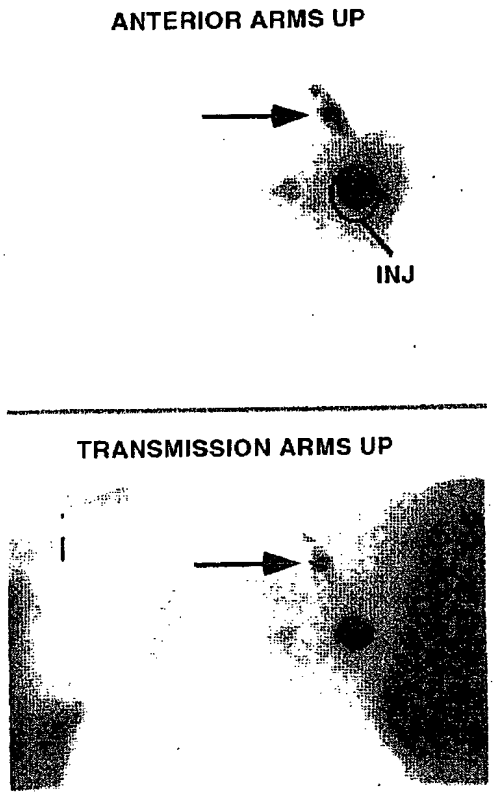

Fig. 7. A lymphoscintigraphy study to locate the sentinel node. In this case the activity has been injected in a breast tumor. In the *upper image*, the sentinel node is visualized (*arrow*), as well as the injection site and part of the activity still in the lymph system. The *lower image* is a transmission image of the patient, which gives the general layout out of the anatomy. If the patient were to be scheduled for a biopsy of the sentinel node, her skin would be marked, and the surgeon would use that mark and the image for the initiation of a gamma probe-guided procedure

sentinel node studies were done with Neoprobe systems. Neoprobe has added new models to its line of detectors. It should be noted that the companies listed in Table 1 have an evolving product line. Some products may have been modified or discontinued, and new products may have been added. Except in the case of DAMRI/ORIS, which is a spin-off of the French CEA, websites have been found and listed to give the reader access to the current product line of each manufacturer.

Summary of clinical applications

The manufacturers in Table 1 make various types of intraoperative probes readily available to the surgeon. They provide instruction in the use of the probes and service the product when there are problems. The industrial support has led to the availability of thousands of these devices at all types of hospitals, although most are in large medical centers. The use of the sentinel node technique requires only the support of a small nuclear medicine service to provide the ^{99m}Tc-labeled colloid and a set of images to help guide the surgeon. This relatively straightforward approach has led to widespread use, and has already spawned a number of editorials [130, 131] that advocate the technique and a number of review articles [77, 96 117, 119] to help teach and evaluate the concepts. In a number of cases, the technique is accepted as being the preferred approach.

The RIGS approach is a more difficult procedure. It requires the ability to work with the MAbs, and apparently the cost is relatively high [70]. Although it is being used in thousands of procedures, the added difficulty of using MAbs has slowed its general acceptance.

The future: imaging probes?

It is difficult to imagine what improvements in intraoperative probes could make a significant improvement in their performance. Even if the detector were perfect, with 100% photopeak efficiency and perfect resolution, the procedures are basically limited by the amount of isotope that can be injected. The next improvement would seem be the development of imaging probes. An imaging probe can cover a larger area than a nonimaging probe and still pinpoint the location of the activity. In cases of relatively poor signal to noise ratio, the image can show the distribution of the activity to pinpoint the hot area, whereas the nonimaging probe simply gives you a tone or an activity reading representing the average activity in the region. There are two types of device that can be considered for the job of an imaging probe: (1) A small probe, 1–2 cm in diameter, to be used as a beta imager. It would be designed for tissue contact readings and would employ low atomic number detectors to minimize interactions with background gamma or x-rays. (2) A gamma imager of the same dimensions as the beta camera, which utilizes higher atomic number detectors and a collimator.

Early intraoperative imaging probes

The earliest imaging probes were a set of prototypes that were developed and evaluated by Barber et al. in 1984 [132]. The devices were based on the concept of the coded aperture. Each probe was cylindrical with a stack of coaxial detectors, and a cylindrical axial collimator with holes that formed the coded aperture. They studied systems with aperture cylinders that rotated about the central detectors to give additional sampling and systems that were stationary to avoid the complication of the mo-

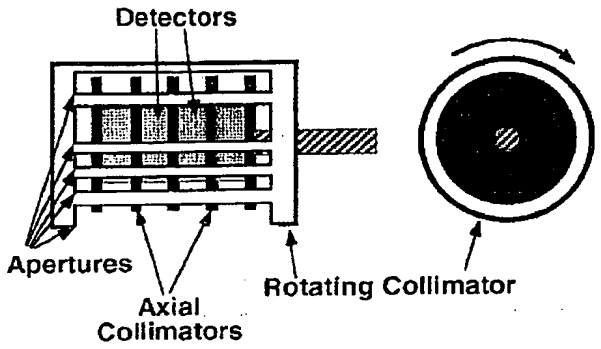

Fig. 8. Configuration of a possible coded aperture imaging probe. The rotating collimator would be inside a protective sleeve, and the diameter of the device could be relatively narrow

tion in system design. A possible configuration is shown in Fig. 8. In this case the coded aperture rotates about a central stack of detectors, which are isolated by axial collimators. The rotating mechanism must provide feedback so that the system knows the location of each aperture when a gamma ray strikes one of the detectors. After the data have been collected, the known response of the system allows the images to be reconstructed by a decoding procedure. The prototypes were capable of imaging high contrast objects, but gave less satisfactory results when the contrast was low. Since one point of going to the added sophistication of imaging was to allow the user to have an instrument that would allow additional discriminating power in lesion detection, the device did not fulfill its purpose and the development has not continued.

Woolfenden and Barber [133] mention the first of a series of semiconductor imaging probes in a review article in 1989. The system had an array of 21 2 mm by 2 mm individual CdTe detectors. The problem with individual detectors is that each pixel requires its own set of electronics, which can be very expensive for even a small imaging devices. The obvious, but difficult to achieve, answer is to have a detector array with some sort of multiplexed readout. Barber et al. [134] described and evaluated such an array in 1994. The device was a 48 by 48 Ge array with 125-μm pixels that utilized a multiplexor for data readout. The authors have used the technique with CdZnTe, but plan to use these devices in a single-photon emission tomography imager, not for imaging probes.

Beta imaging probes

One problem that rekindled interest in beta intraoperative probes was the difficulty of determining tumor margins in brain surgery. It is critical in such surgery that essentially all tumor tissue be removed, but because of the

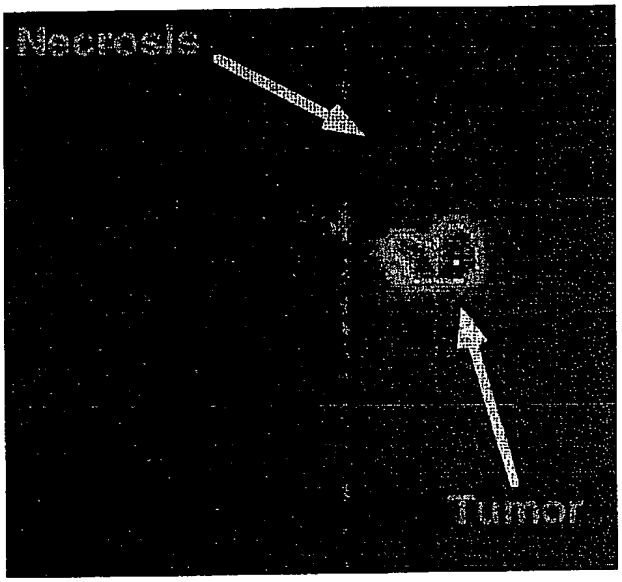

Fig. 9. PET image of ^{18}F-fluorodeoxyuridine demonstrating the high contrast of the tumor relative to healthy tissue in the brain.

possibility of injury to the patient, it is also important to minimize the loss of healthy tissue. The immediate impetus for a beta detector came from PET images of brain tumors with fluorine-18 fluorodeoxyuridine [23] (Fig. 9). The high contrast of ^{18}F-fluorodeoxyuridine made it an ideal agent to label a tumor for an intraoperative probe procedure. However, the high energy (511 keV) of the annihilation radiation would require a relatively large and unwieldy detector with heavy shielding. A more attractive approach was to detect the positrons directly, using a low Z detector, such as a plastic scintillator [22]. The low Z of the plastic greatly reduced the background from the annihilation radiation, and the dual-detector technique (Fig. 5) allowed the measurement and correction for the residual 511 keV background. The short range of the positrons would theoretically allow localization on the order of 1–2 mm.

Scintillator-based beta imaging probes

It was anticipated that the bulk of the tumor would be removed before the probe would be employed to locate residual bits of the tumor. In order to achieve good localization, it was necessary for the detector to be small (ca. 3 mm diameter), and this entailed a large number of readings on the tissue surface. One way to reduce the problem of the large number of readings was to use a relatively large imaging detector (ca. 12 mm diameter) which would allow good localization while covering a much larger area (by ca. a factor of 16). The initial con-

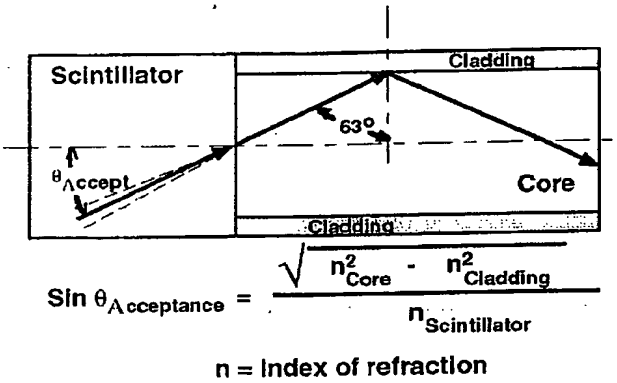

Fig. 10. A scintillator attached to a single clad optical fiber. For this case ncore = 1.59, nCladding = 1.42, and nScintillator = 1.43 for CaF_2(Eu), 1.85 for NaI(Tl), and 1.59 for plastic scintillators. The *solid arrow* in the scintillator indicates the acceptance angle for plastic scintillators (26.7°), and *dashed lines* are for NaI(Tl) (22.7) and CaF_2(Eu) (29.9)

cept of imaging probes was based on the use of scintillators coupled to photodetectors through fiber optics. A major problem with fiber optics was the fact that only a small fraction of the randomly oriented scintillation light would actually be transmitted down the fiber. Generally, fiber optics are noted for their ability to carry light long distances, but in such instances the light is from a source, such as a laser, directed down the center of the fiber. The situation for the probe is illustrated in Fig. 10.

An optical fiber consists of a core, which transports the light, and a thin cladding, which reflects light back into the core. In order for light to travel down a fiber optic, it must be traveling in a direction such that it will strike the cladding beyond the critical angle for total internal reflection between the cladding and core ($n_{core} > n_{Cladding}$). This limits the fraction of the light from the scintillator that will travel down the fiber optic. The fraction depends on the index of refraction of each component and a conc of acceptance is defined by the angle given in the equation in Fig. 10. Thus, if the angle of the light at the interface falls within the cone of acceptance, the light will be beyond the angle of total internal reflection in the fiber and it will be transmitted. The angles of acceptance for NaI(Tl), plastic, and CaF_2 are 22.7°, 26.7°, and 29.9°, respectively, which translate into the respective geometric efficiencies of 3.9%, 5.2%, and 6.7%. Plastic scintillators are the obvious low Z detector of choice for beta imaging, but the problem of getting a strong enough signal at the end of the fiber optic had to be solved. A plastic scintillator produces about 1000 scintillation photons for 100 keV of deposited energy. At 5% geometric efficiency, 50 photons would exit the fiber optic and a PMT would detect about ten of these. This signal strength was too low for a reliable clinical device, and improvement of the signal was given top priority.

In the work of MacDonald et al. [135, 136] a very sensitive solid state photon counter termed a visible light photon counter (VLPC) [137] was used instead of a PMT. The VLPC has a 60%–80% counting efficiency and was able to detect on the order of 30–40 photons per 100 keV. In addition, the VLPC has essentially no noise, and was capable of resolving events that consisted of one, two, or three photons. Thus, the signal to noise ratio was excellent for the 100–200 keV beta energies that would dominate the signal from ^{18}F. The major drawback of the VLPC was that it required cooling to just above liquid helium temperatures, and the problems associated with the cooling meant it was not a practical clinical device.

Fortunately, other aspects of the optimization process brought about an increase in the number of photons transported down the fiber optics. One of the primary improvements came from the realization that CaF_2 had almost ideal properties for this application. Its photon yield is 63% that of NaI and 231% that of a good plastic scintillator. Its low index of refraction means more of the signal will be transported down the fiber. The light yield at the PMT would be 109% that of an NaI(Tl) scintillator and 312% that of a plastic scintillator, or 30–60 photoelectrons in a PMT for 100- to 200-keV beta particles. In addition, the choice of reflector and detector thickness were optimized to increase the total photon flux down the fiber.

The design of an intraoperative beta imaging probe based on a scintillator and fiber optics is shown in Fig. 11 [138, 139]. In this system a thin disk of CaF_2 is the scintillator, and a disk of transparent plastic diffuses the light among a number of fiber optics arranged in a hexagon in the manner of the PMTs on early scintillation cameras.

In this system the diffuser thickness was chosen to provide a uniform flood field image as well as maintain good resolution. Figure 12 shows the flood field image as a function of diffuser image. In this image, the fiber optics are clearly visible with no diffuser in place and they disappear as the diffuser thickness is increased. The uniformity is essentially constant for thicknesses greater than 1.7 mm. However, the resolution was also seen to gradually decrease with the thickness of the diffuser, but at a surprisingly slow rate.

The spatial resolution was found to be 0.63±0.1 mm full-width at half-maximum (FWHM), when measured with a 0.1-mm slit transmission source. The system is designed to be placed in contact with the tissue of the patient with no collimator. The beta particles are emitted in all directions and ^{18}F was found to have an intrinsic spread on the order of 1.2 mm FWHM. The resolving power of this beta imaging system can be seen in the image in Fig. 13.

A potential problem with a beta imaging probe is the annihilation radiation that is present when the beta happens to be a positron [140]. It is possible to get a mea-

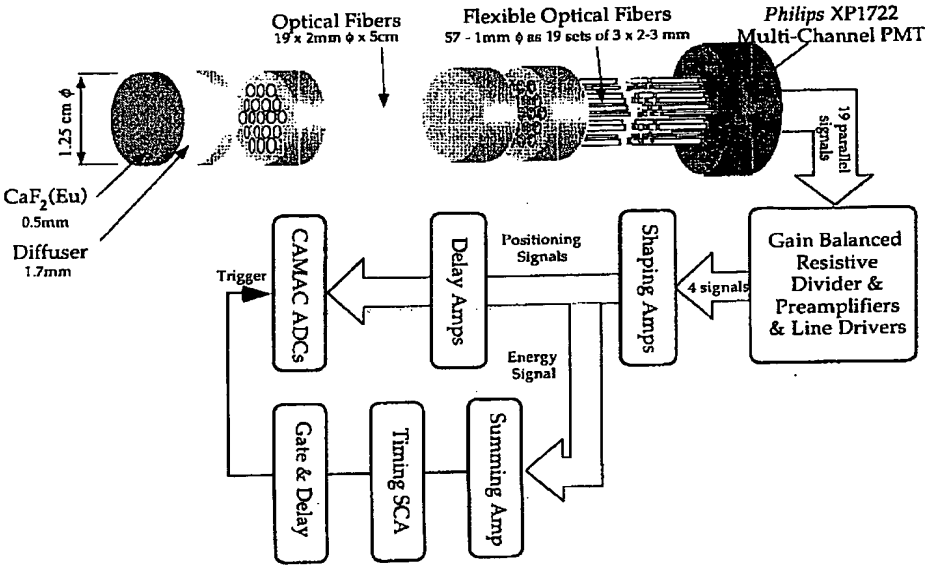

Fig. 11. Diagram of a beta imaging probe. The $CaF_2(Eu)$ disk is optically coupled to a diffuser which is then coupled to 19 2-mm-diameter optical fibers. This set of thick fibers with holders provides a rigid handle for the surgeon to hold. These are then couple to 2–3 m of flexible optical fibers that bring the signal to a multichannel PMT. The signals from the multichannel PMT are fed into a resistive divider network that provides X+, X-, Y+ and Y- positioning signals of the type used in scintillation cameras. These signals are then shaped, amplified, and fed to ADCs, while a sum of the signals is used to set an energy threshold and provide a trigger for the ADCs. This system is still in the prototype stage, and all electronics and data collection are performed with modular research systems

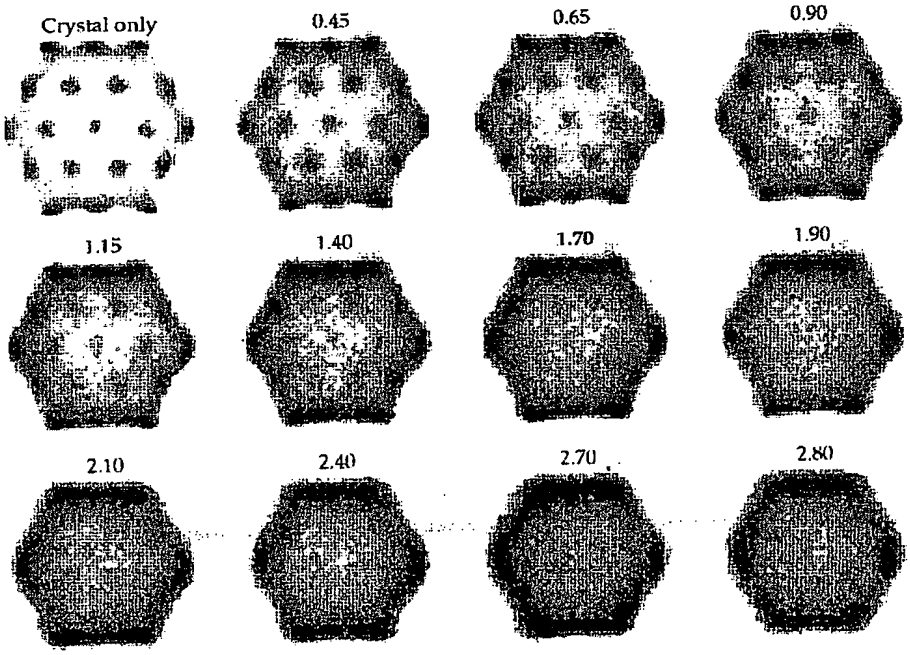

Fig. 12. Flood field images as a function of diffuser thickness. The data are taken with a ^{204}Tl point source at a distance. ^{204}Tl is a pure beta emitter with a maximum beta energy of 763 keV. It is used because it has a half-life of 3.8 years and the energy is conveniently close to that of ^{18}F

surement of this background by simply placing a plastic cap over the face of the imaging probe and taking a second image. In practice this would be cumbersome in a surgery, and it would be difficult to reproduce the position of the probe for the second measurement. A number of methods have been considered for suppression of this background [140–142]. One method that has been implemented and shown to work is illustrated in Fig. 14.

This type of system, generally referred to as a "phoswich," takes advantage of the difference in decay time of the scintillation light between the $CaF_2(Eu)$ and the high Z scintillator [gadolinium orthosilicate (GSO),

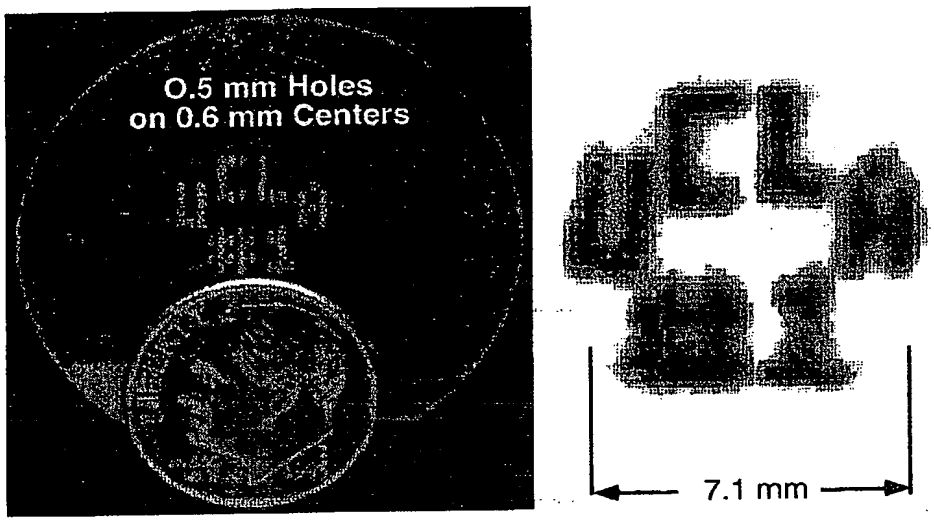

Fig. 13. Transmission image of holes in a copper disk with a ^{204}Tl beta source. The holes are at 0.6-mm centers, which is essentially the same as the resolution of the probe

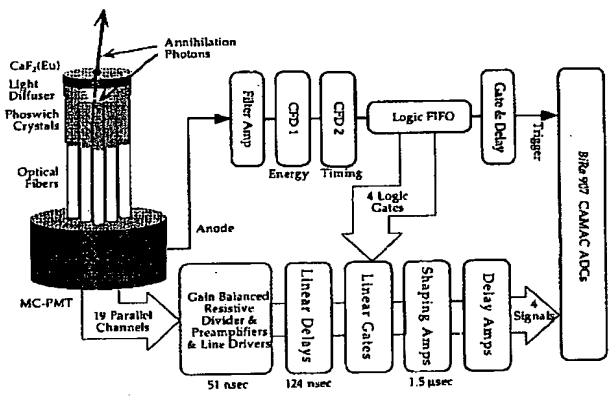

Fig. 14. Diagram of gamma-suppressing beta imaging probe. This system is based on the beta probe shown in Fig. 11, except for two key differences: (1) the first 1–2 cm of the 2-mm-diameter fiber optic is replaced by a high Z scintillation detector; (2) the signals are taken from the multichannel PMT anode, which is the sum of all channels, and these signals are used for energy discrimination and a time pickoff to determine when a gamma ray interacted with the high Z scintillator

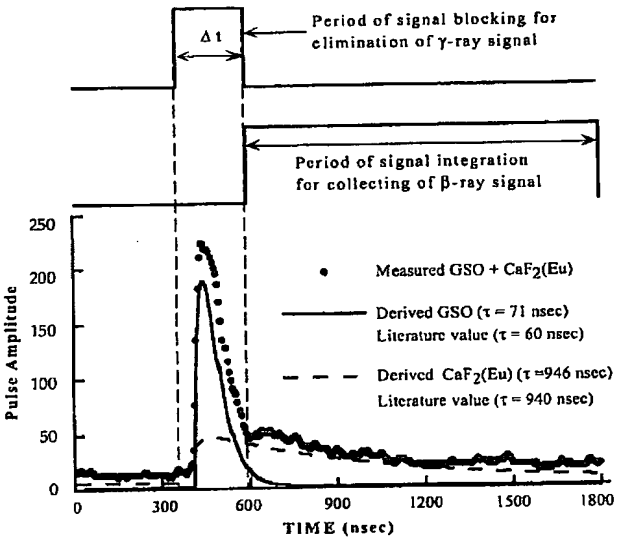

Fig. 15. Plot of phoswich signal from a digital oscilloscope in which the beta [CaF_2(Eu)] and gamma (GSO) components are both present (*dots*). A least squares fitting program was used to extract the two components from the signal with (τ) as a floating parameter. The results are given as a *solid line* (GSO) and a *dashed line* [CaF_2(Eu)]. In the diagram, it can be seen that a large fraction of the beta signal occurs after the GSO signal has gone

bismuth germanate (BGO), or lutetium orthosilicate (LSO)]. When the positron is absorbed by the CaF_2(Eu), the scintillation light passes through the high Z scintillator and down through the optical fibers to give a positioning signal. The positron also annihilates in the CaF_2(Eu) and gives off two 511-keV photons at 180° to each other. Since the high Z scintillators are coupled almost directly to the CaF_2(Eu), there is a very high probability that one of these photons will be detected by the high Z scintillator. The system requires that both types of event occur simultaneously before an event is considered valid. The manner in which this is achieved can be appreciated from the diagram in Fig. 15, which is a digitized version of the signal from the PMT.

In Fig. 15, it is seen that the fast GSO signal rises and falls in about 200 ns and because of this the amplitude is much greater than that of the CaF_2(Eu) signal. The problem with the GSO signal is that it bears very little relationship with the position of the beta signal, yet it must

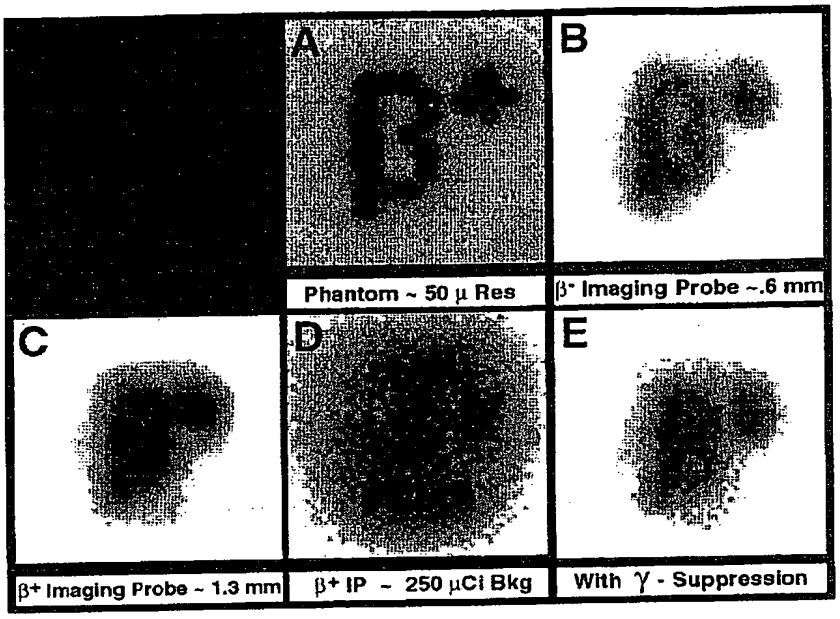

Fig. 16A–E. Images of β^+ phantom with various beta imaging system using ^{18}F. **A** A high-resolution autoradiographic system; **B** original beta imaging prototype (Fig. 11); **C** phoswich prototype with no out of field activity; **D** phoswich prototype with 250 mCi out of field activity, but with no gamma suppression; **E** phoswich prototype with 250 mCi out of field activity, but with gamma suppression

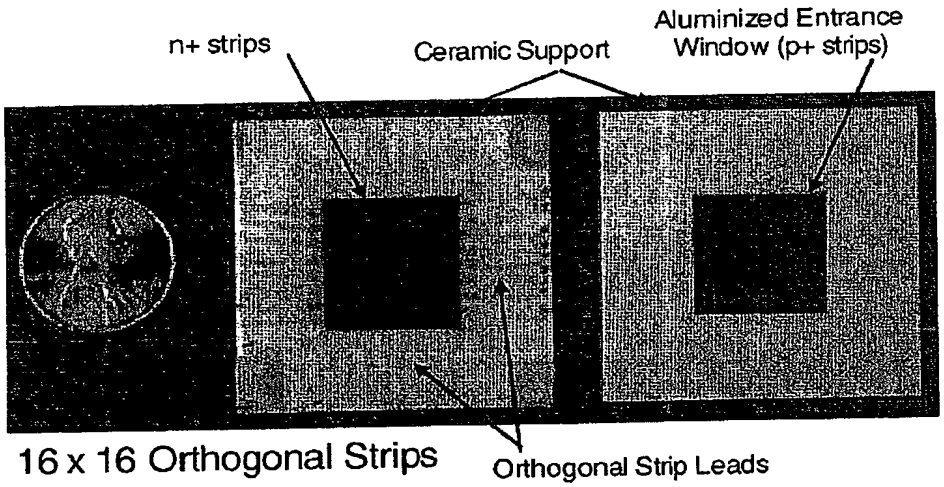

Fig. 17. Photograph of silicon strip prototype for beta imaging probe (front and back). The device is mounted on a large support for convenience in testing. The front face is covered with a thin layer of aluminum to allow the beta particles to penetrate but to block out light that would also produce a signal in the device. The strips have a pitch of 1 mm

travel down the same set of optical fibers. In order to eliminate the GSO signal, the ADC is blocked for about 250 ns, as indicated in Fig. 15, and then is opened for 1 μs to collect the $CaF_2(Eu)$ signal. The results from a prototype of this system are shown in Fig. 16. Cylindrical high Z scintillators were not available and 2 mm by 2 mm by 10 mm crystals were employed in the optical path for proof of principle. The better geometry cylindrical crystals will undoubtedly provide higher resolution results.

The phantom for Fig. 16 was a series of shallow 0.5-mm holes on 0.6-mm centers in the form of a β^+. The variable intensity is due to the difficulty of accurately pipetting volumes on the order of 0.2 μl. Image A was taken with an autoradiography system with 50-μm resolution. Image B was made with the system that produced Fig. 13. Image C was taken with the phoswich system with ^{18}F only in the phantom. The loss of resolution due to the square high Z scintillators is obvious. Image D was taken with 250 μCi in a 400-ml beaker behind the phantom but without gamma suppression, and image E is the same as image D but with suppression. The image is obliterated without suppression (D), and the suppression brings back an image (E) comparable in resolution to image C but noisier.

Solid state beta imaging probes

The use of solid state detectors for gamma probes has had problems due to trapping for high Z detectors and low sensitivity in the case of silicon. However, silicon has more than enough stopping power for beta particles. Recently significant progress in this area has been made in a collaboration between our laboratory and Photon Imaging, Inc. (Northridge, Calif.). Silicon as a direct detector for beta particles has been used for years. The application in this case is to create an imaging array from a small silicon wafer. The device is the same in principle to the one in Fig. 4, except that the electrodes on the front and back sides are made of 16 isolated strips. The backside collects the electron signal from horizontal strips (Fig. 17) to determine the "y" location of the event and the hole signal is collected on the front side from vertical strips to determine the "x" position of the event. Using strip detectors requires only 32 sets of electronics instead of the 256 channels required of fully pixelated devices.

Point sources of ^{18}F gave image resolutions of 1.5±0.07 mm FWHM. The energy resolution was found to be 3.6 keV. Additional preliminary results are given in Fig. 18. The spectrum of ^{18}F is shown directly and after a thin absorber blocked the positrons themselves. The gamma signal is seen to be about 2.5% of the total. A simple image task was done with the stick figure transmission phantom shown on the strip detector. The holes on the arms are at 1-mm centers. Although there is good suppression of the gamma background, it will probably be necessary to provide some method for suppression of subtraction of this background. One concept is to sacrifice the corners of the device with small beta shields. This would allow only gamma rays to be detected at the corners. The average gamma rate could then be subtracted from the image. This assumes there is no structure in the gamma data. A more accurate method would be similar to the "phoswich" method but without the use of the common signal path. PMTs of 10–13 mm diameter are available that could easily be incorporated into the handle of an imaging probe. Thus, a high Z scintillator could be coupled to a small PMT and have a strip detector mounted to its front end. Again, when a positron annihilates in the strip detector, the annihilation photons will strike the high Z scintillator, and the only valid events would have both signals. In this case the events would be recorded only if they occurred within 10–20 ns of each other. The phoswich method required a time window of 1 μs, which meant that there would be a 50–100 times greater probability that an accidental event would be accepted in the background for that technique compared with a true coincidence technique.

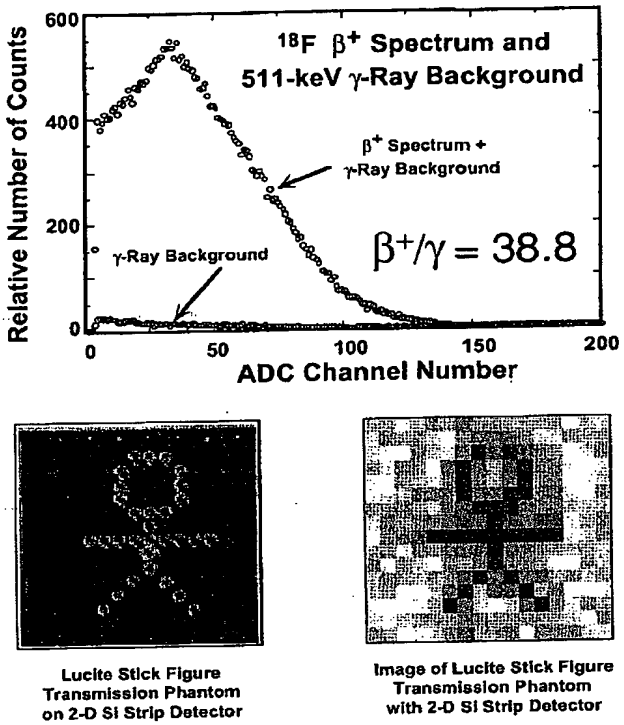

Fig. 18. Preliminary results from silicon strip beta imaging probe. Spectrum of beta and gamma rays from ^{18}F showing the suppression of gamma rays. Stick figure phantom to *left* on strip detector. Image of phantom on *right*

Radiopharmaceuticals for beta probes

An important part of the measurement system for beta imaging probes is the radiopharmaceutical. Most radiopharmaceutical development has emphasized gamma-emitters. The fact that positrons were also betas has been a problem rather than an advantage for PET. With beta probes, whether imaging or nonimaging, the fact that a PET image can be made with the tumor seeker can be an important advantage in planning the surgery. Thus far we have seen that ^{18}F-5-fluorodeoxyuridine [23] and ^{18}F-fluorodeoxyglucose [24, 25, 36, 37] have shown promise for beta probes.

^{99m}Tc has been the isotope of choice for most of nuclear medicine. The reasons for this choice have been its optimal gamma energy and the fact that it has no beta particle associated with its decay. A potential solution to this problem has recently become available in the form of a generator-based beta-emitting analog of ^{99m}Tc. The isotope in question is rhenium-188, which is the 17-h daughter of tungsten-188 (half-life 69 days). The isotope has only a small gamma component, which can be useful in its quality control. ^{188}W is available from double neutron capture on ^{186}W in a high-flux reactor [143, 144]. A

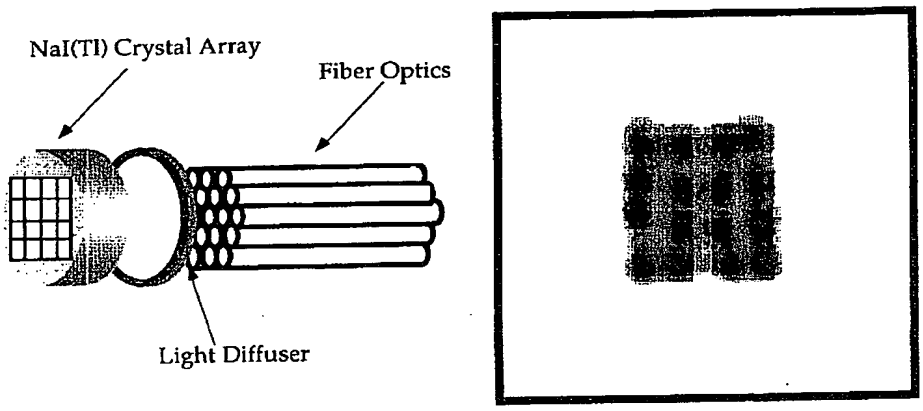

Fig. 19. Diagram of concept for gamma imaging probe. The diffuser and fibers produce an image of the crystal and all counts in each spot correspond to events absorbed in that crystal

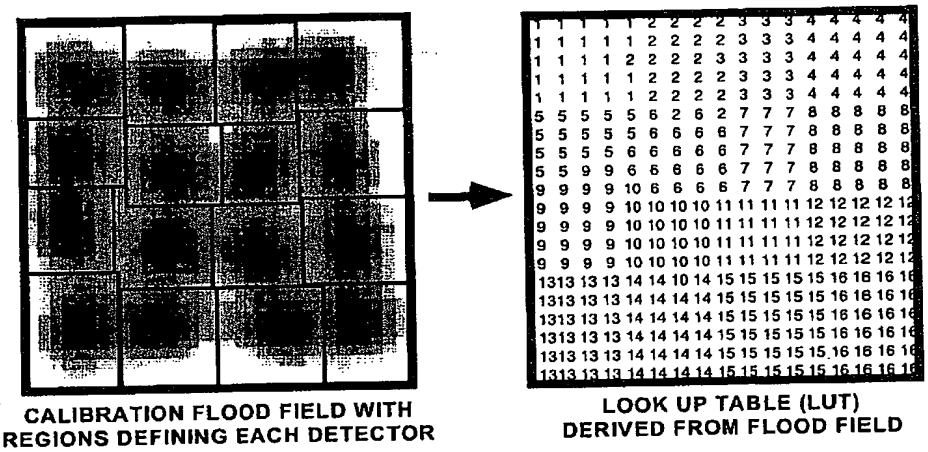

Fig. 20. The technique for creating a detector identification LUT for a discrete crystal imaging system. The calibration on the left allows the drawing of regions of interest (ROIs) on the image matrix. A detector number is assigned to each ROI, and the matrix elements corresponding to each ROI are set equal to these numbers. When image data are collected, the x and y data correspond to the LUT elements and are used to fetch the detector number from the table

$^{188}W/^{188}Re$ generator is available (Isotope Products Laboratories, Burbank, Calif.). Re is in the same column in the periodic table as Tc, and because it is above the lanthanides and is subject to a phenomenon known as the lanthanide contraction, it has a size almost identical to Tc. Its chemistry is in many cases almost identical to that of Tc (e.g., the generator column and eluent are essentially the same as with Tc). An encouraging aspect is that a number of groups are working with this generator system to produce tumor-seeking compounds that can be used for radiotherapy [145–151]. The tumor to tissue ratio requirement is much higher for therapy than diagnosis because of the very high doses used in therapy. Thus, a compound that might be considered inadequate for therapy could be almost perfect for use with a beta imaging probe. Its similarity to technetium means that preliminary localization can be done with ^{99m}Tc and a scintillation camera, as in the sentinel node work.

Gamma imaging probes

Barber and Woolfenden first introduced the concept of gamma imaging probes [134, 152], but used the technology to pursue other avenues. Another approach that used a HgI_2 crystal set up as a 16 by 16 array was successful as a prototype, but was abandoned for more practical approaches based on silicon technology [153]. In our laboratory, the gamma imaging probe was approached in a manner similar to the beta probe. Instead of $CaF_2(Eu)$, NaI(Tl) was the scintillator of choice. Initially a continuous detector was considered, but a 6- to 8-mm-thick by 12-mm-diameter crystal did not allow for good image resolution and thinner crystals did not have the required sensitivity [154]. Crystal arrays allowed for both good resolution and high efficiency, but required that we borrow the principle of the PET block for implementation [154, 155].

The basic physical arrangement is shown in Fig. 19. The light coming from the crystal array is detected as an image of the crystals. The counts in each spot correspond to events in the particular crystal and a large number of

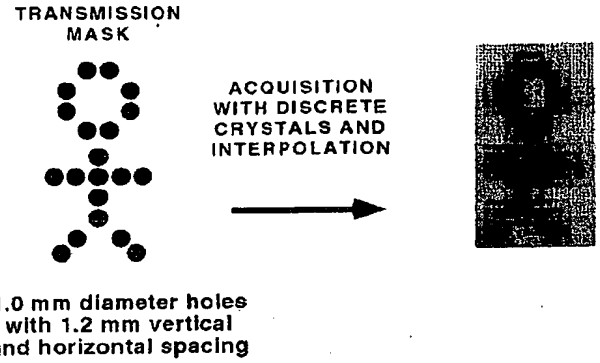

Fig. 21. Image of stick figure similar to that in Fig. 18, except that the absorber is lead instead of plastic. Since the array was only 4 by 4 it was necessary to scan it over the phantom to get an image of the whole figure, and interpolation was done to obtain a less pixelated image

small crystals are required for an image. In order to turn the spot pattern into an image the pattern is decoded in a look up table (LUT). The data from the system are simple x and y values corresponding to the apparent position of the scintillation light. The image of the spot pattern from a flood source is stored in an appropriate sized matrix. This image is shown in Fig. 20. On this calibration image, a set of regions of interest is drawn, and a matrix of numbers with dimensions the same as the image size is created. The values in the matrix correspond to the detector number that is associated with that part of the image. Thus when an x and y combination from the ADCs provide an address location in the matrix, that location is read and it contains the detector number. The location in the image being collected is then incremented by one.

A sample of an image taken with this 4 by 4 matrix is shown in Fig. 21. In this case the crystal array was scanned to get the full image. The intrinsic resolution of a discrete crystal system is defined by the crystal size, and the system resolution will then be defined by the collimator geometry and to some extent by the septal thickness.

Summary

The technology for both beta and gamma intraoperative imaging probes is in place and has been tested on prototype units. Methods have been developed based on scintillation crystals coupled to PMTs with optical fibers. The technology has been developed for suppression of the background due to the gamma rays and annihilation radiation that is associated with a number isotopes. The resolutions achieved are compatible with ^{18}F, which is the lowest energy beta that is likely to be useful with beta imaging probes. If ^{188}Re is developed as a radiopharmaceutical for intraoperative beta probes, there should be a general improvement in the method. ^{188}Re has maximum beta energies of 1.98 and 2.13 MeV, which will cause some blurring of the image, but it also means that there is greater penetration of the tissue. However, the higher energy means the detector window can be stronger and the signal produced in the detector will be higher. For the future, the silicon strip detector has superior properties for the beta imaging probe. The intrinsic resolution, which is already excellent, can be improved by simply making narrower strips. The energy resolution for the prototype was on the order of 3.6 keV, which is superior to that for any imaging detector being considered at this time. The excellent energy resolution allows for the possibility of using energy windowing to provide depth information (i.e., the lower energy betas would tend to originate in deeper tissue, while high energy betas would tend to come from the surface.).

The gamma imaging probe has a major problem in that it would require a collimator for imaging, which would cause an unacceptable drop in sensitivity. The strength of essentially all the intraoperative probes discussed in this review is their high sensitivity. The detectors are only collimated by a "tube" of absorber to eliminate radiation from the side. Even the beta imaging probe is wide open, and when placed against the tissue, it has almost 50% geometric efficiency.

The most likely nuclear medicine intraoperative imaging system would be one of the small scintillation cameras being developed for breast imaging [156–159]. There are a number of cameras reported in the literature that are based on position-sensitive PMTs [156, 157,159], and these have fields of view ranging from 5 cm by 5 cm to a 10 cm diameter. These devices have more bulk than is desirable, but they are much smaller than the portable scintillation camera that is common in the nuclear medicine clinic. In the long run, the PMT cameras should be replaced by cameras consisting of scintillators coupled to solid state photodiode arrays [158]. In these systems the photodetector is an array of photodiodes on a single wafer of silicon. The scintillator can be a continuous crystal or a matrix of crystals designed to be coupled one to one with the elements on the wafer. Early testing shows energy resolutions averaging 8.7% FWHM for ^{99m}Tc for a set of 16 pixels, and best resolution of the set of 6.4% FWHM. The crystal plus electronics need to only be 1–2 cm thick for such a system. With a shallow depth of field collimator, the system could be less than 5 cm thick by perhaps 12 cm in diameter. It would be small enough to bring into a surgery and large enough to image the whole area under suspicion. The high efficiency shallow field collimator and the fact that it might only require a single view of the surgical field would make it the choice relative to a small intraoperative gamma imaging probe.

Discussion

Intraoperative probes have a history of more than 50 years. Yet it is only in the past 10 years that their use has had an impact. In the first 40 years (1946–1986), the field consisted primarily of physician–physical scientist collaborations in the fine tradition of interdisciplinary collaboration. The individuals would meet and find out that together they had a potential solution for a problem. In this case the problem was locating tumors in surgery. They would build a probe system, employ it on a few cases, and publish a paper. Then there was little follow up. A wide variety of technology was employed from the simplest of GM tubes to scintillation detectors to the most advanced solid state detector systems.

Essentially every radiation detector system that could be miniaturized was tested or at least suggested as an intraoperative probe. Many of these systems were good solutions for the instrumentation aspects of the problem. In the last 10+ years, commercial support has developed for the concept. Neoprobe and Carewise seem to dominate the market, but a number of other companies (Table 1) are also supporting the market. Because of this support, a surgeon can simply buy the probe, and the company will supply basic training and technical support. Because of this, it is the surgeon, not the nuclear medicine physician, who is driving the research and development in this field [131]. This can also be inferred from the names of the journals dominating the reference list for this review.

Two types of procedure dominate the literature, and presumably, the clinical practice. Each of these has the properties of a good measurement system, which ensure a good level of success. The first, the RIGS system, overcomes some of the problems of MAbs by using a long-lived label (^{125}I), which gives a much higher contrast at the time of surgery. The low energy of the emissions gives better localization because the absorption of the radiation in tissue causes a rapid drop in signal with distance. The good signal to noise and energy resolution of the detector allow it to be used reliably at such low energy. Any lack of total acceptance of RIGS is due to the checkered history of MAbs as reliable imaging agents. The second procedure is the localization of the sentinel node. Again the nature of the localization is key. In many cases (e.g., Fig. 7), the sentinel node is a "light bulb" with very little background. With the imaging study as a guideline, the localization and biopsy of the sentinel node with an intraoperative probe is becoming a standard procedure. It is sometimes the preferred procedure. Part of the success of this procedure is attributable to the fact that the process that is being observed is the well-understood drainage through the lymph system. Thus, the surgeon is confident of the interpretation of the images and the count rates seen with the probe. It is not clear that improvement in the detectors for intraoperative probes will significantly improve their usefulness. Therefore, a completely different capability, that of imaging, will most likely provide the next major advance in intraoperative probes. Prototypes of beta imaging probes demonstrate the potential of this approach. The use of beta imaging is efficient because no collimator is employed and is highly localizing because of the short range of the beta. On the other hand an equivalent gamma imaging probe has a problem with sensitivity, particularly if a number of images are required over the area of the surgical field. The solution for gamma imaging during surgery is likely to be small scintillation cameras that can image all or most of the surgical field in a single view while still being small enough to be relatively unobtrusive.

Conclusion

The development of the various intraoperative probes systems is another example of the success of interdisciplinary collaborations. However, it is seen that until there is commercial support of such a system, little more than anecdotal research is produced. Many of the early probe systems had the same capability as the systems that are now supplied by commercial vendors, but in the past there was no infrastructure to support the nonexpert user. The supply of the probes and support to the user is as important to the success of this technique as the original development of the probes. The RIGS and sentinel node procedures have established intraoperative probes as useful procedures. Whether or not imaging probes can have a similar impact has yet to be seen. If the past can be used as a predictor, the commercial support of imaging probes will be the key to their success.

Acknowledgements. This work was supported in part by DoE Contract DE-FC03–87ER60615.

References

1. Low-Beer B. Surface measurements of radioactive phosphorus in breast tumors as a possible diagnostic method. *Science* 1946; 104: 399.
2. Moore GE. Use of radioactive diiodofluorescein in the diagnosis and localization of brain tumors. *Science* 1948; 107: 569–571.
3. Selverstone B, Solomon AK. Radioactive isotopes in the study of intracranial tumors. *Trans Am Neurol Assoc* 1948; 73: 115–119.
4. Selverstone B, Solomon AK, Sweet WH. Location of brain tumors by means of radioactive phosphorus. *JAMA* 1949; 140: 227–228.
5. Selverstone B, Sweet WH, Robinson CV. The clinical use of radioactive phosphorus in the surgery of brain tumors. *Ann Surg* 1949; 130: 643–651.
6. Nakayama K. Diagnostic significance of radioactive isotopes in early cancer of the alimentary tract, especially the esophagus and the cardia. *Surgery* 1956; 39: 736–759.

7. Thomas CI, Krohmer JS, Storaasli JP. Detection of intraocular tumors with radioactive phosphorous. *Arch Ophthalmol* 1952; 47: 276–286.
8. Robinson C, Peterson R. A study of small ether argon Geiger-Müller counters. *Rev Sci Instrum* 1948; 19: 911–914.
9. Robinson CV, Selverstone B. Localization of brain tumors at operation with radioactive phosphorus. *J Neurosurg* 1958; 15: 76–83.
10. Ackerman NB, Shahon DB, Marvin JF. The diagnosis of thyroid cancer with radioactive phosphorus. *Surgery* 1960; 47: 615–622.
11. Nelson RS, Dewey WC, Rose RG. The use of radioactive phosphorus ^{32}P and a miniature Geiger tube to detect malignant neoplasia of the gastrointestinal tract. *Gastroenterology* 1964; 46: 8–15.
12. Williamson M, Boyd CM, McGuire EL, Angtuaco T, Westbrook KC, Lang NP, Alston J, Broadwater JR, Navab F, Bersey ML. Precise intraoperative location of gastrointestinal bleeding with a hand-held counter (work in progress). *Radiology* 1986; 159: 272–273.
13. Harris CC, Bigelow RR, Francis JE, Kelley GG, Bell PR. A CsI(Tl)-crystal surgical scintillation probe. *Nucleonics* 1956; 14: 102–108.
14. Morris AC Jr, Barclay TR, Tanida R, Nemcek JV. A miniaturized probe for detecting radioactivity at thyroid surgery. *Phys Med Biol* 1971; 16: 397–404.
15. Swinth KL, Ewins JH. Biomedical probe using a fiber-optic coupled scintillator. *Med Phys* 1976; 3: 109–112.
16. Colton C, Hardy JG. Evaluation of a sterilizable radiation probe as an aid to the surgical treatment of osteoid-osteoma. *J Bone Joint Surg Am* 1983; 65: 1019–1022.
17. Barber HB, Woolfenden J, Donahue DJ, Nevin WS. Small radiation detectors for bronchoscopic tumor localization. *IEEE Trans Nucl Sci* 1980; 27: 496–502.
18. Harvey WC, Lancaster JL. Technical and clinical characteristics of a surgical biopsy probe. *J Nucl Med* 1981; 22: 184–186.
19. Woolfenden J, Nevin W, Barber HB, Donahue DJ. Lung cancer detection using a miniature sodium iodide detector and cobalt-57 bleomycin. *Chest.* 1984; 85: 84-88.
20. Knoll GF, Lieberman LM, Nishiyama H, Beierwaltes WH. A gamma ray probe for the detection of ocular melanomas. *IEEE Trans Nucl Sci* 1972; 19: 76–80.
21. "Technical Specifications of the C-Trak Surgical Guidance System", 1999.
22. Daghighian F, Mazziotta J, Hoffman EJ, Shenderov P, Eshaghian B, Siegel S, Phelps ME. Intraoperative beta probe: a device for detecting tissue labeled with positron or electron emitting isotopes during surgery. *Med Phys* 1994; 21: 153–157.
23. Abe Y, Fukuda H, Ishiwata K, Yoshioka S, Yamada K, Endo S, Kubota K, Sato T, Matsuzawa T, Takahashi T, Ido T. I. Tumor uptakes of [F-18]-5-fluorouracil, [F-18]-5-fluorouridine, and [F-18]-5-fluorodeoxyuridine in animals. *Eur J Nucl Med* 1983; 8: 258–261.
24. Raylman RR, Wahl RL. A fiber-optically coupled positron-sensitive surgical probe. *J Nucl Med* 1994; 35: 909–913.
25. Raylman RR, Fisher SJ, Brown RS, Ethier SP, Wahl RL. Fluorine-18-fluorodeoxyglucose-guided breast cancer surgery with a positron-sensitive probe: validation in preclinical studies. *J Nucl Med* 1995; 36: 1869–1874.
26. Knoll G. *Radiation detection and measurement, 2nd edn.* New York: John Wiley, 1989.
27. Pircher FJ, Anderson B, Cavanaugh PJ, Sharp KW. Experiences with a solid state detector for surface counting of phosphorus-32. *J Nucl Med* 1967; 8: 444–450.
28. Larose JH, Jarrett WH, Hagler WS, Palms JM, Wood RE. Medical problems in eye tumor identification. *IEEE Trans Nucl Sci* 1971; 18: 46–49.
29. Lauber A. Development of miniaturized solid state detectors for the measurement of beta and gamma radiation in superficial and deep parts of living tissue. *Nucl Instrum Methods* 1972; 101: 545–550.
30. Moldofsky PJ, Swinth KL. Avalanche detector arrays for in vivo measurement of plutonium and other low activity, low energy emitters. *IEEE Trans Nucl Sci* 1972; 19: 55–63.
31. Hickernell TS, Barber HB, Barrett HH, Woolfenden JM. Dual-detector probe for surgical tumor staging. *J Nucl Med* 1988; 29: 1101–1106.
32. Matherson KJ, Barber HB, Barrett HH, Hartsough NE, Woolfenden JM. In: Klaisner L, ed. *Conf. Record of the 1993 IEEE Nucl. Sci. Symp. & Med. Imag. Conf., vol 2.* San Francisco: IEEE; 1993: 1312–1316.
33. Hartsough NE, Barrett HH, Barber HB, Woolfenden JM. Intraoperative tumor detection: relative performance of single-element, dual-element, and imaging probes with various collimators. *IEEE Trans Med Imaging* 1995; 14: 259–265.
34. Saffer JR, Barrett HH, Barber HB, Woolfenden JM. Surgical probe design for a coincidence imaging system without a collimator. *Image and Vision Computing* 1992; 10: 333–341.
35. Watabe H, Nakamura T, Takahashi H, Itoh M, Matsumoto M, Yamadera A. Development of a miniature gamma-ray endoscopic probe for tumor localization in nuclear medicine. *IEEE Trans Nucl Sci* 1993; 40: 88–94.
36. Raylman RR, Wahl RL. Evaluation of ion-implanted-silicon detectors for use in intraoperative positron-sensitive probes. *Med Phys* 1996; 23: 1889–1895.
37. Raylman RR, Wahl RL Beta-sensitive intraoperative probes utilizing dual, stacked ion-implanted silicon detectors: proof of principle. *IEEE Trans Nucl Sci* 1998; 45: 1730–1736.
38. Arnold MW, Schneebaum S, Berens A, Petty L, Mojzsik C, Hinkle G, Martin EW Jr. Intraoperative detection of colorectal cancer with radioimmunoguided surgery and CC49, a second-generation monoclonal antibody. *Ann Surg* 1992; 216: 627–632.
39. Arnold MW, Schneebaum S, Berens A, Mojzisik C, Hinkle G, Martin EW Jr. Radioimmunoguided surgery challenges traditional decision making in patients with primary colorectal cancer. *Surgery* 1992; 112: 624–630.
40. Arnold MW, Young D, Hitchcock CL, Schneebaum S, Martin EW Jr. Radioimmunoguided surgery in primary colorectal carcinoma: an intraoperative prognostic tool and adjuvant to traditional staging. *Am J Surg* 1995; 170: 315–318.
41. Bell J, Mojzisik C, Hinkle. G, Derman H, Schlom J, Martin EW Intraoperative radioimmunodetection of ovarian cancer using monoclonal antibody B72.3 and a portable gamma-detecting probe. *Obstet Gynecol* 1990; 76: 607–611.
42. Kim JA, Triozzi PL, Martin EW Jr. Radioimmunoguided surgery for colorectal cancer. *Oncology* 1993; 7: 55–64.
43. Martin EW Jr., Carey LC. Second-look surgery for colorectal cancer. The second time around. *Ann Surg* 1991; 214: 321–327.
44. Nieroda CA, Mojzisik C, Sardi A, Ferrara P, Hinkle G, Thurston MO, Martin EW Jr. The impact of radioimmunoguided surgery (RIGS) on surgical decision-making in colorectal cancer. *Dis Colon Rectum* 1989; 32: 927–932.

45. Nieroda C, Mojzisik C, Sardi A, Ferrara P, Hinkle G, Thurston MO, Martin EW Jr. Radioimmunoguided surgery in primary colon cancer. *Cancer Detect Prev* 1990; 14: 651–656.
46. O'Dwyer PJ, Mojzisik CM, Hinkle GH, Rousseau M, Olsen J, Tuttle SE, Barth RF, Thurston MO, McCabe DP, Farrar WB, Martin EW Intraoperative probe-directed immunodetection using a monoclonal antibody. *Arch Surg* 1986; 121: 1391–1394.
47. Sardi A, Workman M, Mojzisik C, Hinkle G, Nieroda C, Martin EW Intra-abdominal recurrence of colorectal cancer detected by radioimmunoguided surgery (RIGS system). *Arch Surg* 1989; 124: 55–59.
48. Waddington WA, Davidson BR, Todd-Pokropek A, Boulos PB, Short MD. Evaluation of a technique for the intraoperative detection of a radiolabelled monoclonal antibody against colorectal cancer. *Eur J Nucl Med* 1991; 18: 964–972.
49. Schneebaum S, Arnold MW, Houchens DP, Greenson JK, Cote RJ, Hitchcock CL, Young DC, Mojzisik CM, Martin EW Jr. The significance of intraoperative periportal lymph node metastasis identification in patients with colorectal carcinoma. *Cancer*. 1995; 75: 2809–2817.
50. Nabi H, Doerr RJ, Balu D, Rogan L, Farrell EL, Evans NH. Gamma probe assisted ex vivo detection of small lymph node metastases following the administration of indium-111-labeled monoclonal antibodies to colorectal cancers. *J Nucl Med* 1993; 34: 1818–1822.
51. Adams S, Baum RP, Hertel A, Wenisch HJ, Staib-Sebler E, Herrmann G, Encke A, Hšr G. Intraoperative gamma probe detection of neuroendocrine tumors. *J Nucl Med* 1998; 39: 1155–1160.
52. Aflab F, Stoldt HS, Testori A, Imperatori A, Chinol M, Paganelli G, Geraghty J. Radioimmunoguided surgery and colorectal cancer. *Eur J Surg Oncol* 1996; 22: 381–388.
53. Arnold MW, Hitchcock CL, Young D, Burak WE Jr., Bertsch DJ, Martin EW Jr. Intra-abdominal patterns of disease dissemination in colorectal cancer identified using radioimmunoguided surgery. *Dis Colon Rectum* 1996; 39: 509–513.
54. Badalament RA, Burgers JK, Petty LR, Mojzisik CM, Berens A, Marsh W, Hinkle GH, Martin EW Jr. Radioimmunoguided radical prostatectomy and lymphadenectomy. *Cancer*. 1993; 71: 2268–2275.
55. Benevento A, Dominioni L, Carcano G, Dionigi R. Intraoperative localization of gut endocrine tumors with radiolabeled somatostatin analogs and a gamma-detecting probe. *Semin Surg Oncol* 1998; 15: 239–244.
56. Burak WE Jr., Schneebaum S, Kim JA, Arnold MW, Hinkle G, Berens A, Mojzisik C, Martin EW Jr. Pilot study evaluating the intraoperative localization of radiolabeled monoclonal antibody CC83 in patients with metastatic colorectal carcinoma [see comments]. *Surgery* 1995; 118: 103–108.
57. Cohen AM, Martin EW Jr., Lavery I, Daly J, Sardi A, Aitken D, Bland K, Mojzisik C, Hinkle G. Radioimmunoguided surgery using iodine 125 B72.3 in patients with colorectal cancer. *Arch Surg* 1991; 126: 349–352.
58. Cote RJ, Houchens DP, Hitchcock CL, Saad AD, Nines RG, Greenson JK, Schneebaum S, Arnold MW, Martin EW Jr. Intraoperative detection of occult colon cancer micrometastases using ^{125}I-radiolabeled monoclonal antibody CC49. *Cancer* 1996; 77: 613–620.
59. de Nardi P, Stella M, Magnani P, Paganelli G, Mangili F, Fazio F, di Carlo V. Combination of monoclonal antibodies for radioimmunoguided surgery. *Int J Colorectal Dis* 1997; 12: 24–28.
60. Di Carlo V, Stella M, De Nardi P, Fazio F. Radioimmunoguided surgery: clinical experience with different monoclonal antibodies and methods. *Tumori*. 1995; 81: 98–102.
61. Di Carlo V, De Nardi P, Stella M, Magnani P, Fazio F. Preoperative and intraoperative radioimmunodetection of cancer pretargeted by biotinylated monoclonal antibodies. *Semin Surg Oncol* 1998; 15: 235–238.
62. Greiner JW, Smalley RV, Borden EC, Martin EW, Guadagni F, Roselli M, Schlom J. Applications of monoclonal antibodies and recombinant cytokines for the treatment of human colorectal and other carcinomas. *J Surg Oncol Suppl* 1991; 2: 9–13.
63. Heij HA, Rutgers EJ, de Kraker J, Vos A. Intraoperative search for neuroblastoma by MIBG and radioguided surgery with the gamma detector. *Med Pediatr Oncol* 1997; 28: 171–174.
64. Krag DN, Haseman MK, Ford P, Smith L, Taylor MH, Schneider P, Goodnight JE. Gamma probe location of 111indium-labeled B72.3: an extension of immunoscintigraphy. *J Surg Oncol* 1992; 51: 226–230.
65. Manayan RC, Hart MJ, Friend WG. Radio-immunoguided surgery for colorectal cancer. *Am J Surg* 1997; 173: 386–389.
66. Martelli H, Ricard M, Larroquet M, Wioland M, Paraf F, Fabre M, Josset P, Helardot PG, Gauthier F, Terrier-Lacombe MJ, Michon J, Hartmann O, Tabone MD, Patte C, Lumbroso J, Gruner M. Intraoperative localization of neuroblastoma in children with ^{123}I- or ^{125}I-radiolabeled metaiodobenzylguanidine. *Surgery*. 1998; 123: 51–57.
67. Nieroda CA, Milenic DE, Carrasquillo JA, Scholm J, Greiner JW. Improved tumor radioimmunodetection using a single-chain Fv and gamma-interferon: potential clinical applications for radioimmunoguided surgery and gamma scanning. *Cancer Res* 1995; 55: 2858–2865.
68. Peltier P, Curtet C, Chatal J, Le Doussal JM, Daniel G, Aillet G, Gruaz-Guyon A, Barbet J, Delaage M. Radioimmunodetection of medullary thyroid cancer using a bispecific anti-CEA/anti-indium-DTPA antibody and an indium-111-labeled DTPA dimer. *J Nucl Med* 1993; 34: 1267–1273.
69. Roveda L. [Radioimmunoscintigraphy with mono-clonal antibodies in recurrences and metastases of colorectal tumors]. *Medicina* 1990; 10: 160–161.
70. Rutgers EJ. Radio-immunotargeting in colorectal carcinoma. *Eur J Cancer* 1995; 31A: 1243–1247.
71. Schneebaum S, Papo J, Graif M, Baratz M, Baron J, Skornik Y. Radioimmunoguided surgery benefits for recurrent colorectal cancer [see comments]. *Ann Surg Oncol* 1997; 4: 371–376.
72. Stella M, De Nardi P, Paganelli G, et al. Surgery for colorectal cancer guided by radiodetecting probe. Clinical evaluation using monoclonal antibody B72.3. *Eur J Surg* 1991; 157: 485–488.
73. Stella M, De Nardi P, Paganelli G, et al. Avidin-biotin system in radioimmunoguided surgery for colorectal cancer. Advantages and limits. *Dis Colon Rectum* 1994; 37: 335–343.
74. Williams HT, Sorsdahl OA, Lawhead RA, Letton AH, Sommerville JC. Colorectal and gynecological malignancies: comparison of B72.3 monoclonal antibody imaging, CT, and serum tumor antigens. *Am Surg* 1995; 61: 195–196.
75. Barbera-Guillem E, Arnold MW, Nelson MB, Martin EW Jr. First results for resetting the antitumor immune response by immune corrective surgery in colon cancer. *Am J Surg* 1998; 176: 339–343.
76. Martin EW Jr, Mojzisik CM, Hinkle GH, et al. Radioimmunoguided surgery using monoclonal antibody. *Am J Surg* 1988; 156:386-392.

77. Alazraki NP, Eshima D, Eshima LA, Herda SC, Murray DR, Vansant JP, Taylor AT. Lymphoscintigraphy, the sentinel node concept, and the intraoperative gamma probe in melanoma, breast cancer, and other potential cancers. *Semin Nucl Med* 1997; 27: 55–67.
78. Albertini JJ, Cruse CW, Rapaport D, Wells K, Ross M, DeConti R, Berman CG, Jared K, Messina J, Lyman G, Glass F, Fenske N, Reintgen DS. Intraoperative radio-lympho-scintigraphy improves sentinel lymph node identification for patients with melanoma. *Ann Surg* 1996; 223: 217–224.
79. Alex JC, Weaver DL, Fairbank JT, Rankin BS, Krag DN. Gamma-probe-guided lymph node localization in malignant melanoma. *Surg Oncol* 1993; 2: 303–308.
80. Alex JC, Krag DN. Gamma-probe guided localization of lymph nodes. *Surg Oncol* 1993; 2: 137–143.
81. Alex JC, Krag DN. The gamma-probe-guided resection of radiolabeled primary lymph nodes. *Surg Oncol Clin North Am* 1996; 5: 33–41.
82. Alex JC, Krag DN, Harlow SP, Meijer S, Loggie BW, Kuhn J, Gadd M, Weaver DL. Localization of regional lymph nodes in melanomas of the head and neck. *Arch Otolaryngol Head Neck Surg* 1998; 124: 135–140.
83. Ames SE, Krag DN, Brady MS. Radio-localization of the sentinel lymph node in Merkel cell carcinoma: a clinical analysis of seven cases. *J Surg Oncol* 1998; 67: 251–254.
84. Bartolomei M, Testori A, Chinol M, Gennari R, De Cicco C, Leonardi L, Zoboli S, Paganelli G. Sentinel node localization in cutaneous melanoma: lymphoscintigraphy with colloids and antibody fragments versus blue dye mapping. *Eur J Nucl Med* 1998; 25: 1489–1494.
85. Berclaz G, Crazzolara AO, Altermatt HJ, Aebi S, Fey MF, Haenggi W, Dreher E. Sentinel lymphadenectomy: an alternative to axillary lymphadenectomy in breast cancer. *Schweiz Med Wochenschr* 1998; 128: 1730–1736.
86. Bombardieri E, Crippa F, Maffioli L, Draisma A, Chiti A, Agresti R, Greco M. Nuclear medicine approaches for detection of axillary lymph node metastases. *Q J Nucl Med* 1998; 42: 54–65.
87. Borgstein PJ, Pijpers R, Comans EF, van Diest PJ, Boom RP, Meijer S. Sentinel lymph node biopsy in breast cancer: guidelines and pitfalls of lymphoscintigraphy and gamma probe detection. *J Am Coll Surg* 1998; 186: 275–283.
88. Brobeil A, Kamath D, Cruse CW, Rapaport DP, Wells KE, Shons AR, Messina JL, Glass LF, Berman CG, Puleo CA, Reintgen DS. The clinical relevance of sentinel lymph nodes identified with radiolymphoscintigraphy. *J Florida Med Assoc* 1997; 84: 157–160.
89. Büchels HK, Vogt H, Bachter D. [Scintillation probe guided sentinel lymphadenectomy in malignant melanoma]. *Chirurg* 1997; 68: 45–50.
90. Crossin JA, Johnson AC, Stewart PB, Turner WW Jr. Gamma-probe-guided resection of the sentinel lymph node in breast cancer. *Am Surg* 1998; 64: 666–668; discussion 669.
91. de Hullu JA, Doting E, Piers DA, Hollema H, Aalders JG, Koops HS, Boonstra H, van der Zee AG. Sentinel lymph node identification with technetium-99m-labeled nanocolloid in squamous cell cancer of the vulva. *J Nucl Med* 1998; 39: 1381–1385.
92. Dresel S, Weiss M, Heckmann M, Rossmüller B, Konz B, Tatsch K, Hahn K. [Diagnosis of sentinel lymph node in malignant melanoma: preoperative lymphoscintigraphy and intraoperative gamma probe guidance]. *Nuklearmedizin* 1998; 37: 177–182.
93. Glass LF, Messina JL, Cruse W, Wells K, Rapaport D, Miliotes G, Berman C, Reintgen D, Fenske NA. The use of intraoperative radiolymphoscintigraphy for sentinel node biopsy in patients with malignant melanoma. *Dermatol Surg* 1996; 22: 715–720.
94. Greco M, Agresti R, Giovanazzi R. Impact of the diagnostic methods on the therapeutic strategies. *Q J Nucl Med* 1998; 42: 66–80.
95. Gulec SA, Moffat FL, Carroll RG, Krag DN. Gamma probe guided sentinel node biopsy in breast cancer. *Q J Nucl Med* 1997; 41: 251–261.
96. Gulec SA, Moffat FL, Carroll RG, Serafini AN, Sfakianakis GN, Allen L, Boggs J, Escobedo D, Pruett CS, Gupta A, Livingstone AS, Krag DN. Sentinel lymph node localization in early breast cancer. *J Nucl Med* 1998; 39: 1388–1393.
97. Hader D, Moss K, Geier N. Sentinel lymph node biopsy using lymphoscintigraphy. *AORN J* 1998; 68: 572–576, 579–582, 585–588.
98. Kapteijn BA, Nieweg OE, Liem I, Mooi WJ, Balm AJ, Muller SH, Peterse JL, Valdés Olmos RA, Hoefnagel CA, Kroon BB. Localizing the sentinel node in cutaneous melanoma: gamma probe detection versus blue dye. *Ann Surg Oncol* 1997; 4: 156–160.
99. Kapteijn BA, Nieweg OE, Muller SH, Liem IH, Hoefnagel CA, Rutgers EJ, Kroon BB. Validation of gamma probe detection of the sentinel node in melanoma. *J Nucl Med* 1997; 38: 362–366.
100. Koch WM, Choti MA, Civelek AC, Eisele DW, Saunders JR. Gamma probe-directed biopsy of the sentinel node in oral squamous cell carcinoma. *Arch Otolaryngol Head Neck Surg* 1998; 124: 455–459.
101. Krag DN, Meijer SJ, Weaver DL, Loggie BW, Harlow SP, Tanabe KK, Laughlin EH, Alex JC. Minimal-access surgery for staging of malignant melanoma. *Arch Surg* 1995; 130: 654-658; discussion 659-660.
102. Krag D, Weaver D, Ashikaga T, Moffat F, Klimberg VS, Shriver C, Feldman S, Kusminsky R, Gadd M, Kuhn J, Harlow S, Beitsch P. The sentinel node in breast cancer–a multicenter validation study. *N Engl J Med* 1998; 339: 941–946.
103. Lieber KA, Standiford SB, Kuvshinoff BW, Ota DM. Surgical management of aberrant sentinel lymph node drainage in cutaneous melanoma. *Surgery* 1998; 124: 757–761; discussion 761–762.
104. Meijer S, Collet GJ, Pijpers HJ, van Hattum L, Hoekstra OS. [Less axillary dissection necessary due to sentinel node biopsy in patients with breast carcinoma]. *Ned Tijdschr Geneeskd* 1996; 140: 2239–2243.
105. Mudun A, Murray DR, Herda SC, Eshima D, Shattuck LA, Vansant JP, Taylor AT, Alazraki NP. Early stage melanoma: lymphoscintigraphy, reproducibility of sentinel node detection, and effectiveness of the intraoperative gamma probe. *Radiology* 1996; 199: 171–175.
106. Nieweg OE, Jansen L, Kroon BB. Technique of lymphatic mapping and sentinel node biopsy for melanoma. *Eur J Surg Oncol* 1998; 24: 520–524.
107. O'Brien CJ, Uren RF, Thompson JF, Howman-Giles RB, Petersen-Schaefer K, Shaw HM, Quinn MJ, McCarthy WH. Prediction of potential metastatic sites in cutaneous head and neck melanoma using lymphoscintigraphy. *Am J Surg* 1995; 170: 461–466.
108. Offodile R, Hoh C, Barsky SH, Nelson SD, Elashoff R, Eilber FR, Economou JS, Nguyen M. Minimally invasive

breast carcinoma staging using lymphatic mapping with radiolabeled dextran. *Cancer*. 1998; 82: 1704–1708.
109. Paganelli G, De Cicco C, Cremonesi M, Prisco G, Calza P, Luini A, Zucali P, Veronesi U. Optimized sentinel node scintigraphy in breast cancer. *Q J Nucl Med* 1998; 42: 49–53.
110. Pijpers R, Collet GJ, Meijer S, Hoekstra OS. The impact of dynamic lymphoscintigraphy and gamma probe guidance on sentinel node biopsy in melanoma. *Eur J Nucl Med* 1995; 22: 1238–1241.
111. Pijpers R, Borgstein PJ, Meijer S, Hoekstra OS, van Hattum LH, Teule GJ. Sentinel node biopsy in melanoma patients: dynamic of lymphoscintigraphy followed by intraoperative gamma probe and vital dye guidance. *World J Surg*. 1997; 21: 788–792; discussion 793.
112. Pijpers R, Meijer S, Hoekstra OS, Collet GJ, Comans EF, Boom RP, van Diest PJ, Teule GJ. Impact of lymphoscintigraphy on sentinel node identification with technetium-99m-colloidal albumin in breast cancer. *J Nucl Med* 1997; 38: 366–368.
113. Reintgen D, Rapaport D, Tanabe KK, Ross M. Lymphatic mapping and sentinel node biopsy in patients with malignant melanoma. *J Florida Med Assoc* 1997; 84: 188–193.
114. Rettenbacher L, Koller J, Gmeiner D, KŠssmann H, Galvan G. [Selective regional lymphadenectomy in malignant melanoma using a gamma probe]. *Acta Med Austriaca* 1997; 24: 79–80.
115. Schneebaum S, Stadler J, Cohen M, Yaniv D, Baron J, Skornick Y. Gamma probe-guided sentinel node biopsy–optimal timing for injection. *Eur J Surg Oncol* 1998; 24: 515–519.
116. Snider H, Dowlatshahi K, Fan M, Bridger WM, Rayudu G, Oleske D. Sentinel node biopsy in the staging of breast cancer. *Am J Surg* 1998; 176: 305–310.
117. Stewart KC, Lyster DM. Interstitial lymphoscintigraphy for lymphatic mapping in surgical practice and research. *J Invest Surg* 1997; 10: 249–262.
118. Thompson JF, Niewind P, Uren RF, Bosch CM, Howman-Giles R, Vrouenraets BC. Single-dose isotope injection for both preoperative lymphoscintigraphy and intraoperative sentinel lymph node identification in melanoma patients. *Melanoma Res* 1997; 7: 500–506.
119. Tiourina T, Arends B, Huysmans D, Rutten H, Lemaire B, Muller S. Evaluation of surgical gamma probes for radioguided sentinel node localisation. *Eur J Nucl Med* 1998; 25: 1224–1231.
120. van der Veen H, Hoekstra OS, Paul MA, Cuesta MA, Meijer S. Gamma probe-guided sentinel node biopsy to select patients with melanoma for lymphadenectomy. *Br J Surg* 1994; 81: 1769–1770.
121. Veronesi U, Paganelli G, Galimberti V, Viale G, Zurrida S, Bedoni M, Costa A, de Cicco C, Geraghty JG, Luini A, Sacchini V, Veronesi P. Sentinel-node biopsy to avoid axillary dissection in breast cancer with clinically negative lymph-nodes [see comments]. *Lancet* 1997; 349: 1864–1867.
122. Vidal-Sicart S, Piulachs J, Pons F, Castel T, Palou J, Herranz R, Setoain J. [Detection of sentinel lymph nodes by lymphatic gammagraphy and intraoperative gamma-ray probe in patients with malignant melanoma. Initial results]. *Rev Esp Med Nucl* 1998; 17: 15–20.
123. Cohen M, Gat A, Haddad R, Avital S, Even-Sapir E, Skornick Y, Shafir R, Schneebaum S. Single-injection gamma probe-guided sentinel lymph node detection in 40 melanomatous lymphadenectomies. *Ann Plast Surg* 1998; 41: 397–401.
124. Pijpers R, Borgstein PJ, Meijer S, Krag DN, Hoekstra OS, Greuter HNJM, Teule GJJ. Transport and retention of colloidal tracers in regional lymphoscintigraphy in melanoma: influence on lymphatic mapping and sentinel node biopsy. *Melanoma Res* 1998; 8: 413–418.
125. Guliano AE, Kirgan DM, Guenther JM, Morton DL. Lymphatic mapping and sentinel lymphadenectomy for breast cancer. *Ann Surg* 1994; 220: 391–401.
126. Kohler G, Milstein C. Continuous cultures of fused cell secreting antibody of predefined sensitivity. *Nature*. 1975; 256: 495–497.
127. Thurston MO, Kaehr JW, Martin EW III, Martin EW Jr. Radionuclide of choice for use with an intraoperative probe. *Antibody Immunoconj Radiopharm* 1991; 4: 595–601.
128. Morton DL, Wen DR, Wong JH, Economou JS, Cagle LA, Storm FK, Foshag LJ, Cochran AJ. Technical details of intraoperative lymphatic mapping for early stage melanoma. *Arch Surg* 1992; 127: 392–399.
129. Krag DN, Weaver DL, Alex JC, Fairbank JT. Surgical resection and radiolocalization of the sentinel lymph node in breast cancer using a gamma probe. *Surg Oncol* 1993; 2: 335–339; discussion 340.
130. Perkins A. Peroperative nuclear medicine [editorial]. *Eur J Nucl Med* 1993; 20: 573–575.
131. Alazraki N. Lymphoscintigraphy and the intraoperative gamma probe [editorial; comment]. *J Nucl Med* 1995; 36: 1780–1783.
132. Barber HB, Barrett HH, Wild WJ, Woolfenden JM. Development of small in vivo imaging probes for tumor detection. *IEEE Trans Nucl Sci* 1984; 31: 599–604.
133. Woolfenden JM, Barber HB. Radiation detector probes for tumor localization using tumor-seeking radioactive tracers. *Am J Roentgenol* 1989; 153: 35–39.
134. Barber HB, Augustine FL, Barrett HH, Dereniak EL, Matherson KL, Meyers TJ, Perry DL, Venzon JE, Woolfenden JM, Young ET. Semiconductor arrays with multiplexer readout for gamma-ray imaging: results for a 48*48 Ge array. *Nucl Instrum Methods Phys Res Sect A* 1994; 353: 361–365.
135. MacDonald LR, Tornai MP, Levin CS, Park J, Atac M, Cline DB, Hoffman EJ. Investigation of the physical aspects of beta imaging probes using scintillating fibers and visible light photon counters. *IEEE Trans Nucl Sci* 1995; 42: 1351–1357.
136. MacDonald LR. Ph.D. Thesis, UCLA, 1996.
137. Petroff M, Staepelbroek M. Photon counting solid-state photomultiplier. *IEEE Trans Nucl Sci* 1989; NS-36: 158–162.
138. Tornai MP, MacDonald LR, Levin CS, Siegel S, Hoffman EJ, Park J, Atac M, Cline DB In: Park J, ed. *Imaging detectors in high energy, astroparticle and medical physics*. Singapore: World Scientific Co.; 1996: 133–148.
139. Tornai MP, Macdonald LR, Levin CS, Siegel S, Hoffman EJ. Design considerations and initial performance of a 1.2 cm(2) beta imaging intra-operative probe. *IEEE Trans Nucl Sci* 1996; 43: 2326–2335.
140. Levin CS, Tornai MP, MacDonald LR, Hoffman EJ. Annihilation gamma-ray background characterization and rejection for a small beta ray camera imaging positron emitters. *IEEE Trans Nucl Sci* 1997; NS-44: 1120–1126.
141. Tornai MP, Levin CS, MacDonald LR, Holdsworth CH, Hoffman EJ. A miniature phoswich detector for gamma-ray localization and beta imaging. *IEEE Trans Nucl Sci* 1998; NS-45: 1166–1173.

142. Hoffman EJ, Tornai MP, Levin CS, MacDonald LR, Holdsworth CH. A dual detector beta-ray imaging probe with gamma-ray background suppression for use in intra-operative detection of radiolabeled tumors. *Nuclear Instrum Methods Phys Res Sect A: Accelerators Spectrometers Detectors and Associated Equipment.* 1998; 409: 511–516.
143. Knapp FF Jr., Beets AL, Guhlke S, Zamora PO, Bender H, Palmedo H, Biersack HJ. Availability of rhenium-188 from the alumina-based tungsten-188/rhenium-188 generator for preparation of rhenium-188-labeled radiopharmaceuticals for cancer treatment. *Anticancer Res* 1997; 17: 1783–1795.
144. Ehrhardt GJ, Ketring AR, Ayers LM. Reactor-produced radionuclides at the University of Missouri Research Reactor. *Appl Radiat Isotopes* 1998; 49: 295–297.
145. Kairemo KJ. Radioimmunotherapy of solid cancers: a review. *Acta Oncol* 1996; 35: 343–355.
146. Kairemo KJ, Stršmberg S, Nikula TK, Karonen SL. Expression profile of vascular cell adhesion molecule-1 (CD106) in inflammatory foci using rhenium-188 labelled monoclonal antibody in mice. *Cell Adhesion Commun* 1998; 5: 325–333.
147. Prakash S, Went MJ, Blower PJ. Cyclic and acyclic polyamines as chelators of rhenium-186 and rhenium-188 for therapeutic use. *Nucl Med Biol* 1996; 23: 543–549.
148. Rhodes BA, Lambert CR, Marek MJ, Knapp FF Jr, Harvey EB. Re-188 labelled antibodies. *Appl Radiat Isotopes* 1996; 47: 7–14.
149. Truitt KE, Nagel T, Suen LF, Imboden JB. Structural requirements for CD28-mediated costimulation of IL-2 production in Jurkat T cells. *J Immunol* 1996; 156: 4539–4541.
150. Zamora PO, Bender H, Gulhke S, Marek MJ, Knapp FF Jr, Rhodes BA, Biersack HJ. Pre-clinical experience with Re-188-RC-160, a radiolabeled somatostatin analog for use in peptide-targeted radiotherapy. *Anticancer Res* 1997; 17: 1803–1808.
151. Zamora PO, Bender H, Knapp FF Jr., Rhodes BA and Biersack HJ. Targeting peptides for pleural cavity tumor radiotherapy: specificity and dosimetry of Re-188-RC-160. *Hybridoma.* 1997: 16: 85–91.
152. Woolfenden JM, Barber HB. In: Freeman LM, ed. *Nuclear medicine annual.* New York: Raven Press; 1990: 151–173.
153. Patt BE, Tornai MP, Iwanczyk JS, Levin CS, Hoffman EJ. Development of an intraoperative gamma camera based on a 256-pixel mercuric iodide detector array. *IEEE Trans Nucl Sci* 1997; NS-44: 1242–1248.
154. Tornai MP, Levin CS, MacDonald LR, Hoffman EJ. Investigation of crystal geometries for fiber coupled gamma imaging intra-operative probes. *IEEE Trans Nucl Sci* 1997; NS-44: 1254–1261.
155. Hoffman EJ, Tornai MP, Levin CS, MacDonald LR, Siegel S. Design and performance of gamma and beta intra-operative imaging probes. *Phys Med* 1997; XIII: S243–S247.
156. Pani R, De Vincentis G, Scopinaro F, Pellegrini R, Soluri A, Weinberg IN, Pergola A, Scafe R, Trotta G. Dedicated gamma camera for single photon emission mammography (SPEM). *IEEE Trans Nucl Sci* 1998; NS-45: 3127–3133.
157. Weinberg IN, Pani R, Pellegrini R, Scopinaro F, DeVincentis G, Pergola A, Soluri A. Small lesion visualization in scintimammography. *IEEE Trans Nucl Sci* 1997; NS-44: 1398–1402.
158. Patt BE, Iwanczyk JS, Rossington Tull C, Wang NW, Tornai MP, Hoffman EJ. High resolution CsI(Tl)/Si-PIN detector development for breast imaging. *IEEE Trans Nucl Sci* 1998; NS-45: 2126–2131.
159. Levin CS, Hoffman EJ, Tornai MP, MacDonald LR. PSPMT and PIN diode designs of a small scintillation camera for imaging malignant breast tumors. *IEEE Trans Nucl Sci* 1997; NS-44: 1513–1520.

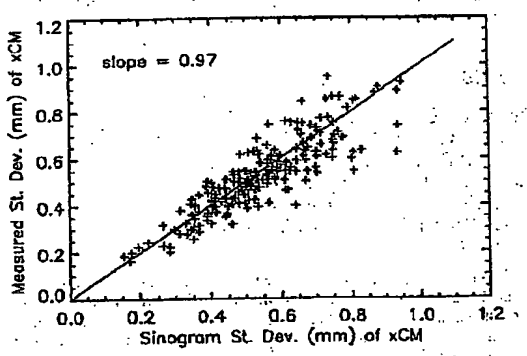

No. 67

IMPROVED QUANTITATIVE IMAGING FOR ^{111}In-PROSTASCINT® USING CT/SPECT AND DUAL-ENERGY RECONSTRUCTION. K. H. Wong*, H. R. Tang, A. J. Da Silva, M. C. Wu, K. Iwata, and B. H. Hasegawa, University of California at San Francisco, San Francisco, CA. (101096)

Objectives: We have developed and tested new iterative reconstruction techniques for the UCSF CT/SPECT system that enhance the quantitative accuracy of ^{111}In-ProstaScint® imaging. **Methods:** We use high-resolution CT scans to correct for attenuation, and calibration measurements to correct for collimator resolution loss and energy-dependent efficiency. Because ^{111}In emits photons at both 171 and 245 keV, our reconstruction also fully models its dual-energy emissions, using either (1) separate energy windows and attenuation maps or (2) a combined energy window and an 'effective attenuation map', which accounts for the prefatential attenuation of the 171 keV photons. We have tested these reconstruction algorithms in phantom studies, using a 20 cm diameter cylindrical tank containing spheres (38-18 mm diameter) representing tumors, with a tumor:background activity ratio of 8:1. The tank also contained ^{99m}Tc to simulate the blood-pool imaging used in ^{111}In-ProstaScint® scans. We acquired SPECT projections using energy windows at 140, 171, and 245 keV. CT slices of the phantom were acquired, registered to SPECT data, and scaled to produce attenuation maps. We then reconstructed the SPECT data using the new dual-energy methods, filtered backprojection, and a conventional ML-EM code with no dual-energy capabilities; quantitative accuracy was determined by measuring the activity in the spheres and comparing against their known activity. **Results:** The dual-energy methods produced the least error (11%), followed by conventional ML-EM (48%) and filtered backprojection (>100%). Furthermore, the combined window method produced results within 10% of the separate window method, while requiring roughly 50% less reconstruction time. **Conclusion:** Our new dual-energy methods can significantly improve quantitation of ^{111}In-ProstaScint® images.

No. 68

AN INNOVATIVE HIGH EFFICIENCY AND HIGH RESOLUTION PROBE FOR PROSTATE IMAGING. L. Zhang*, N. H. Clinthorne, S. J. Wilderman, C. Hua, T. J. Kragh, and W. L. Rogers, University of Michigan, Ann Arbor, MI. (101356)

High resolution imaging of the prostate is essential to improve detection of prostate cancer, but is difficult to achieve by conventional imaging methods. We have designed a transrectal imaging probe based on Compton camera techniques that promises high sensitivity and high resolution. Initial investigations were performed using Monte Carlo simulations. A simulated probe consisting of a $1\times4\times1$cm^3 Si detector with 1mm^3 detector elements was placed at the center of a simulated human body. Two $40\times40\times2$cm^3 planar CZT cameras were located 5cm below and above the body and served as the second detectors. The human body was simulated by a $40\times40\times20$cm^3 thick slab phantom with prostate located 1cm from the center plane. A "Y" shaped array of point source with 5mm spacing was placed at the location of the prostate. All effects of scattering, attenuation, detector penetration and Doppler broadening were included in the simulation. List-mode likelihood method was used for image reconstruction. Reconstructions of the simulated prostate are shown below for γ-ray energies of 140kev, 364kev and 511kev (L-R). Best performance is obtained at 364kev which gives 2mm FWHM resolution at a detection efficiency (including attenuation) of 1.2×10^{-3}. Resolution at 140 and 511kev is 2.5 and 2.3mm, respectively. The initial results demonstrate that the Compton probe has high resolution and high efficiency at energies ranging from 140 to 511kev, which include the emissions from ^{111}In used in ProstaScint.

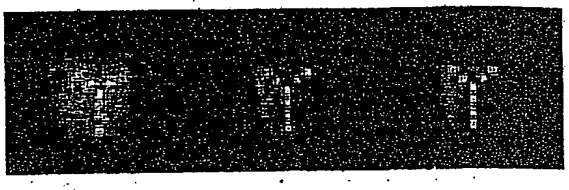

No. 69

REGIONAL LEFT VENTRICULAR FUNCTION AND PERFUSION FROM GATED SPECT ^{201}Tl SCANS: A 4D MODEL USING SPHERICAL HARMONICS. P. M. Mansour*, M. F. Smith, V. Dilsizian, and S. L. Bacharach, The National Institutes of Health, Bethesda, MD. (101305)

Objectives: It is desirable to quantify the absolute regional LV motion and perfusion from gated ^{201}Tl SPECT studies. Image noise and poor spatial resolution make this difficult. We approach this problem by fitting the inherently 4D data to a single 4D analytic function. **Methods:** Using a modified spherical coordinate system, 144 radial profiles (12 θ and 12 ϕ) are generated from short-axis LV slices for the 8 time-points. Each 1D profile is modeled as a square wave convolved with a PSF with fwhm = 15mm. The (θ, ϕ)-dependences of the endocardial border (r_n), the width (w), the myocardial perfusion (M) and background are described by spherical harmonic series (max. polar and azimuthal orders 6 and 4). Blood-pool activity is modeled as a constant. The time-dependences of r_n and w are modeled by 1 Fourier harmonic. The parameters of the fit are the coefficients of the basis functions. The estimated r_n and w are used to compute 2 LV indices: max. regional width (*MRW*) and regional thickening (*RT*). Using ROIs drawn on a gated patient PET ammonia study, we generated 10 noisy realizations of simulated SPECT data to assess the error in *M*, *MRW* and *RT*. Our 4D model was compared to a 2D version, which fit the 144 radial profiles independently, from which the regional indices *M*, *MRW* and *RT* also were computed. **Results:** The relative variability (%σ) in *M* fell from 19% (2D) to 12% (4D), while the %rms error rose from 12% (2D) to 15% (4D). The %σ in the estimate of *MRW* fell from 25% (2D) to 17% (4D), and %rms rose from 31% (2D) to 32% (4D). For *RT* %σ fell from 55% (2D) to 44% (4D) and the %rms also fell from 88% (2D) to 67% (4D). **Conclusion:** A 4D model of gated SPECT ^{201}Tl scans reduces the variability in estimates of regional indices of LV function/perfusion, while accuracy either remains nearly constant or improves.

No. 70

LESION DETECTABILITY OF MAP RECONSTRUCTION USING COMPUTER OBSERVER: A THEORETICAL STUDY. J. Qi*, and R. H. Huesman, Lawrence Berkeley National Laboratory, Berkeley, CA. (101417)

Objectives: Statistical image reconstruction methods based on *maximum a posteriori* principle (MAP) have been developed for emission tomography due to the low signal to noise ratio in emission data. Examples have been shown that statistical methods improve image quality compared to the conventional filtered backprojection (FBP) method. However, these results depend on isolated data sets. Here we will derive theoretical results of the lesion detectability of MAP reconstruction, which do not rely on any particular object structure. **Methods:** Since resolution and noise properties of MAP algorithm are nonlinear and object dependent, approximations are typically required to make the problem tractable. Resolution and noise properties of MAP reconstructions have been analyzed at the fixed point of the objective function. Using the local invariant approximation we have previously developed,